University of Alberta

GDF11 in Ocular Development and MOTA Mapping

by

Robertino Ralph Karlo Peralta Mateo

A thesis submitted to the Faculty of Graduate Studies and Research
in partial fulfillment of the requirements for the degree of

Master of Science

In

Medical Sciences – Medical Genetics

Fall 2012
Edmonton, Alberta

Abstract

Vision relies on the ability of the eye to receive, process, and send signals to the brain for interpretation. To perform these functions, the eye must properly form during embryogenesis which requires the interaction of genes encoding proteins with various functions during development such as cellular differentiation, migration, and proliferation. In this thesis, I investigate ocular formation and disease. One project assesses the role of *gdf11* in a zebrafish animal model to study the eye formation. I also explore the effect of human *GDF11* sequence variants in ocular disorders. The second project involves mapping a genomic interval responsible for an autosomal recessive disorder known as Manitoba Oculotrichoanal syndrome. The interval detected is in the vicinity of *FREM1*, whose paralogs cause Fraser Syndrome, a disease with phenotypic overlaps. Understanding the molecular basis of ocular diseases can aid the development of new methods to potentially better manage, treat, and reduce their occurrences.

Acknowledgements

The work presented in this thesis would not have been possible without the aid and guidance of many individuals. First of all I would like to thank my mentor Dr. Ordan J. Lehmann for accepting me as a trainee. I have been privileged to study in the Department of Medical Genetics and Dr. Lehmann's position as a clinical-scientist allowed for the pursuit of projects regarding ocular development and disease. His high expectations, patience, and understanding made me a better scientist in terms of my ability to plan experiments, analyze data, and develop the skills required to write a manuscript. I thank my committee members Dr. Andrew J. Waskiewicz and Dr. Michael A. Walter for their input and guidance in my training at committee meeting presentations or at various poster presentations. I would also like to thank Dr. Nipavan Chiamvimonvat from the University of California Davis for recommending the University of Alberta as an institution where I can continue my studies.

I wish to express my gratitude to the following individuals who have trained me in numerous molecular assays and analytical techniques. To Dr. Mika Asai-Coakwell and Ming Ye I thank you both for offering assistants and guidance in trouble shooting GC rich PCRs, molecular cloning, cell transfection and western analysis training. To Dr. Xiao Hua thanks you for creating template plasmids for subsequent cloning assays. I thank past and present members of the Waskiewicz especially Karyn Berry who guided me in performing in situ hybridization, morpholino injections, and demonstrating the patience and dedication required to perform zebrafish for experiments as well as Curtis French, Timothy Erickson,

Patricia Gongal, and Laura Pillay for their encouragement and the occasional Friday afternoon beers. To Dr. Ted Allison and his trainee Michele DuVal, thank you for your assistance and supply of photoreceptor antibodies. A special thanks goes to Azam Khorshidi for training me in the use of PLINK and GenomeStudio software suite for my mapping project. To Dr. Hardeep P. Singh and Dr. Sameer D. Pant I thank for their opinions and input on my mapping project and paper. To Dr. Sarah Hughes, thank you for letting me use your confocal microscope facility. I would also like to thank technicians May Yu for plating and upkeep of cells used for western analysis, Aleah McCoury for maintaining a healthy zebrafish facility, and Erin Strachan for helping to keep the Lehmann lab running smoothly.

I would like to thank the various funding sources I have been fortunate to receive in my time as a graduate research assistant. First off, I would like to thank Dr. Lehmann for providing and supplementing my stipend from some of the lab's funding sources, notably from the Canadian Institute of Health Research and Alberta Innovates Health Solutions. Secondly I would like to thank the Department of Medical Genetics for paying half of my annual tuition, which as an international is quite a substantial sum. I would like to also recognize the Faculty of Medicine & Dentistry and Alberta Health Services for the Graduate Student Recruitment Studentship and a Graduate Research Assistantship awards and the Women and Children Health Research Institute (WCHRI) for financing a Graduate Studentship. The work presented in this thesis made it possible to attend conferences at the provincial, national, and international level. I also enjoyed presenting at several research days organized in Edmonton by WCHRI,

Team to Prevent Blindness, or the Medical Genetics Students' Association. I lastly thank my friends and family members for their support whether they are in Edmonton, California, or the Philippines. I am grateful for the experiences I have had and I am proud call Canada my home.

Table of Contents

List of Figures

List of Tables

Abbreviations

BAF	B-allele frequency
BMP	bone morphogenetic protein
BMP4	bone morphogenetic protein 4
BMP7	bone morphogenetic protein 7
BNAR	bifid nose, renal agenesis
bp	base pair
cDNA	complementary DNA
CER1	cerberus 1
CNV	copy number variation
CRX	cone rod homebox
CSPG	chonrdoitin sulfacte proteo glycan
CSPG4	chondroitin sulfate proteoglycan 4
DIG	digoxigenin
DNA	deoxyribonucleic acid
dpf	days post fertilization
ECM	extracellular matrix
ECR	evolutionary conserved region
ef1alpha	Elongation factor 1-alpha
EGF	epidermal growth factor
FGF	Fibroblast growth factor
FOXL2	forkhead box L2
FRAS1	Fraser syndrome 1
FREM1	FRAS1-related extracellular matrix protein 1
FS	Fraser Syndrome
GDF11	growth differentitation factor 11
GDF3	growth differentiation factor 3
GDF6	growth differentiation factor 6
GDF8	growth differentiation factor 8
gDNA	genomic DNA
hpf	hours post fertilization
IBD	identical by descent
IBS	identical by state
IHC	immunohistochemistry
kb	kilobase
LCA	Lebers Congenital Amaurosis
LRR	Log_2 R ratio
LTBP2	latent-transforming growth factor beta-binding protein 2
MAC	micropthalmia, anophthalmia & coloboma

Mb	megabase
MOs	morpholinos
MOTA	Manitoba Oculotrichoanal
mRNA	messanger RNA
neuroD	neurogenic differentiation
NR2E3	nuclear receptor subfamily 2, group E, member 3
OTX2	orthodenticle homeobox 2
p53	tumor protein 53
PABP2	poly(A)-binding protein 2
PCR	polymerase chain reaction
POAG	primary open angle glaucoma
RGCs	retinal ganglion cells
rh1	rhodopsin 1
RNA	ribonucleic acid
RP	retinitis pigmentosa
RPCs	retinal precursor cells
RPE65	Retinal pigment epithelium-specific 65 kDa
RT-PCR	real time polymerase chain reaction
runx1	runt-related transcription factor 1
SDM	site directed mutagenesis
SDS-PAGE	sodium dodecyl sulfate polyacrylamide gel electrophoresis
Smad	short for mothers against decapentaplegic
SNP	single nucleotide polymorphism
SRY	(Sex determining region Y)-box 2
TGFβ	transforming growth factor beta
UTR	untranslated region
WISH	whole embryo in-situ hybridization
ZDHHC21	zinc finger, DHHC-type containing 21

Chapter 1 General Introduction

The visual system in brief

Vision relies on the ability the eye to focus and detect light, which is then sent as electrochemical signals to the visual processing centers of the brain. To perform this function, the eye must properly form during embryonic development. This process requires the interaction of many genes encoding proteins needed by cells to form structures in the eye such as the light sensitive laminated substructure of the eye known as the retina. Photons are received by photoreceptor cells in the retina to initiate an electrophysiological signal that is relayed by horizontal, bipolar, and amacrine cells to the retinal ganglion cells whose axons transmit these signals to the brain.

Ocular morphogenesis

Ocular morphogenesis of the vertebrate eye, as reviewed by Lamb et al. 2007 [1], begins with the neural tube, the precursor of nervous system. Proliferating neural crest cells migrate dorsally causing the ventral invagination of the endoderm (**Fig. 1.1**). Optic vesicles extend outwards, followed by the proliferation of neural crest cells to eventually separate the endoderm and ectoderm. Once this occurs, the optic vesicles come in contact with surface ectoderm to induce the formation of the lens placode. After making contact with the surface ectoderm, the optic vesicles invaginate to form a bilayered cup consisting of retinal pigment epithelium (RPE) and retinal precursors. The retina and the RPE grow circumferentially whilst lens placode cells proliferate and differentiate until it eventually separates the surface ectoderm.

Anterior segment and eyelid morphogenesis

The development of the anterior segment requires the coordinated movement of surface ectoderm and mesenchyme cells (continue in **Fig. 1.1**)[2]. Future anterior structures such as the cornea (which covers the iris, pupil, and anterior chamber) and eyelids begin development by the migration of mesenchymal cells between the lens, followed by the invagination of eyelid folds in the surface ectoderm**.** Mesenchyme cells proliferate as the eyelids migrate across the cornea. Periderm arms of the eyelid emerge and spread across the corneal surface as mesenchyme cells dissociate from the lens to form the anterior chamber. The eyelid has temporarily fused [3-4] while lens and cornea continue to separate structures as mesenchyme cells continue to differentiate to eventually form the iridocorneal angle, ciliary body, Schlemm's canal, and trabecular meshwork present in the adult eye.

The temporarily fused eyelids are separated via EGF activation of apoptosis [4-6]. Extracellular matrix, ECM, proteins such as EGF can directly bind to proteins containing *chondroitin sulfate proteoglycan* (CSPG) domains [7-8] altering the bioavailability of extracellular growth factors like EGF to affect processes such as epithelial separation of the eyelid. Investigating genes that potentially interact with CSPG and EGF can elucidate disease mechanisms for disorders involving improper eyelid development.

Retinal Development

Retinal cell types differentiate in an orderly manner to form a laminated tissue called the retina. During optic cup formation, the neural retina consists of undifferentiated immature progenitor cells. Retinal ganglion cells (RGCs) are the first retinal cells to develop followed by the differentiation of horizontal cells, cones, amacrines, rods, bipolar cells, and then Müller glial cells [9]. Rod photoreceptors differentiate during embryogenesis but continue to develop after birth [9]. Retinal proliferation is complete by postnatal day 7 but maturation, formation of proper synaptic connections between cell types, and morphological maturation continues until postnatal day 21 [10].

The differentiation and specification of retinal precursor cells (RPCs) into specific neuro-retinal cell types is controlled by many factors. Generally speaking, RPCs grow and proliferate and neuoro-retinal cell types are born after the exit of these RPCs from cell cycle growth. Commitment of RPCs to certain cell fates are controlled by extrinsic growth factors and signaling molecules as well as intrinsic transcription factors [11]. Examples of extrinsic factors that determine retinal development and cell fate include and sonic hedgehog (*SHH*), fibroblast growth factor (*FGF*), epidermal growth factor (*EGF*). *SHH* is expressed by RGCs and through an "auto-regulatory feedback loop" inhibits RGC development to promote RPC proliferation and development in later born cell types like rod photoreceptors [12-13]. Loss of *FGF* signaling partially results in a change of cell fates of amacrines and photoreceptor cells in to Müller glial cells [14].

Increasing *EGF* signaling by viral introduction of *EGF* receptors results in an increase of Müller glial cells [15].

Many intrinsic transcription factors induce retinal cell fates [10] and genes pursued in this thesis are discussed subsequently. *NeuroD* is expressed at low levels in early developing RGCs [16] while overexpression results in the genesis of later born rod photoreceptors [10, 17-18]. RPCs require the expression of cone-rod homeobox (*Crx*) to form the photoreceptor outer segment [19]. Orthodenticle homeobox 2 (*Otx2*) is an upstream activator of *Crx* and loss of *Otx2* results in an increase of amacrines at the expense of photoreceptors [20]. Time-lapse documentation and algorithmic analysis of single isolated RPCs developed a predictive model for differentiation as the correct proportion of each retinal cell type differentiated [21]. RPCs are heterogeneous in their expression profile as performed in a study of 42 RPCs isolated from the same time point [22]. It may be that undifferentiated RPCs in different positions of the eye respond to different external factors (or environmental cues) that are spatially and temporally specific. Studies investigating genes that potentially regulate intrinsic transcription factors, such as the BMPs, can further progress the understanding of their roles in retinal differentiation and their contribution to ocular disease.

Zebrafish as a Visual System Model Organism

Zebrafish (*Danio rerio*) is a powerful model organism utilized in embryonic and larval developmental studies. Zebrafish exhibit several traits that make their use in the laboratory setting highly desirable. For example, zebrafish reach sexual maturity by 3-4 months of age. A breeding pair can yield hundreds of fertilized

eggs. These embryos are transparent and can be visualized and monitored using a dissecting microscope.

The anatomy of the zebrafish retina consists of the seven major cell types found in other vertebrates [23]. By 24 hours post fertilization (hpf), the zebrafish eye is composed of undifferentiated RPCs which can be monitored for development of retinal cell types of interest. Photoreceptors make up 70% of the retina but percent composition of rods and cones varies according to the activity and needs of a particular species. For example, the mouse retina is rod dominant to accommodate their nocturnal activity and contains only 2-3% cone photoreceptors [23-24]. The cone photoreceptor population in the human and zebrafish retina are 5% and 30% respectively, likely due to their diurnal activity [25-26]. Unlike humans, the zebrafish photoreceptor layer is a highly regular grid like pattern of alternating photoreceptor sub types during development which persist in adulthood [27]. The similar retinal anatomy, comparable cone photoreceptor composition, relative ease of visually monitoring development, as well as tools for genetic manipulation make the zebrafish an excellent model for studying ocular development. Manipulation of gene activity in zebrafish can be accomplished with morpholinos.

Morpholino utility, strengths, and weaknesses

Morpholinos (MOs) affect gene activity by inhibiting translation of mRNA or interfering with RNA splicing [28]. MOs are 25 nucleotides in length and are complementary to the translational initiation sequence or span exon-intron junctions. Shorter MOs that are 22 nucleotides in length have been generated for

use in knocking down microRNAs. MO technologies have several strengths. MOs are relatively inexpensive and quick to use as compared to the more time consuming and expensive process of generating knockouts. They are not degraded by cells as there are no enzymes known to act on MOs [29]. MO knockdown methods can be used to target maternally deposited or zygotically expressed genes. MOs can be also designed to bind to specific splice isoforms of target genes [30]. MOs are injected between the 1-4 cell stages of development to inhibit gene activity. MOs can be assayed for gene knockdown efficacy by several means. One mechanism is to test for rescue of the phenotype by co-injecting morpholinos with RNA that does not contain the MO binding sites. Injection with RNA may be difficult if genes normally exhibit low levels of expression. Another problem could arise if the activity of genes requires spatially specific expression. Injection with RNA in a vector contain tissue specific promoters could augment the problem of unspecific spatial expression. When available, antibodies for the gene of interest can be used to show the efficacy of MO inhibition on protein levels. Alternate methods include assaying the splice blocking MOs by showing retention of intronic sequence which introduces premature stop codons in mRNA by reverse transcription PCR.

MOs are excellent tools but they are associated with caveats. Phenotypes thought to be attributed to MOs are observed in the first 3 to 5dpf. MO knockdowns are variable and incomplete so proteins with long half lives may accumulate and retain activity. MOs exert their effects by binding directly to RNA within cells so as embryos grow, the finite amount of MO becomes diffuse eventually becoming

ineffective. A common effect observed is the activation of *p53* activity in response to MOs is their ability to cause non specific cell death [31]. To partially augment this deficit, MOs are co-injected with *p53* targeting MOs to prevent non specific cell death. An issue complicating use of zebrafish in genetic studies is the existence of two paralogs for at least 20% of human genes [32]. Paralogous genes in zebrafish may perform similar roles but de-novo functions not found in their human counterpart could have developed in paralogs that complicate studies. Another issue that arises is that injection of reproducible volumes in small embryos may not be precise which introduces further variability in MO inhibition studies. While imperfect, the use of MO technology coupled with ease of visualization, high number of offspring, and a similar retinal anatomy to humans make zebrafish an ideal tool to study ocular development and disorders.

Ocular Disease

The importance of studying ocular diseases is apparent in the toll on the quality of life that visual impairment entails. Estimates from the World Health Organization suggest that over 138 million people are visually impaired worldwide [33]. Loss of vision can be caused by injuries to the eye, nutritional deficiencies, complications arising from other diseases such as type II diabetes, or malformations during development. By studying genes required for eye development, inherited ocular conditions can be better understood with the ultimate goal to improve diagnosis, treatment, and anticipation of such genetic disorders. The effort placed in the importance of ocular genetics is apparent in the fact that of the approximately 20,000 entries in the Online Mendelian Inheritance

in Man (OMIM), 30% are associated with ocular development or vision loss [11]. Childhood blindness can result from nutritional deficiencies, but they may also be due to genetic factors which result in malformations and impaired development of the eye. Microphthalmia and Anophthalmia are rare congenital ocular conditions occurring at 1 to 3.2 cases per 10,000 births [34-35]. Microphthalmia is a term used to describe reduced eye size while anopthalmia is the lack of ocular structures required to form an eye globe and both conditions can present unilaterally or bilaterally [36]. Approximately 50% of microphthalmia and Anophthalmia present with systemic anomalies [37]. Non-ocular systemic phenotypes are illustrated by SRY (Sex determining region Y)-box 2 (*SOX2*) transcription factor whose mutations can account for 4-20% of Microphthalmia and Anophthalmia cases [38]. Systemically, patients with *SOX2* mutations can have non-ocular symptoms such as genital, kidney, and esophagus malformations [39]. Coloboma is a rare congenital condition occurring at a rate of 2.6 cases per 10,000 live births which can occur in patients with micropthalmia [40]. Coloboma is a congenital abnormality caused by defective closure of the optic cup fissure during embryonic development. This results in visible malformations in the anterior portions of the eye such as the iris or posterior structures like retina, choroid (the vascular support tissue of the eye), or the optic disk, the area of the eye where optic nerves exit the eye.

TGF-β family and BMP signaling

Genes that play a role in the development of ocular structures in the eye include those that encode for Bone Morphogenetic Proteins (BMPs). The BMP genes

belong to the transforming growth factor β, TGF-β, super family. The human genome contains at least 42 different genes in the TGF-β superfamily of growth factors [41]. BMP protein were originally named for their ability to induce bone and cartilage tissue formation, but have since been documented to play roles in patterning of organs such as the brain and controlling axis patterning by controlling biological processes such as cell proliferation, differentiation, migration, or apoptosis [42]. These ligands are secreted by cells and exist in the ECM as disulfide-linked homodimers or heterodimers. This "homo-hetero dimer duality" is thought to contribute to the variability of the BMP ligands to activate different cellular processes. BMP signaling can be prevented by the direct binding of antagonistic proteins such as Follistatin, Chordin, and Cerberus or by pseudo receptors such as Bambi which compete for ligand binding but lack transmembrane activity [41]. Canonical signal transduction of BMPs (**Fig. 1.2**) involves ligand binding via type I and type II transmembrane serine/threonine kinase BMP receptors to initiate canonical signaling by phosphorylating Smad proteins (short for mothers against decapentaplegic). Certain signaling ligands utilize receptor smads R-Smad1, R-Smad5, and R-Smad8 (*GDF6* and *GDF3*) while other ligands signal via R-Smad2 and R-Smad3 (*GDF11*) [43]. R-Smads then heterodimerize with common Smad4 to continue the cascade or can be inhibited by inhibitory Smads to down regulate BMP signaling. This results in the translocation of this complex to the nucleus to regulate transcription of target genes. Alternatively, BMP signaling can initiate the p38 mitogen-activated

protein kinases (MAPK) cascade. This process is demonstrated by *BMP2* to cause neuronal differentiation [44] or apoptosis [45].

Role of BMPs in eye and retinal development

BMP signaling plays key roles in lens formation, optic cup invagination, and retinal development [41]. Targeted deletion of a type I receptor gene resulted in lens fiber cells which degenerate shortly after birth [46], while *BMP4* homozygous mice fail to induce the formation of the lens [47]. One gene shown to be required for proper optic cup development is Growth Differentiation Factor 6, *GDF6*. A hemizygous deletion of chromosome 8q22.1 encompassing *GDF6* was defined in a patient with bilateral coloboma and systemic anomalies such as bilateral soft-tissue syndactyly of the toes and cardiac defects [48]. Bioinformatic analysis of candidate genes narrowed causal genes to *GDF6* on account of its developmental role in BMP signaling while zebrafish studies on its paralog, *gdf6a* ocular anomalies failure of fissure closure, lens defects, and loss of normal retinal lamination [48]. Further studies revealed that *gdf6a* is required to induce dorsal and ventral patterning of the retina [49-50]. *GDF6* missense mutations are associated in a patient panel with MAC (Microphthalmia, Anophthalmia, and Coloboma) ocular conditions as well as skeletal anomalies such as Klippel-Feil syndrome and hemivertebrae [51]. Other BMP genes have also been associated with eye effects. For example, *GDF3* missense variants were identified in patients with ocular or skeletal anomalies, further implicating other BMP genes in perturbed ocular development syndromes such as Microphthalmia, Anophthalmia, and Coloboma (MAC) [52]. Interestingly, *Gdf11* mutant mice exhibit ocular

phenotypes such as ventral coloboma, altered retinal cell type composition, and increased number of vertebrae [20, 53]. *BMP7* and *BMP4* mutations can cause a spectrum of ocular, ear, and skeletal malformations in human patients further adding support that altered BMP signaling causes MAC [54-55]. Loss of the receptor *Bmpr1b*, results in reduced growth of the retina as well as altered dorsal ventral patterning [56]. This axis directing role of BMP signaling is demonstrated in chicken embryos which require *Bmp4* to induce cell death in the dorsal optic cup [57]. Abnormalities in the anterior structures of the eye have been documented in patients with heterozygous *BMP4* mutations [58]. These data strongly suggest that BMP signaling plays a critical role in the development of the eye and elucidating the roles and mechanism of other members of this gene family will define their contributions to disease.

Retinal dystrophies

Another group of ocular diseases caused by mutations in genes are the retinal dystrophies. As of early 2012, there are 238 mutated genes known to cause a retinal dystrophies annotated on the RetNet online database [59]. This database contains information for retinal dystrophies such Leber Congenital Amaurosis (LCA), juvenile Retinitis Pigmentosa (RP), macular degeneration, Usher syndrome, and various rod cone dystrophies. LCA and juvenile RP lie in a continuum as the most severe cases are deemed LCA while later onset manifestations during childhood are referred to as juvenile RP [60]. Both syndromes display reduced electroretinogram amplitudes indicative of rod cone dystrophies [60]. LCA is an early onset blindness resulting in severe vision loss

by the first year of life and estimates suggest a population frequency of 1:30,000 individuals [61]. LCA exhibits genetic heterogeneity as it is known to be associated with mutations in at least 14 genes in 70% of cases, some of which encode proteins required for proper photoreceptor cell development, metabolism, or protein trafficking [62]. Four missense and 7 frameshift *CRX* mutations are present in patients afflicted with autosomal dominant Cone-Rod Dystrophy 2 or LCA7 [63-67] and it is estimated that mutations in *CRX* are associated with 1-3% of all LCA cases [59]. Whole gene deletions of *OTX2* as well as missense and frameshift mutations occur in patients exhibiting micropthalmia [68-70]. Patients exhibiting micropthalmia as well as short stature with hormonal deficiencies carry heterozygous *OTX2* nonsense or frameshift mutations [71-72]. Successful investigations for ocular genetic disease have identified genes responsible for congenital and early onset disorders. These *OTX2* and *CRX* studies suggest a link between ocular developmental malformations such as micropthalmia and retinal dystrophies.

Gene mapping strategies and SNP arrays

Mapping genes associated with ocular disorders can be done by various means. The particular strategy employed is generally determined by the mode of inheritance of disease (for example autosomal or dominant) and whether the disease is hypothesized to multi-factorial or to be due to a mutation in a single gene. With regards to the work presented in this thesis, homozygosity mapping was employed in the mapping of an autosomal recessive disease. The ability to trace ancestral regions was first proposed by Lander and Botstein in 1987 to map

recessive traits in inbred children [73]. This technique requires analysis of markers that are spaced across the genome for genotype homozygosity to infer shared ancestry (**Fig. 1.3**). Microsatellites were used as markers and followed for segregation with disease or phenotypes across multiple generations. Studies employing high density Single Nucleotide Polymorphism (SNP) arrays have become the preferred technique to their higher throughput capability as compared to the more time consuming and labor intensive microsatellites.

The SNP array platform employed in a project in this thesis was developed by Illumina and is capable of detecting genotype status, annotated as B-Allele Frequency (BAF), and Copy Number variation (CNV) [74-75]. The workflow starts with DNA denaturation, followed by amplification of DNA, then digestion using enzymes. DNA is then precipitated and resuspended in hybridization buffer to incubate on a bead chip. Single base extensions occur for each SNP to differentially label each genotype. The labels are excited by lasers to emit fluorescence signals collected by a reader as data to be interpreted by software, in this case GenomeStudio.

BAF is the relative frequency of one genotype against another with the following formula, $BAF = N_{B\text{-allele}}/(N_{A\text{-allele}}+N_{B\text{-allele}})$. A homozygous SNP can have either a BAF=1 when 2/(0+2) or 0 when 0/(2+0) while a heterozygous SNP has a BAF=1/(1+1) or 0.5. In the Illumina SNP array, a genotype of a DNA sample can be visualized by their theta (θ) value. The Illumina platform uses an algorithm based on 4 formulas to calculate the visualized BAF value to achieve similar

calculations to the general BAF calculation previously stated. SNPs vary in their probe intensity levels leading to variability of θ and the corresponding BAF value.

The intensity of a SNP is represented with an R value and CNVs are calculated with the formula Log_2 R ratio, where the R ratio= $R_{observed}/R_{expected}$. Theoretically, an LRR = 0 is the expected value for a SNP with no change in CNV value. Deletions are observed when an LRR < 0 while amplifications are observed when an LRR > 0. However, these values are approximate guideline and making an absolute call for one marker can be difficult. To augment this, a plug-in called "CNVPartition" can be used in tandem with visualizations of LRR values to infer possible copy number. It is important to visualize both CNV and BAF for a SNP as deletions will give a false homozygous genotype since only one allele is present.

There are several issues one must consider before defining a region homozygous. Regions can be homozygous by chance, or Identical By State (IBS) or Identical by Descent (IBD). IBS regions can exist for a given interval if the particular marker lacks heterogeneity in the population to be studied creating a homozygous region by chance. To limit the misidentification of these regions, algorithms used in homozygosity mapping studies set certain criteria. A commonly utilized software is PLINK, whose default criteria define regions of homozygosity include regions that are ≥ 1Mb, have a minimum of 100 SNPs per region, and have a density of at least 1 SNP per 50kb [76]. The sensitivity of the PLINK algorithms can be adjusted since homozygous regions can be missed if the region that is the homozygous region is broken up by heterozygous SNPs or if the IBD region is

much smaller than default thresholds. This thesis uses a SNP array with a mean average of 1 SNP per 2.7kb and adjusts homozygosity length to increase sensitivity of detecting smaller regions. IBD regions are revealed by comparing several probands which identifies intervals thought to represent regions of common ancestry, to further define the critical consensus region of homozygosity responsible for disease. Traditionally, the next step is to sequence candidate genes within the interval of IBD region for mutations responsible for disease. However, homozygosity mapping has its limitations due to its mono-allelic assumption that two copies of an ancestral chromosomal region, each harboring the same allele, are inherited by probands. Homozygosity mapping fails to map genes for disorders when a combination of two different alleles in a proband, arising from two different ancestral chromosomes comprised of different markers [77]. One condition that could potentially aid homozygosity mapping is if the population of the probands to be studied exhibit high levels of consanguinity or homogeneity which occurs if the population is geographically isolated making it less likely that other disease causing alleles in rare disorders are introduced from foreign populations.

In this thesis entitled "*GDF11* in Ocular Development and MOTA Mapping" I investigate two separate projects. The first involves investigating a *GDF11* in ocular development and disease. At the commencement of this first project, a growing number of mutations in genes required for ocular development have been implicated in ocular disorders such as MAC and LCA. By utilizing a candidate gene approach, *GDF11*, and its zebrafish paralog, *gdf11*, were investigated to

model aspects of ocular development. MAC is considered a genetically heterogeneous group of disorders. The functions of BMP family members in the eye and sequence variants in humans which alter gene activity documented in other studies make studying other members of this family of an appealing project. No reports examining *GDF11* in human disease were previously reported but *Gdf11* has been investigated in neurosensory tissues such as the eye and the olfactory epithelium [78-79] of mice as well as in aspects of liver and development in zebrafish [80]. Although there are caveats, MO inhibition of gene activity in zebrafish is a common and potential powerful practice to study genes evolved in development of the embryo. I hypothesize that if *GDF11* activity is altered, ocular tissues may be affected in a zebrafish model organism. Furthermore, analyzing *GDF11* sequence variants in patients with MAC, LCA, and Primary Open Angle Glaucoma (POAG), then biochemically characterizing the effects of these mutations could progress the understating of the role of BMPs involved in ocular development and disease

The second project in thesis involves identifying genetic factors in a disorder affecting the eyelid present in Canadian native aboriginals known as Manitoba Oculotrichoanal (MOTA) syndrome. At the commencement of that study, no known mutations in genes were known to cause disease, but MOTA exhibits an autosomal recessive inheritance pattern. Homozygosity mapping is a technique that was developed in the 1987 to map autosomal recessive traits in probands exhibiting consanguinity [73]. I hypothesize that if MOTA syndrome is due to

genetic factors, then employing homozygosity mapping will identify the chromosomal interval responsible for disease.

Both projects required extensive training in the use of modern biochemical techniques which were subsequently followed with careful data analysis. The data in this thesis contributes to the constantly growing body of information of genes required for ocular development or are implicated in inherited ocular conditions.

Figure 1.1 Optic cup and eyelid development.

Eye formation begins with neural plate consisting of ectoderm (light brown) and endoderm (blue). Neural crest cells (red) migrate dorsally and the neural tube invaginates. Optic vesicles begin to extend outwards to the surface ectoderm while neural crest cells continue their growth and proliferation to eventually cause neural tube closure. The endoderm comes in contact with the surface ectoderm to induce lens formation (grey) while a bilayered optic cup forms consisting of retinal pigment epithelium (purple) and retinal precursors (green). The eye grows circumferentially while the lens vesicle continues to proliferate until its separation from the surface ectoderm. Anterior structure progresses with the migration of mesenchyme cells (while eyelid folds develop on the surface ectoderm. Periderm arms (dark brown) extend from surface ectoderm tissue to cause the temporary eyelid fusion. Anterior segment structures develop while separation of the eyelid occurs by a mechanism of controlled cell death to form the adult eye.

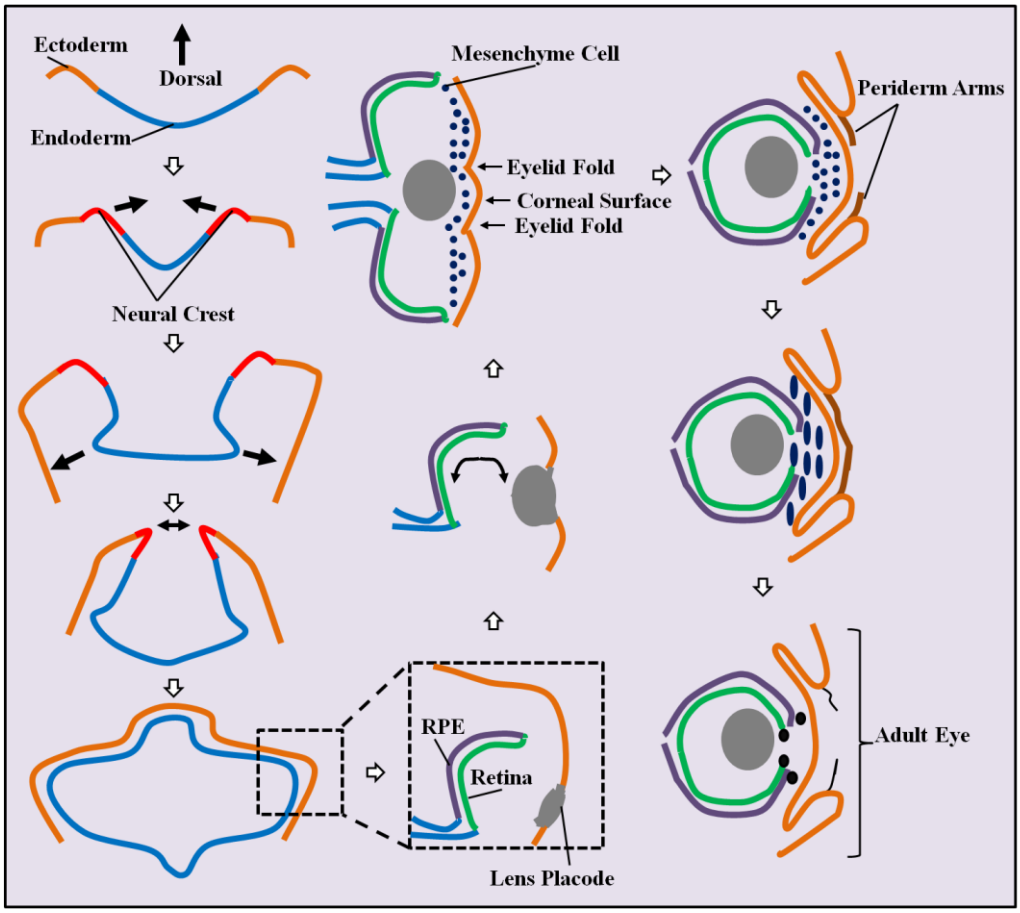

Figure 1.2 General diagram of BMP/TGF-β signaling.

A diagram depicting canonical BMP signaling pathway. The BMPs (green) are ligands which exist in the extracellular space. BMP dimers bind to Type I and Type II kinase receptors or be inhibited by antagonistic proteins tgat prevent downstream signaling. After binding, BMP activation of the kinase receptors causes the phosphorylation of a receptor Smad protein (R-Smad) in the cytoplasm. The phosphorylated form of R-Smad associates with common Smads (Co-Smad) to form a complex which translocates to the nucleus to control expression of target genes.

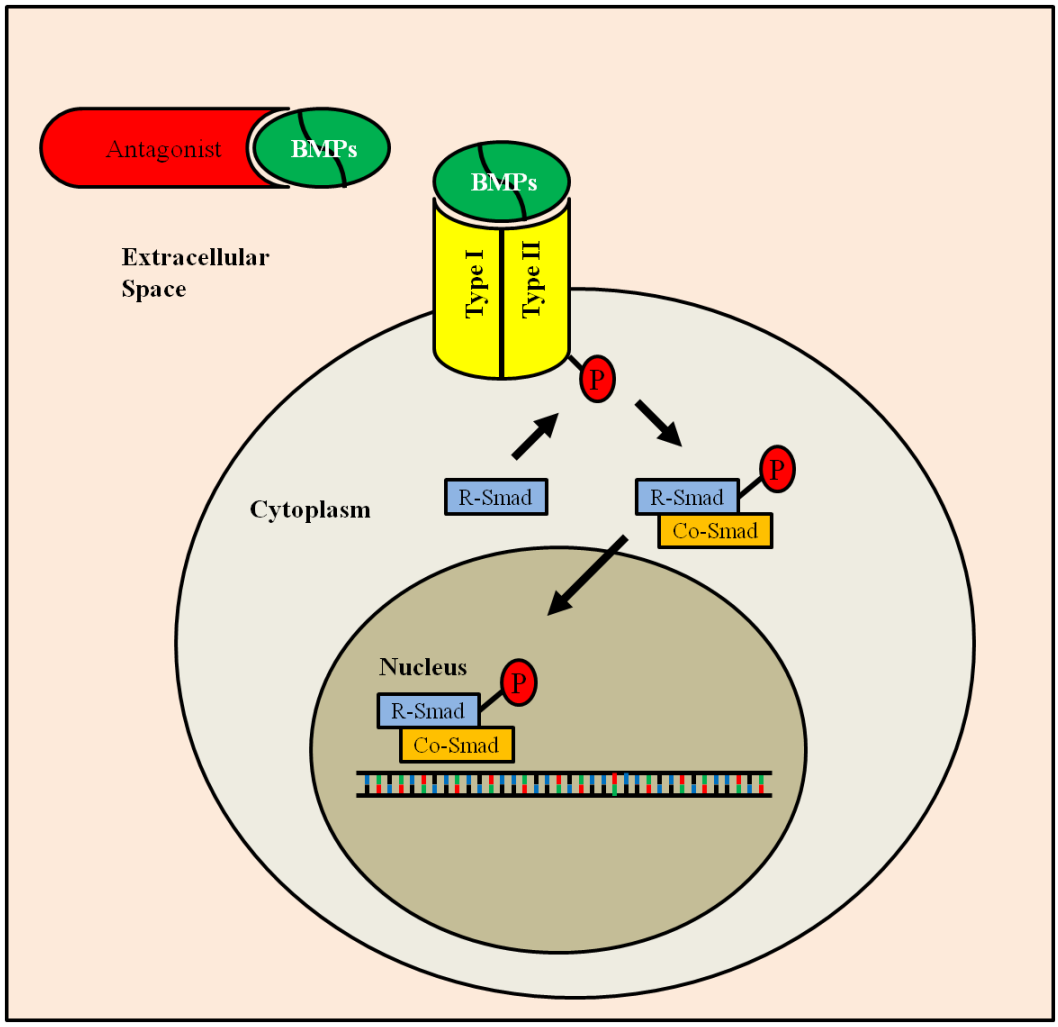

Figure 1.3 Schematic depicting the reunion of an ancestral allele in a consanguineous pedigree

An example allele of interest present on an ancestral chromosome (red) is depicted with a black star. The colored horizontal bars represent chromosomes with unique genotypes. Horizontal lines along the chromosomes represent meiotic recombination events. With each successive generation, the chromosomal segment containing the locus of interest can become shorter while incorporating other unique chromosomal segments. The reunion of this ancestral chromosome, a region that is "Identical By Descent" (illustrated by a dash line), is depicted in a male proband that is an offspring of a first cousin marriage.

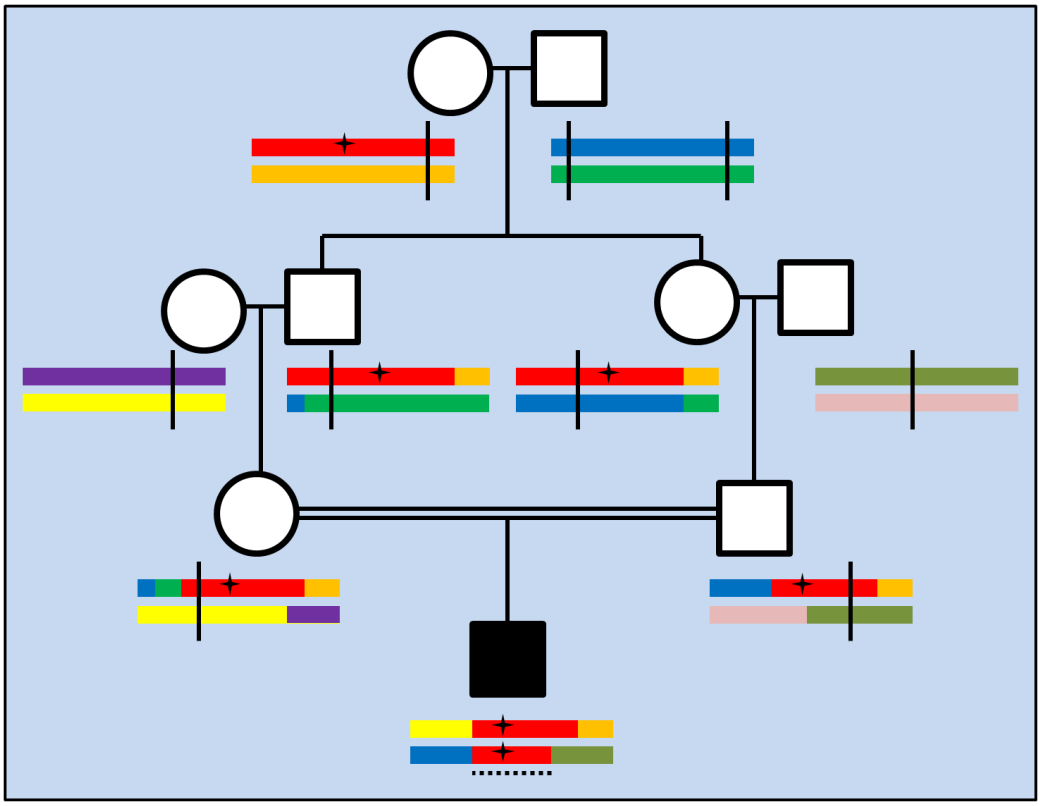

References

1. Lamb TD, Collin SP, Pugh EN, Jr. Evolution of the vertebrate eye: opsins, photoreceptors, retina and eye cup. Nat Rev Neurosci 2007; 8(12):960-76.

2. Gage PJ, Zacharias AL. Signaling "cross-talk" is integrated by transcription factors in the development of the anterior segment in the eye. Dev Dyn 2009; 238(9):2149-62.

3. Harris MJ, McLeod MJ. Eyelid growth and fusion in fetal mice. A scanning electron microscope study. Anat Embryol (Berl) 1982; 164(2):207-20.

4. Findlater GS, McDougall RD, Kaufman MH. Eyelid development, fusion and subsequent reopening in the mouse. J Anat 1993; 183 (Pt 1):121-9.

5. Carpenter G, Cohen S. Epidermal growth factor. Annu Rev Biochem 1979; 48:193-216.

6. Smith JM, Sporn MB, Roberts AB, Derynck R, Winkler ME, Gregory H. Human transforming growth factor-alpha causes precocious eyelid opening in newborn mice. Nature 1985; 315(6019):515-6.

7. Burg MA, Tillet E, Timpl R, Stallcup WB. Binding of the NG2 proteoglycan to type VI collagen and other extracellular matrix molecules. J Biol Chem 1996; 271(42):26110-6.

8. Goretzki L, Burg MA, Grako KA, Stallcup WB. High-affinity binding of basic fibroblast growth factor and platelet-derived growth factor-AA to the core protein of the NG2 proteoglycan. J Biol Chem 1999; 274(24):16831-7.

9. Young RW. Cell differentiation in the retina of the mouse. Anat Rec 1985; 212(2):199-205.

10. Wallace VA. Concise review: making a retina--from the building blocks to clinical applications. Stem Cells 2011; 29(3):412-7.

11. Swaroop A, Kim D, Forrest D. Transcriptional regulation of photoreceptor development and homeostasis in the mammalian retina. Nat Rev Neurosci 2010; 11(8):563-76.

12. Levine EM, Roelink H, Turner J, Reh TA. Sonic hedgehog promotes rod photoreceptor differentiation in mammalian retinal cells in vitro. J Neurosci 1997; 17(16):6277-88.

13. Wallace VA. Proliferative and cell fate effects of Hedgehog signaling in the vertebrate retina. Brain Res 2008; 1192:61-75.

14. McFarlane S, Zuber ME, Holt CE. A role for the fibroblast growth factor receptor in cell fate decisions in the developing vertebrate retina. Development 1998; 125(20):3967-75.

15. Lillien L. Changes in retinal cell fate induced by overexpression of EGF receptor. Nature 1995; 377(6545):158-62.

16. Berson DM, Dunn FA, Takao M. Phototransduction by retinal ganglion cells that set the circadian clock. Science 2002; 295(5557):1070-3.

17. Ohsawa R, Kageyama R. Regulation of retinal cell fate specification by multiple transcription factors. Brain Res 2008; 1192:90-8.

18. Ochocinska MJ, Hitchcock PF. NeuroD regulates proliferation of photoreceptor progenitors in the retina of the zebrafish. Mech Dev 2009; 126(3-4):128-41.

19. Furukawa T, Morrow EM, Li T, Davis FC, Cepko CL. Retinopathy and attenuated circadian entrainment in Crx-deficient mice. Nat Genet 1999; 23(4):466-70.

20. Omori Y, Katoh K, Sato S, Muranishi Y, Chaya T, Onishi A, Minami T, Fujikado T, Furukawa T. Analysis of transcriptional regulatory pathways of photoreceptor genes by expression profiling of the Otx2-deficient retina. PLoS One 2011; 6(5):e19685.

21. Cohen AR, Gomes FL, Roysam B, Cayouette M. Computational prediction of neural progenitor cell fates. Nat Methods 2010; 7(3):213-8.

22. Trimarchi JM, Stadler MB, Cepko CL. Individual retinal progenitor cells display extensive heterogeneity of gene expression. PLoS One 2008; 3(2):e1588.

23. Goldsmith P, Harris WA. The zebrafish as a tool for understanding the biology of visual disorders. Semin Cell Dev Biol 2003; 14(1):11-8.

24. Carter-Dawson LD, LaVail MM. Rods and cones in the mouse retina. I. Structural analysis using light and electron microscopy. J Comp Neurol 1979; 188(2):245-62.

25. Roorda A, Williams DR. The arrangement of the three cone classes in the living human eye. Nature 1999; 397(6719):520-2.

26. Curcio CA, Sloan KR, Kalina RE, Hendrickson AE. Human photoreceptor topography. J Comp Neurol 1990; 292(4):497-523.

27. Fadool JM, Dowling JE. Zebrafish: a model system for the study of eye genetics. Prog Retin Eye Res 2008; 27(1):89-110.

28. Nasevicius A, Ekker SC. Effective targeted gene 'knockdown' in zebrafish. Nat Genet 2000; 26(2):216-20.

29. Summerton J, Weller D. Morpholino antisense oligomers: design, preparation, and properties. Antisense Nucleic Acid Drug Dev 1997; 7(3):187-95.

30. Draper BW, Morcos PA, Kimmel CB. Inhibition of zebrafish fgf8 pre-mRNA splicing with morpholino oligos: a quantifiable method for gene knockdown. Genesis 2001; 30(3):154-6.

31. Danilova N, Kumagai A, Lin J. p53 upregulation is a frequent response to deficiency of cell-essential genes. PLoS One 2010; 5(12):e15938.

32. Postlethwait J, Amores A, Cresko W, Singer A, Yan YL. Subfunction partitioning, the teleost radiation and the annotation of the human genome. Trends Genet 2004; 20(10):481-90.

33. Resnikoff S, Pascolini D, Etya'ale D, Kocur I, Pararajasegaram R, Pokharel GP, Mariotti SP. Global data on visual impairment in the year 2002. Bull World Health Organ 2004; 82(11):844-51.

34. Forrester MB, Merz RD. Descriptive epidemiology of anophthalmia and microphthalmia, Hawaii, 1986-2001. Birth Defects Res A Clin Mol Teratol 2006; 76(3):187-92.

35. Morrison D, FitzPatrick D, Hanson I, Williamson K, van Heyningen V, Fleck B, Jones I, Chalmers J, Campbell H. National study of microphthalmia, anophthalmia, and coloboma (MAC) in Scotland: investigation of genetic aetiology. J Med Genet 2002; 39(1):16-22.

36. Ragge NK, Subak-Sharpe ID, Collin JR. A practical guide to the management of anophthalmia and microphthalmia. Eye (Lond) 2007; 21(10):1290-300.

37. Tucker S, Jones B, Collin R. Systemic anomalies in 77 patients with congenital anophthalmos or microphthalmos. Eye (Lond) 1996; 10 (Pt 3):310-4.

38. Schneider A, Bardakjian T, Reis LM, Tyler RC, Semina EV. Novel SOX2 mutations and genotype-phenotype correlation in anophthalmia and microphthalmia. Am J Med Genet A 2009; 149A(12):2706-15.

39. Williamson KA, Hever AM, Rainger J, Rogers RC, Magee A, Fiedler Z, Keng WT, Sharkey FH, McGill N, Hill CJ, Schneider A, Messina M, Turnpenny PD, Fantes JA, van Heyningen V, FitzPatrick DR. Mutations in SOX2 cause anophthalmia-esophageal-genital (AEG) syndrome. Hum Mol Genet 2006; 15(9):1413-22.

40. Stoll C, Alembik Y, Dott B, Roth MP. Congenital eye malformations in 212,479 consecutive births. Ann Genet 1997; 40(2):122-8.

41. Wordinger RJ, Clark AF. Bone morphogenetic proteins and their receptors in the eye. Exp Biol Med (Maywood) 2007; 232(8):979-92.

42. Liu A, Niswander LA. Bone morphogenetic protein signalling and vertebrate nervous system development. Nat Rev Neurosci 2005; 6(12):945-54.

43. Massague J, Seoane J, Wotton D. Smad transcription factors. Genes Dev 2005; 19(23):2783-810.

44. Iwasaki S, Iguchi M, Watanabe K, Hoshino R, Tsujimoto M, Kohno M. Specific activation of the p38 mitogen-activated protein kinase signaling pathway

and induction of neurite outgrowth in PC12 cells by bone morphogenetic protein-2. J Biol Chem 1999; 274(37):26503-10.

45. Kimura N, Matsuo R, Shibuya H, Nakashima K, Taga T. BMP2-induced apoptosis is mediated by activation of the TAK1-p38 kinase pathway that is negatively regulated by Smad6. J Biol Chem 2000; 275(23):17647-52.

46. Beebe D, Garcia C, Wang X, Rajagopal R, Feldmeier M, Kim JY, Chytil A, Moses H, Ashery-Padan R, Rauchman M. Contributions by members of the TGFbeta superfamily to lens development. Int J Dev Biol 2004; 48(8-9):845-56.

47. Furuta Y, Hogan BL. BMP4 is essential for lens induction in the mouse embryo. Genes Dev 1998; 12(23):3764-75.

48. Asai-Coakwell M, French CR, Berry KM, Ye M, Koss R, Somerville M, Mueller R, van Heyningen V, Waskiewicz AJ, Lehmann OJ. GDF6, a novel locus for a spectrum of ocular developmental anomalies. Am J Hum Genet 2007; 80(2):306-15.

49. French CR, Erickson T, French DV, Pilgrim DB, Waskiewicz AJ. Gdf6a is required for the initiation of dorsal-ventral retinal patterning and lens development. Dev Biol 2009; 333(1):37-47.

50. Gosse NJ, Baier H. An essential role for Radar (Gdf6a) in inducing dorsal fate in the zebrafish retina. Proc Natl Acad Sci U S A 2009; 106(7):2236-41.

51. Asai-Coakwell M, French CR, Ye M, Garcha K, Bigot K, Perera AG, Staehling-Hampton K, Mema SC, Chanda B, Mushegian A, Bamforth S, Doschak MR, Li G, Dobbs MB, Giampietro PF, Brooks BP, Vijayalakshmi P, Sauve Y, Abitbol M, Sundaresan P, van Heyningen V, Pourquie O, Underhill TM,

Waskiewicz AJ, Lehmann OJ. Incomplete penetrance and phenotypic variability characterize Gdf6-attributable oculo-skeletal phenotypes. Hum Mol Genet 2009; 18(6):1110-21.

52. Ye M, Berry-Wynne KM, Asai-Coakwell M, Sundaresan P, Footz T, French CR, Abitbol M, Fleisch VC, Corbett N, Allison WT, Drummond G, Walter MA, Underhill TM, Waskiewicz AJ, Lehmann OJ. Mutation of the bone morphogenetic protein GDF3 causes ocular and skeletal anomalies. Hum Mol Genet 2010; 19(2):287-98.

53. Lee YJ, McPherron A, Choe S, Sakai Y, Chandraratna RA, Lee SJ, Oh SP. Growth differentiation factor 11 signaling controls retinoic acid activity for axial vertebral development. Dev Biol 2010; 347(1):195-203.

54. Wyatt AW, Osborne RJ, Stewart H, Ragge NK. Bone morphogenetic protein 7 (BMP7) mutations are associated with variable ocular, brain, ear, palate, and skeletal anomalies. Hum Mutat 2010; 31(7):781-7.

55. Bakrania P, Efthymiou M, Klein JC, Salt A, Bunyan DJ, Wyatt A, Ponting CP, Martin A, Williams S, Lindley V, Gilmore J, Restori M, Robson AG, Neveu MM, Holder GE, Collin JR, Robinson DO, Farndon P, Johansen-Berg H, Gerrelli D, Ragge NK. Mutations in BMP4 cause eye, brain, and digit developmental anomalies: overlap between the BMP4 and hedgehog signaling pathways. Am J Hum Genet 2008; 82(2):304-19.

56. Murali D, Yoshikawa S, Corrigan RR, Plas DJ, Crair MC, Oliver G, Lyons KM, Mishina Y, Furuta Y. Distinct developmental programs require

different levels of Bmp signaling during mouse retinal development. Development 2005; 132(5):913-23.

57. Trousse F, Esteve P, Bovolenta P. Bmp4 mediates apoptotic cell death in the developing chick eye. J Neurosci 2001; 21(4):1292-301.

58. Chang B, Smith RS, Peters M, Savinova OV, Hawes NL, Zabaleta A, Nusinowitz S, Martin JE, Davisson ML, Cepko CL, Hogan BL, John SW. Haploinsufficient Bmp4 ocular phenotypes include anterior segment dysgenesis with elevated intraocular pressure. BMC Genet 2001; 2:18.

59. The University of Texas-Houston Health Science Center. RetNet:Genes and Mapped Loci Causing Retinal Diseases. 2012 [cited 24 January 2012]; Available from: https://sph.uth.tmc.edu/retnet/

60. Lorenz B, Gyurus P, Preising M, Bremser D, Gu S, Andrassi M, Gerth C, Gal A. Early-onset severe rod-cone dystrophy in young children with RPE65 mutations. Invest Ophthalmol Vis Sci 2000; 41(9):2735-42.

61. Koenekoop RK. An overview of Leber congenital amaurosis: a model to understand human retinal development. Surv Ophthalmol 2004; 49(4):379-98.

62. den Hollander AI, Roepman R, Koenekoop RK, Cremers FP. Leber congenital amaurosis: genes, proteins and disease mechanisms. Prog Retin Eye Res 2008; 27(4):391-419.

63. Freund CL, Gregory-Evans CY, Furukawa T, Papaioannou M, Looser J, Ploder L, Bellingham J, Ng D, Herbrick JA, Duncan A, Scherer SW, Tsui LC, Loutradis-Anagnostou A, Jacobson SG, Cepko CL, Bhattacharya SS, McInnes RR. Cone-rod dystrophy due to mutations in a novel photoreceptor-specific

homeobox gene (CRX) essential for maintenance of the photoreceptor. Cell 1997; 91(4):543-53.

64. Swain PK, Chen S, Wang QL, Affatigato LM, Coats CL, Brady KD, Fishman GA, Jacobson SG, Swaroop A, Stone E, Sieving PA, Zack DJ. Mutations in the cone-rod homeobox gene are associated with the cone-rod dystrophy photoreceptor degeneration. Neuron 1997; 19(6):1329-36.

65. Freund CL, Wang QL, Chen S, Muskat BL, Wiles CD, Sheffield VC, Jacobson SG, McInnes RR, Zack DJ, Stone EM. De novo mutations in the CRX homeobox gene associated with Leber congenital amaurosis. Nat Genet 1998; 18(4):311-2.

66. Swaroop A, Wang QL, Wu W, Cook J, Coats C, Xu S, Chen S, Zack DJ, Sieving PA. Leber congenital amaurosis caused by a homozygous mutation (R90W) in the homeodomain of the retinal transcription factor CRX: direct evidence for the involvement of CRX in the development of photoreceptor function. Hum Mol Genet 1999; 8(2):299-305.

67. Nakamura M, Ito S, Miyake Y. Novel de novo mutation in CRX gene in a Japanese patient with leber congenital amaurosis. Am J Ophthalmol 2002; 134(3):465-7.

68. Wyatt A, Bakrania P, Bunyan DJ, Osborne RJ, Crolla JA, Salt A, Ayuso C, Newbury-Ecob R, Abou-Rayyah Y, Collin JR, Robinson D, Ragge N. Novel heterozygous OTX2 mutations and whole gene deletions in anophthalmia, microphthalmia and coloboma. Hum Mutat 2008; 29(11):E278-83.

69. Ashkenazi-Hoffnung L, Lebenthal Y, Wyatt AW, Ragge NK, Dateki S, Fukami M, Ogata T, Phillip M, Gat-Yablonski G. A novel loss-of-function mutation in OTX2 in a patient with anophthalmia and isolated growth hormone deficiency. Hum Genet 2010; 127(6):721-9.

70. Dateki S, Fukami M, Sato N, Muroya K, Adachi M, Ogata T. OTX2 mutation in a patient with anophthalmia, short stature, and partial growth hormone deficiency: functional studies using the IRBP, HESX1, and POU1F1 promoters. J Clin Endocrinol Metab 2008; 93(10):3697-702.

71. Henderson RH, Williamson KA, Kennedy JS, Webster AR, Holder GE, Robson AG, FitzPatrick DR, van Heyningen V, Moore AT. A rare de novo nonsense mutation in OTX2 causes early onset retinal dystrophy and pituitary dysfunction. Mol Vis 2009; 15:2442-7.

72. Dateki S, Kosaka K, Hasegawa K, Tanaka H, Azuma N, Yokoya S, Muroya K, Adachi M, Tajima T, Motomura K, Kinoshita E, Moriuchi H, Sato N, Fukami M, Ogata T. Heterozygous orthodenticle homeobox 2 mutations are associated with variable pituitary phenotype. J Clin Endocrinol Metab 2010; 95(2):756-64.

73. Lander ES, Botstein D. Homozygosity mapping: a way to map human recessive traits with the DNA of inbred children. Science 1987; 236(4808):1567-70.

74. Gunderson KL, Steemers FJ, Ren H, Ng P, Zhou L, Tsan C, Chang W, Bullis D, Musmacker J, King C, Lebruska LL, Barker D, Oliphant A, Kuhn KM, Shen R. Whole-genome genotyping. Methods Enzymol 2006; 410:359-76.

75. Gibbs JR, Singleton A. Application of genome-wide single nucleotide polymorphism typing: simple association and beyond. PLoS Genet 2006; 2(10):e150.

76. Nothnagel M, Lu TT, Kayser M, Krawczak M. Genomic and geographic distribution of SNP-defined runs of homozygosity in Europeans. Hum Mol Genet 2010; 19(15):2927-35.

77. Miano MG, Jacobson SG, Carothers A, Hanson I, Teague P, Lovell J, Cideciyan AV, Haider N, Stone EM, Sheffield VC, Wright AF. Pitfalls in homozygosity mapping. Am J Hum Genet 2000; 67(5):1348-51.

78. Kim J, Wu HH, Lander AD, Lyons KM, Matzuk MM, Calof AL. GDF11 controls the timing of progenitor cell competence in developing retina. Science 2005; 308(5730):1927-30.

79. Wu HH, Ivkovic S, Murray RC, Jaramillo S, Lyons KM, Johnson JE, Calof AL. Autoregulation of neurogenesis by GDF11. Neuron 2003; 37(2):197-207.

80. Farooq M, Sulochana KN, Pan X, To J, Sheng D, Gong Z, Ge R. Histone deacetylase 3 (hdac3) is specifically required for liver development in zebrafish. Dev Biol 2008; 317(1):336-53.

Chapter 2 Investigating the role of *GDF11* in ocular development and disease

Introduction

Growth differentitation factor 11 (*Gdf11*) expression was originally documented in developing mouse limb and *Xenopus* experiments suggested a role in patterning during embryogenesis, specifically in the limb and spinal cord neural tissues [1]. Cryosections reveal *Gdf11* expression in the mouse olfactory epithelium, hindbrain and retina [2]. Mice exhibit dose dependent transformations in the anterior posterior axis, displaying an increase in the number of vertebrae and ribs in *Gdf11* homozygous mice while heterozygous mutants exhibited a milder phenotype [3-4]. Early studies noted the amino acid sequence similarity of *Gdf11* to *Gdf8*, which codes for myostatin, an inhibitor of skeletal muscle growth [5]. In developing chicken limb cell cultures, addition of *Gdf11* protein inhibits bone and muscle formation consistent with the idea that BMPs/TGF-B ligands have redundant functions [6-7]. *Gdf11* exhibits an autoregulatory to inhibit the proliferation of olfactory neurons in homozygous mutants resulting in an increased number of progenitors and mature olfactory receptor neurons [8]. In the retina, *Gdf11* homozygous mutants exhibit alterations in cell fate as they display an increase in the number of retinal ganglion cells, a decrease in amacrine and photoreceptor cell number in the absence of any detectable differences in proliferation or apoptosis, and a ventral coloboma at E 14.5 [9].

Zebrafish *gdf11* exhibits 80% amino similarity to mouse and human *GDF11* and real-time PCR analysis demonstrate that *gdf11* is maternally deposited as it is expressed in unfertilized eggs [10]. Zygotically expressed genes are turned on

approximately 3.5hpf [11]. Zebrafish *gdf11* morphants display a gross decrease in eye size at 2-3dpf (see figure 12 of Farooq et al. 2008) [12]. Whether or not this is due to *Gdf11*'s role in determining retinal cell fate decisions [9] was not investigated, but suggested that loss of *gdf11* activity could contribute to microphthalmic-like phenotypes at 3dpf. Adult phenotypes in zebrafish with reduced *gdf11* activity resulted in an anterior posterior axis change of pelvic fin positioning observed at 44-60dpf [13].

Mutations in the BMP and TGF-β ligand encoding genes *GDF6*, *GDF3*, *BMP4* and *BMP7* display variable penetrance and cause a spectrum of ocular phenotypes like MAC and skeletal or digital anomalies [14-17]. In the case of *GDF6,* ocular phenotypes compatible with micropthalmia and coloboma are observed in zebrafish when *gdf6a* activity is decreased by MO inhibition or in null mutant strains that resulting in a loss of dorsal cell identity in the eye and an expansion of ventral markers [18-19]. Missense *GDF3* and *GDF6* variants were identified in patients with Klippel-Feil syndrome, hemi-vertebrae and post-axial polydactyly [15, 20]. MAC is a disorder exhibiting genetic and phenotypic heterogeneity caused by mutations in members of TGF-β and may be accompanied with changes in skeletal patterning. *Gdf11*'s role in ocular and skeletal patterning suggests that it may make a candidate gene with mutations in *GDF11* contributing to MAC.

In disease, *GDF11* attributable sequence variants have never been documented but an RT-PCR study analysis of colorectal tissue demonstrating increased levels of *GDF11* mRNA in tumor tissue as compared to controls suggests that this may

be used as a bio marker for colorectal cancers [21]. In 2007, a region on 12q spanning *GDF11* and approximately 250 other genes was identified as a causative chromosomal locus for an autosomal dominant excavated optic disc phenotype, however no *GDF11* sequence changes were discovered [22]. Excavated optic disc is indicative of RGC cell death which Fingert et al. 2007 attribute to a glaucoma type phenotype however, certain coloboma can affect ocular structures such as the optic disc. This mapping data implicates *GDF11* in a human disease compatible with MAC.

The aims of this current study are to investigate zebrafish *gdf11* expression in the early developing eye and to characterize the phenotypes of reducing *gdf11* activity by MOs inhibition. I describe *gdf11* expression 18hpf-3dpf in the eye and hindbrain, differences in overall eye size at 3dpf & 5dpf, changes observed in genes thought to mark specific retinal cell types as well evidence for a decreased number of photoreceptors. I also present the pursuit of identifying sequence variants in MAC, juvenile RP, and POAG disease panels and show the effects of such alterations on protein processing. This work further investigates *gdf11* in zebrafish and its contribution to human disease.

Methods

Zebrafish Usage and Growth

The majority of the experiments were performed with the AB strain from the Zebrafish International Resource Center (ZIRC Eugene, OR USA). The *rh1*-GFP strains were used to visualize GFP expression in rod photoreceptors. Zebrafish trios were set consisting of two females and one male one day prior to mating. 2-6 hours post fertilization, the dead or unfertilized embryos were removed while the remaining viable embryos were raised in embryo media (0.875g/L NaCl, 37.5mg/L KCL, 0.145g/L CaCl-2H20, 20.5mg/L KH_2PO4, 7.1mg/L NaH_2PO_4 anhydrous, 0.245g/L $MgSO_4$-$7H_20$, 60mg/L NaHCO3, and 400µl of 0.05M Metranitozol). Following MO injection, embryos were raised in injection embryo media supplemented with Penicillin-Streptomycin antibiotics on the first day of birth. At 24hpf injection media was replaced with embryo media containing 0.003% N-Phenylthiourea (Sigma) to inhibit pigment formation. Embryos were grown in incubators at 25.5-33°C for 1-5 days with media replacement once a day. Post embryonic reference staging was performed according to Parichy et al. 2009 [23].

Zebrafish *gdf11* DIG labeled probe synthesis

RNA was isolated from approximately 50 27hpf zebrafish embryos. Primers (**Table 2.1** and **Fig. 2.2**) were used to amplify a 962bp segment of *gdf11* cDNA

using the SuperScript® III *One-Step RT-PCR* System with Platinum® Taq DNA Polymerase (Invitrogen). PCR products were run on 1% agarose gels to visualize an expected product size of 962bp and extracted using Qiagen's Gel Extraction kit.

Table 2.1 Primers to amplify zebrafish *gdf11* for in situ hybridization

	Primer Sequence (5'-3')	Annealing Temp (°C)	Extension Time (s)	Amplicon Size (bp)
F-z*gdf11*	AGCCGAACCTCTTTCTAGC	55	60	962
R-z*gdf11*	CTGCACCAGATGGGTATGTG			

Cloning of *gdf11* PCR product

The pCR-4TOPO Kit (Invitrogen) was used to sub clone and propagate *gdf11*. 2µl of gel extracted partial *gdf11* cDNA, and 0.5µl salt solution. Plasmid containing *gdf11* was transformed into 25µl of TOP10 one-shot cells and grown on agar plates containing carbenicillin overnight at 37°C. Single colonies were selected for further growth using QIAprep Spin miniprept kit protocol (Qiagen). Plasmids were isolated and sequenced by the Amersham DYEnamic ET mix with M13F sequencing primer. Sequencing reactions were ethanol purified and sent to the Molecular Biology Servicing Unit located in the Department of Biological Sciences at the University of Alberta for sequencing with an ABI 3730 Sequencer. Colonies containing *gdf11* amplicons were grown using the Qiagen Maxiprep kit to achieve high quality DNA for probe synthesis.

DIG labeled Probe Synthesis

Following sequencing confirming the orientation of the *gdf11* insert, 10 ug of *gdf11* in PCR-4TOPO plasmid containing *gdf11* was digested with *NotI* (New England Biolabs) at 37°C for 2 hours in order to generate linearize the DNA. Digested products underwent phenol chloroform extraction by addition of 160µl DEPC treated H20 and 200µl phenol chloroform and vortexed for 20 sec followed by a 5min spin at ≥ 13,000rpm. Upper aqueous layer was transferred and precipitated with 3 times volume of 100% EtOH and 1/10th volume 3M NaAc (pH 5.2), kept on ice 15 min, spun 20 min, washed with 100% EtOH, and resuspended in 10µl DEPC H20. 2µg of linearized *gdf11* in pCR-4Topo plasmid DNA were used as template anti-sense probe synthesis using the digoxigenin-UTP labeling kit (Roche) with T3 RNA polymerase. Probe synthesis occurred for 2 hours with replenishment of an additional 1µl of T3 RNA Polymerase was added 1 hour into the reaction. RNAse free DNAse was added to digest pCR-4Topo plasmid following incubation at 37°C for 5 minutes. 0.2M EDTA was added to stop reaction and purified using the Post Reaction Purification Columns (Sigma). Probes were stored in -80°C.

Whole embryo In Situ Hybridization

Embryos were fixed in 4% paraformaldehyde in PBST (Phosphate buffer solution with Tween-20.8g/L NaCl, 0.2g/L KCl, 1.44g/L Na_2HPO_4 (dibasic anhyrdrous), 0.24g/L KH2PO4 (monobasic anhydrous) pH = 7.4 and 0.1% Tween-20 for 4-5 hours at room-temp or overnight at 4°C. Embryos were washed 5 times, 5

minutes per wash, in PBST, and dechorionated manually, if needed. Embryos were permeablized with 10ug/ml of Proteinase K (Invitrogen) in PBST for 5-35 minutes depending on age (5min for 24hpf, 7min 28hpf, 15 min 3dpf, 25 min 4 dpf, and, 35 min 5dpf). Embryos were refixed in 4% PFA/PBST for 20 minutes and washed 5 times, 5 minutes per wash, in PBST. Embryos were incubated with prehybdrization (prehyb) solution at 65°C for 1 hour (prehyb-50% Formamide, 5X SSC (20X SSC: 21.91g/L NaCl, 10.275g/L Sodium Citrate), 50ug/mL heparin, 500ug/mL tRNA, 0.1% Tween-20, and .092M Citric Acid pH = 6.0. Prehyb solution was removed and 200µl of hyb and probe was added (containing approximately 100ng of digoxigenin (DIG) labeled probe) and incubated for 65°C overnight.

The next day, embryos were washed for 5 minutes each at 65°C in 66% hyb mix (no tRNA)/33% 2 x SSC, 33% hyb mix (no tRNA)/ 66% 2 x SSC, and 5 min in 2 x SSC at 65°C. Stringency washes followed with a 1 time 20 minute wash containing 0.2x SSC, 0.1% Tween-20 for 65°C, followed by 2 times 20 minute wash of 0.1 x SSC, 0.1$ Tween-20 at 65°C. Embryos were then washed 1 time each for 5 minutes in 66% 0.2 x SSC/33% PBST , 33% 0.2 x SSC/66% PBST, and then 100% PBST at room temperature. Following the washes embryos were blocked by incubating in blocking solution made in PBST containing 2% Sheep Serum and 2% BSA 1 hour. Anti-digoxigenin-AP antibody was diluted 1:5000 in blocking solution and incubated at 2 hours at RT or overnight at 4°C then washed 5 times, 15 minutes per wash, in PBST.

For coloration, embryos were washed 4 times, 5minutes/wash, with coloration buffer (100mM Tris-HCl pH=9.5, 50 mM $MgCl_2$, 100 mM NaCl, and 0.1% Tween 20). 45µl of nitro-blue tetrazolium (NBT) stock and 35 µl of bromo-4-chloro-3-indoyl phosphate (BCIP) from Boehringer were added per 10mL of coloration buffer. 500µl of NBT/BCIP in coloration buffer were added to embryos and incubated in the dark at room temperature until a blue reaction product was visible on the embryos. Embryos were washed with STOP solution (PBST @ pH = 5.5 quickly 2 times, 1 minute/wash, and then 2 times, 15minute per wash. Embryos were then washed 2 time, 5 minute per wash, with PBST (pH = 7.4) and stored in PBST in the dark at 4°C. Embryos were deyolked with insect pins and underwent a gradient sinks of 30%, 40%, and 70% glycerol made in PBST. Embryos or were mounted on coverslips with 70% glycerol. For fluoroscein based in situs embryos were incubated overnight at 4°C with 1:10,000 dilution of alkaline phosphatase-conjugate anti-fluorescein antibody (Roche). Embryos were washed 5 times in PBST, 15 minutes each. Following PBST washes, embryos were washed 4 times, 5 minutes each, with coloration buffer. Fluorescein coloration solution consist of 5ml of coloration buffer, 17.5ul INT Red (Iodo-Nitrotetrazolum Violet) (Sigma) and 17.5uL of BCIP. Coloration reactions were stopped by rinsing two times with coloration buffer, followed by MiliQ-H_20 and 5 PBST washes. Embryos were stores in 4% PFA at 4°C.

Whole Embryo Immunohistochemistry

Embryos that were fixed in 4% PFA were rehydrated in 90%, 70%, 50%, 30%, 10% methanol in PBST. 5dpf embryos were permeabilized with Proteinase K at

10ug/mL for 55 minutes at room temp on a shaker. Then, embryos were re-fixed in 4% PFA for 20 minutes at room temp on a shaker, followed by washing 4 times PBSDTT (PBS and 1% DMSO, 1% Tween-20, 1% Triton X-100), 5 minutes per wash. Embryos were then placed in blocking buffer (2.5% Goat Serum, 0.1% Triton-X-100, 2mg/mL BSA in PBST) for 1 hour at room temp on a shaker. Primary antibodies were diluted in blocking buffer at the following concentrations, 1D1 (rods) 1:100, 4C12 (rods) 1:200, Zpr-1 (red-green cones) 1:100 and incubated with embryos at 4°C overnight on a shaker. Primary antibody solutions were decanted and embryos were washed 5 times, 5 minutes per wash, with PBSDTT. Then embryos were placed in blocking buffer for 1 hour at room temp on a shaker. Fluorescent secondary antibodies (Santa-Cruz) were added to blocking buffer (1:500) and incubated with embryos for 2 hours in the dark at room temperature on a shaker, then washed with PBSDTT 3 times, 5minutes per wash. Embryos were stores in PBST for longer storage in the dark at 4°C. Left eyes were removed and mounted anterior of the eye down on slides.

Microscopy and automated cell counting

Dissected eyes that were processed for in situ hybridization were photographed with a Zeis AxioImager.Z1 scope with an Axiocam HRm camera with RGB filters. Embryos that had the yolk were imaged using a Zeiss Discovery, V8 stereoscope fitted with a QImaging micropublisher camera. IHC processed eyes were imaged with a Zeiss 700 confocal microscope, kindly provided by Dr. Sarah Hughes, using the Plan-Apochromat 20x/0.8 M27 lens. Each eye was imaged every 0.87uM and representative images are merged z-stacks of 60-80 individuals

slices as Maximum Intensity Projection. Confocal images were processed using ImageJ 1.44p. Automated cell counting was performed using the Image based Tool for Counting Nuclei. To calculate the surface for each eye, the total height of the z-stacks for each eye was utilitzed as the radius. The formula for surface of half a sphere = $2\pi r^2$.

Morpholino use and injection

MOs were ordered from GeneTools (Philomath, OR, USA). MO sequences are listed in **Table 2.2**. The *gdf11* translation blocking morpholino, *gdf11*^{ATGMO}, was designed to bind to the 5'UTR of *gdf11* mRNA 35bp upstream of the ATG start codon whilst the splice blocking *gdf11*^{spliceMO} spans exon1 and intron1 (**Fig. 2.2**). 6ng of *gdf11*^{ATGMO} or 10ng of *gdf11*^{spliceMO} were microinjected into embryos between 1-4 cell stages. To prevent non-specific side effects accompanying morpholino use [24-25], 4ng of a translation blocking *p53*^{MOATG} were co-injected with *gdf11*^{ATGMO} or *gdf11*^{spliceMO}. 6ng of a control morpholino, *gdf11*^{ATGMMMO}, containing a 5bp mismatch substitutions was used as a control to test *gdf11*^{ATGMO} efficacy. Unless indicated, microinjections were performed using embryos from the AB strain of zebrafish. The *rh1*-GFP strain was used to visualize rod photoreceptors and red-green cones in the same embryo.

Table 2.2 *gdf11* morpholino sequences

	Morpholino Sequence (5'-3')
gdf11^{ATGMO}	ATCAGGAAACAATGGTTTTCTCTTG
gdf11^{ATGMMMO}	ATCACGAATCAATCGTTTACTCTTC
gdf11^{spliceMO}	GAAGTTTTGTAACTCACGCTCTGAA
p53^{ATGMO}	GCGCCATTGCTTTGCAAGAATTG

Reverse transcription PCR for morpholino efficacy studies

Approximately 50 24hpf zebrafish that were injected with with *gdf11*^{spliceMO} and p53^{MO} or just control *p53*^{MO} were store in RNAlater. Afterwards, cDNA was synthesized using the SuperScript III reverse transcription PCR system (Invitrogen) with oligodT template. PCR using cDNA template of splice injected or control morpholino only was performed using primers listed in **Table 2.3**.

Table 2.3 Primers used for morpholino efficacy studies (5'-3')

F1	CATAGACGCCGATGAGTATC
R1	AGCAAGAAAGCATGTTTGTG
R2	CATTGCCACTTTCATCATAG
ef1alpha-F	GACAGACCCGTGAGCACGCC
ef1alpha-R	TGTCGGTGGGACGGCTAGGG

Screening *GDF11* in human DNA samples

Four primer pairs were used to screen *GDF11* in disease cohorts by PCR amplification. Primers were designed by Primer3 to amplify the exon coding base pairs of *GDF11* including exon/intron boundaries. A GC rich PCR protocol was used to amplify *GDF11*. Primers are listed in Table as well as annealing temperatures and extension times. PCR amplification cycle is as follows, Step 1) 95℃, 2 min Step 2) 95℃, 30 sec Step 3) 55-60°C, 30 sec Step 4) 72°C, 30 sec - 1min Step 5) Repeat Steps 2-5 34 times Step 6) 72℃ 5 min, Step 7) Hold at 15℃. Each reaction was performed in a 25µl volume with final concentration of 1X final PCR buffer (10X Standard Taq Reaction Buffer containing New England Biolabs), 2µM forward and reverse primers, 200µM dNTP (Invitrogen), 10% glycerol (Anachemia), and 5% Formamide (Sigma) and 2.5units of TAQ DNA Polymerase (New England BioLabs) using gDNA at concentrations of 15-60ng/reaction. Amplicons were run on ethidium bromide stained 1% agarose gels (Invitrogen) for electrophoresis and visualized on a Pharmacia Biotech capture system. Samples were purified with post reaction clean up columns (Sigma) before sequencing. PCR amplicons were sent to The Applied Genomic Centre (Edmonton, Canada) or to the Centre hospitalier universitaire de Québec (Quebec, Canada). Sequencing reactions were performed with the Applied Biosystems Big Dye Terminator v3.1 Cycle sequencing kit and were run on the 3130 /3130XL or 3730Xl Genetic Analyzer with 1 of the 2 primers for economic reasons and are indicated in **Table 2.4**.

Table 2.4 Primer sequences and conditions for screening human *GDF11*.

	Primer Sequence	Annealing Temp (°C)	Extension Time (s)	Amplicon Size (bp)
exon1-part1-For	CCAGTCCTCCCTCCCCTCCCC	59.5	30	381
exon1-part1-Rev*	GTCGTGTAGGTCCAGGATCTG			
exon1-part2-For	GAGCGCTCCAGCCGGCCAG	58.3	30	386
exon1-part2-Rev*	CCG CTT GGA GCA GAA GG			
exon2-For	CCACCCAGGACTACTGATCC	56.5	35	576
exon2-Rev*	AGTAATGCTGGTCCCCAACC			
exon3-For*	CTGAGAAGTCAGCAGTCTCTATTCTG	55.1	60s	842
exon3-Rev	GTCTCTGCCTCGTCTGTCTCTTC			

*Sequencing Primer

Restriction enzyme digestion: The *GDF11* G210V and G44A sequence variants were validated and screened in population controls by restriction enzyme digestion of PCR amplicons flanking the base pair substitutions. Primers used for amplification are listed in **Table 2.5** and PCR was performed using the same GC-rich sequencing protocol.

Table 2.5 Restriction enzyme digestion primer sequences and conditions.

	Primer Sequence (5'-3')	Annealing Temp (°C)	Extension Time (s)	Amplicon Size (bp)
G44A HgaI-F*	GGCGGCGGCGGCGGCGGCGGC GGCGGCAGCGGCGGGGGAC	58.3	30s	331
G44A HgaI-R	TCTCCTGGGCCATGCTAATGAC GGTCTCG			
G210V TspRI-F	ACCCTTTGCTGATGCTGTGCCC	59.5	30s	350
G210V TspRI-R	GCTCTGTGGCTGGCGGAACC			

G44A primers were designed as follows: a T>A bp substitution was introduced into the forward primer sequence in order to create a second cut site within the amplicon designed for G44A detection in controls. The G44A forward primer was also designed to contain extra wildtype sequence specific nucleotides to aid in visualization of control samples. G44A causes a gain of a second *HgaI* (New England Biolabs) cut site within the designed 331bp amplicon. 3µl of G44A PCR product, 1 unit of *HgaI* enzyme, and 0.5µl 10X Buffer 1 (New England Biolabs) were brought to a final volume of 5µl per sample. Samples were incubated for 8 hours at 37°C followed by heat inactivation for 65°C 20 min. G210V results in a gain of a cut second cut site for *TspRI* (New England Biolabs). 5µl of G210V PCR Product, 2 units of *TspRI*, 1x BSA (.005mg) (New England Biolabs), were brought to a final volume of 7µl per sample. Samples were incubated for 8 hours at 65°C. Both G44A and G210V restriction enzyme digestion population control PCR products were loaded on ethidium bromide stained 3% agarose gels for electrophoresis and visualized on a Pharmacia Biotech capture system.

Size Fragment Genotyping

Primer pairs were designed to screen the *GDF11* polyalanine and +10_+11insT sequence variants in population controls. The three primer pairs for each variant are listed in **Table 2.6** and were amplified using the same GC rich PCR protocol as previously described. For economy, PCR products were combined into one genotyping reaction. FAM or VIC fluorescence labeled PCR products were diluted to 1:10-1:100 and sent to The Applied Genomic Centre (Edmonton, Canada) or at the Centre hospitalier universitaire de Québec (Quebec, Canada) to be further diluted in H20 and HiDi formamide to be run on a 3130xl automated genetic analyzer with a Liz500 size standard DNA ladder. Genotyping data were analyzed using Peak Scanner Software v1.0 (Applied Biosystems). As performed by Dr. Xiao Hua, PCR amplicons spanning the polyalanine stretch were amplified using the *GDF11*exon1-part1 primer pair to confirm polyalanine number (**Table 2.4**). DNA samples containing insertions or deletions were amplified and sub-cloned into vectors using the TA Cloning kit (Invitrogen) and sequenced to confirm alanine number.

Table 2.6 Genotyping primers and conditions for *GDF11* indel variants

+10_+11InsT Variant	Primer Sequence (5'-3')	Amplicon Size (bp)	Annealing Temp (°C)	Extension Time (s)
Forward *FAM	GCTGTGGCTGCTCTTAAGGT			
Rev-120bp	GTTCGCGGGAAGAGTGG	120	55.4	30
Rev-135bp	GGGCAACGGTGTGAT	135	55.4	30
Rev-159bp	TGTTGTATTGCACACGGCTT	159	51.3	30
Poly Ala Variant				
Forward *VIC	CCAGTCCTCCCTCCCCTCCCC			
Rev-193bp	GCCACGGACGGGGCTGG	193	59.4	30
Rev-219bp	ACACGGGGCAGCCGTCC	219	60.3	30
Rev-235bp	GCTGCCGCCAAACGCACAC	235	57.5	30

Constructions of expression vectors containing sequence variants for western analysis

Wildtype *GDF11* in V-5 c-terminal labeled expression constructs, pcdna3.2, were created by site directed mutagenesis (SDM) for base pair substitutions using the QuikChange Lightning Site-Directed Mutagenesis Kit (Stratagene). Primers for SDM are listed in **Table 2.7** and were designed using the QuikChange Primer Design Program located on the Agilent website.

Table 2.7 Primer sequences for site directed mutagenesis

	Primer Sequence (5'-3')
G210V-Sense	AGGGACCGCAGTGGGAGGGGGCG
G210V-Antisense	CGCCCCCTCCCACTGCGGTCCCT
G44A-Sense	GCGGGGGTCGCGGGGGAGCGC
G44A-Antisense	GCGCTCCCCCGCGACCCCCGC

Each reaction was performed in a 50µl volume using Agilent QuickChange Lightning reagents. 5µl 10X Reaction Buffer, 125ng Sense and 125ng Anti Sense primers, 1µl of dNTP mix, (2.5µl of 100% DMSO (Sigma), 31.5µl DRF H20 and 1µl of QuikChange Lightning enzyme . *GDF11* cDNA in pENTR223.1 (Open Biosystems) was used as a template. PCR amplification cycles are as follows Step 1) 95℃, 2 min Step 2) 95℃, 20 sec Step 3) 60℃, 10 sec Step 4) 68℃, 1min 30 sec Step 5) Repeat Steps 2-5 17 times 6) 68℃ 5min. 2µl of *DpnI* RE digest were added directly to the mixture following PCR amplification and incubated at 37°C for 5 minutes to digest the parental non-mutated template *GDF11* plasmid. Amplified *GDF11* plasmids were transformed into One Shot Top10 Chemically Competent E. Coli (Invitrogen) and grown in bacterial culture under kanamycin selection pressure.

Construction of *GDF11* polyalanine vectors

GDF11 polyalanine variants were created by creating an ~400bp PCR fragment using a *GDF11* specific pENTR primer (**Table 2.8**) and plasmid DNA templates containing various *GDF11* alanine sequences provided by Dr. Xiao Hua. This ~400bp PCR fragment was used as a "forward primer" for amplification of full length *GDF11* cDNA with using wildtype *GDF11* cDNA as a template. *GDF11* cDNA products containing various polyanine number were visualized on a 1% agarose gel, and the approximately 1200bp products were isolated using a Qiagen Gel Extraction Kit. *GDF11* cDNA products were ligated into p-ENTR/SD/D-TOPO plasmid (Invitrogen), transformed into One Shot Top10 Chemically Competent E. Coli (Invitrogen) as previously described for growth on plates and subsequent liquid culture. Plasmids were prepped with mini-plasmid isolation kits (Qiagen), sequenced with M13F and M13R to screen which colonies had the desired variants, shuttled into pcDNA3.2/V5-Dest (Invitrogen) according to manufacturer guidelines, and grown in Top 10 cells for midi prep plasmid isolation.

Table 2.8 Primer sequences and conditions used to clone full length *GDF11*

	Primer Sequence (5'-3')	Amplicon Size (bp)	Annealing Temp (°C)	Extension Time (s)
pENTR-GDF11-F	CACCATGGTGCTCGCGGCCC CGCT	400	63	30
R3	GTCGTGTAGGTCCAGGATCT G			
TCA-GDF11 FLR	TGAAGAGCAGCCACAGCGAT CCACC	1200	63	90

Each reaction was performed in a 150µl volume , with a final concentration of 1X *Pfx50* PCR Mix (Inivitrogen), dNTP at 200µM (Invitrogen), 10% glycerol (Anachemia), 5% Formamide (Sigma), 2.5 units of *Pfx50* (Invitrogen), 2µl of the Large Forward GDF11 PCR Product, 2µM of the Reverse Primer and *GDF11* cDNA in pENTR223.1. PCR amplification cycles employed is a follows Step 1) 95°C, 5 min Step 2) 95°C, 45 sec Step 3) 63°C, 1min Step 4) 68°C, 1min 30 sec Step 5) Repeat Steps 2-5 29 times 6) Hold at 15°C.

Transient transfection and maintenance of COS cells for v-5 tagged westerns

COS cells were kindly plated by May Yu (Walter Laboratory) to reach 50-80% confluence in 10cm plates with a concentration of 10^6 cells per 100mm plate. 6ug of each plasmid were incubated with 18µl of FuGENE (a 3:1 ratio) in 776µl of Dulbecco's Modified Eagle Medium (DMEM) for 30 minutes at RT in a tissue culture hood then dispensed in a drop-wise spiral pattern evenly over the cells. Cells were swirled for optimal dispersion of transfection reagent and plasmid. Cells were placed in 37°C incubators containing 5% CO_2 for 24 hours. Media was replaced with 3mL of DMEM after 24 hours. Protein fractions were harvested 2 days post transfection. For media protein extraction, all 3mL of media were collected and mixed with 8mL of 100% acetone and incubated at -80°C for 1 hour. The mixture was then spun at 10,000 x g at 4°C for 15 minutes. Lysis Buffer was made as follows: 25mL 0.5 HEPES, 2.5mL 5M NaCl, 5.0mL 0.5M EDTA, 25.0mL Glycerol, and 3.5mL Triton X and Mili-Q H_20 up to 250mL. Supernatants were aspirated and protein pellets were resuspended in

125µl of a solution containing 10µl Protease Inhibitor Cocktail (Sigma), 5µl 0.1M PMSF, and 985µl of lysis buffer.

For whole cell lysate protein extraction each plate was washed with 5mL of PBS two times. Following the washes, 10µl 0.1M PMSF was added to 1mL of cold PBS and added to each plate. Plates were scraped to harvest cells and pipette into pre-chilled tubes. Tubes were spun at 3000rpm at 4°C for 5 minutes to pellet cells. Supernatants were aspirated and cell pellet resuspended in 200µl of the same solution as used to resuspend media protein isolates followed by a 1 hour incubation at 4°C in a rotating platform. Media and whole cell lysate protein samples were recollected and spun briefly prior to sonication. Sonication was performed using a Sonic Dismembrator (Fisher) for 10 seconds 4 Watts RMS. Samples were re-spun at 13,000 rpm at 4°C for 5 minutes to pellet the insoluble fraction and the supernatant contain isolated protein samples were transferred to new tubes at stored at -80°C.

Protein Quantification

A Bradford assay was performed to quantify protein yields using a DU-640 spectrophotometer (Beckman) configured to read protein concentration at 595nm. A 1x assay reagent consisting of 5x Bio-Rad Protein Assay Reagent (Bio-Rad), 3µl of 5M NaCl, and 797 Mili-Q H20 was prepared for every sample to be assayed as well as for each control in the standard curve. A protein standard curve for 0, 1.0, 2.5, 5.0, 7.5, and 10.0ug/µl was set by adding the corresponding amount of a 1ug/µl BSA reagent. The spectrophotometer was standardized with a

lysis buffer only sample prior to reading protein samples. 1.0µl of each protein isolated were added to 1mL of 1x assay reagent and measured and calculated to give a final protein concentration in ug/µl.

Western Assay

Buffers necessary for western analysis include 5x Running Buffer, containing 15.1g Tris Base, 72.0g glycine, and 5.0g sodium dodecyl sulfate per 1L, 4x separating buffer containing 90.86g Tris Base, 2.0g SDS per 500mL at a pH=8.8, 4x stacking buffer containing 6.05g Tris Base, 4.0 mL of 10% SDS made in MiliQ-H20, per 100mL at a pH=6.8. Sodium Dodecyl Sulfate PolyAcrylamide Gel Electrophoresis (SDS-PAGE) gels were cast in a two step fashion using a 75mm Biorad apparatus. First, the separating portion of the gel, which consisted of 4mL Acrylamide: Bis, 2.5mL of 4x separating buffer, 3.5 mL of Mili-Q H_20, 60 µl of 10% APS, and 13.4 µl of Temed to make a 12% SDS page gel. Second, the stacking portion of the gel was poured and consisted of 400 µl Acrylamide: Bis, 750 4x stacking buffer, 1.85 mL of Mili-Q H_20, 20 µl of 10% APS, and 6.7 µl of Temed. Between 10-40ug of protein were loaded into each well and gel was ran at 120 Volts for the first 15 mins followed by 80 V for 60 minutes to separate proteins. Separated proteins were transferred to nitrocellulose membrane blot (BioRad) by running at 100 V for approximately 1 hour in the cold room. Western blots were then placed in a washing tray and blocked with 5% Milk in TBST or 1 hour at room temp on a shaker. Blots were rinsed 3x with TBST 10 minutes each and a final wash of TBS for 15 minutes. Block was removed and replaced with primary antibody in 5% milk in TBST and Sodium Azide, for 1

hour at RT or overnight at 4℃ on a shaker. Primary antibodies were decanted for future use. Blots were quickly rinsed 3 times with TBST, and washed 2 times with TBST for 15min. Species specific secondary antibodies were diluted at 1:5000 in 5% Milk in TBST for 1 hour. Blots were briefly rinsed 3x with TBST followed by a 15 min TBST wash, followed by a brief rinse of TBS and 15 min TBS wash. Blots were placed over saran wrap and ECL reagents (Pierce ThermoScientific) were mixed at a 1:1 ratio and spread evenly over blots. Blots were secured in saran wraps and taped within an x-ray cassette. X-ray film was placed over blots for exposure. Western blots were sequentially re-probed for multiple proteins following stripping with 0.2M NaOH for 20 minute at RT on a shaker, followed by a quick MiliQ-H20 wash, rehydrated in TBS, reblocked in 5% Milk in TBST re-probed for proteins of interest.

Results

Expression pattern of *gdf11* in the eye, brain, and olfactory epithelium

The expression of *gdf11* is first detected in the lens and surrounding retina at 29hpf (**Fig. 2.1A**). At 3dpf (**Fig. 2.1B**), expression of *gdf11* persists but is detected in the inner retina which contains retinal ganglion and amacrine cells. As previously observed by Farooq et al. 2008 [12], the expression of *gdf11* is detected in the hindbrain at 2 and 3dpf (**Fig. 2.1C-D**). At 21 and 27hpf *gdf11* is not expressed in the eye but is present in the presumptive olfactory epithelium (**Fig. 2.1E-F**).

Efficacy of splice blocking *gdf11* morpholino

Two morpholinos were used in these studies, a translation blocking MO binding to *gdf11*'s 5'UTR, $gdf11^{\text{MO-ATG}}$, and a splice blocking MO spanning exon 1 and intron 1, $gdf11^{\text{MO-splice}}$ (**Fig. 2.2A**). The efficacy of $gdf11^{\text{MO-splice}}$ was validated by a PCR primer reaction containing 1 forward primer and 2 reverse primers [13]. The 392bp band representing an amplicon corresponding to processed *gdf11* mRNA is detected only in controls (**Fig. 2.2B lane 1**), which is not deteted in the $gdf11^{\text{MO-splice}}$ injected group (**Fig. 2.2B lane 2**). The 525bp product is not expected to be detected in cDNA amplified with oligoDT primers and could indicate genomic DNA contamination. The intron spanning *ef1alpha* 339bp PCR product suggest no gDNA contamination as it would have been 426bp if it contained the genomic 87bp intron 4-5 and equal loading of PCR amplicons

(lanes 4-5) while the 925bp amplicon used to generate the *gdf11* anti-sense probe (lane 7) is not detected in the *gdf11*^{MOsplice} injected (lane 8) cDNA as it is likely that part of the 119kb intron 1 is retained and cannot be amplified. Lanes 3, 6, and 9 are PCR reactions performed without any template.

Phenotypes as a result of inhibiting *gdf11* in zebrafish at 3-5dpf

Inhibiting *gdf11* results in several phenotypes present in the eye, hindbrain, yolk extension, and tail. Phenotype counts are listed in **Table 2.9** for *gdf11* morphants injected with either *gdf11*$^{MO\text{-}ATG}$ + *p53*^{MO}, *gdf11*^{MOsplice} + *p53*^{MO}, or control *p53*^{MO} alone. The *gdf11*$^{MO\text{-}ATG}$ yielded a reduced eye phenotype as seen in a previous publication [12] and was used for the majority of subsequent studies. At 3dpf, the ventral yolk extension is present in controls (**Fig. 2.3A**) but is decreased in 48% (96/200) of *gdf11* morphants (**Fig. 2.3B**). Hindbrain hydrocephaly, is observed in 50% (100/200) of *gdf11* morphants, but only in 1% (2/185) of controls. The *gdf11* morphants display a slightly smaller eye size but at 5dpf, a gross difference in overall eye size is detected in 46% (64/140) of *gdf11*$^{MO\text{-}ATG}$ larvae compared to 2% in controls (**Fig. 2.3D**). Cardiac edemas are detected in 42% (59/140) of *gdf11* morphants as opposed to the 2% (3/139) in controls. Tail anomalies are detected in 31% (44/140) of *gdf11* morphants as opposed to 7% (10/139) in controls. To account for differences as a result of developmental delay, fish were phenotyped for tail ossification and early anal fin condensation (**Fig. 2.3E-H**) and suggest no gross differences in controls and *gdf11* morphants using Parichy et al. 2009's normal table of development as a reference [23]. The *gdf11*$^{MO\text{-}splice}$ treated fish did not yield phenotypes comparable to *gdf11*$^{MO\text{-}ATG}$ treated larvae at 3dpf but

did yield higher than control phenotype counts at 5dpf possibly due to the fact that *gdf11* is maternally deposited [10]. Embryos injected with the *gdf11*$^{MO\text{-}ATGMM}$ did not develop display phenotypes observed by either *gdf11* morpholino.

Altered expression of amacrine (*runx1*) and rod (*neuroD*) cell markers

Runt-related transcription factor 1 (*runx1*), a marker for a subpopulation of amacrine cells, was investigated in *gdf11* morphants to examine amacrine cell abundance [26]. Expression of *runx1* was detected proximal to the lens of controls at 2dpf (**Fig. 2.4A**) but is not detected in *gdf11* (**Fig. 2.4B**) morphants. At 3dpf, *runx1* persists as a ring like pattern (**Fig. 2.4C**) whereas *gdf11* morphants display reduced expression and lack the ring like organization in controls. *Neurogenic differentiation* (*neuroD*) is a marker for rod photoreceptor cells [27-29]. At 4dpf, *gdf11* morphants exhibit a gross increase of *neuroD* expression in the eye and olfactory epithelium as compared to controls (**Fig. 2.5A-B**). The expression of *neuroD* is expanded throughout the whole eye at 4dpf but is primarily restricted to the outer nuclear layer in controls (**Fig. 2.5C-D**). At 5dpf, *neuroD* expression is decreased in controls but continues to persist in *gdf11* morphants.

Increased expression of photoreceptor developmental markers *crx* and *otx2*

Cone-rod homeobox, *crx*, and orthodenticle homolog 2, *otx2*, were investigated in *gdf11* morphants as these transcription factors play key roles in photoreceptor differentiation and development [30-32]. At 4 & 5dpf, *crx* expression is increased in *gdf11* morphant eyes compared to controls (**Fig. 2.6A-D**). At 5dpf, the

expression of *otx2* is detected within the ganglion cell layer of the eye (**Fig. 2.6E**), but is expanded throughout the eye in *gdf11* morphants (**Fig. 2.6F**).

Decreased photoreceptor number in *gdf11* morphant retinas

Rod photoreceptors were quantified on whole eyes in controls and *gdf11* morphants at 5dpf. 1D1 IHCs controls displayed a mean average of 412 rods per eye (n=9) while *gdf11* morphants exhibited 183 rods per eye (n=8) (**Fig. 2.7A-B**), a statistically significant decrease (**Fig. 2.8A** t-test p=0.0005). A complementary assay performed with another rod antibody, 4C12, showed that controls have a mean of 463 rods per eye (n=8) and *gdf11* morphants had a decrease of 261 rods per eye (**Fig. 2.7C-D**) n=10, p=0.026. A third assay (**Fig. 2.7E-F**) utilizing transgenic *rh1*-GFP which express rhodopsin driven GFP in rod photoreceptors was simultaneously processed with zpr-1, which marks red green cones, resulted in controls displaying 492 rods per eye (n=10) and *gdf11* morphants displayed 246 rods per eye (n=9) ($p<0.0001$). Control eyes exhibited greater intensity of the zpr-1 conjugated Texas Red secondary antibody as compared to morphants suggesting a decrease in red green cone photoreceptors. Correction for the surface area of eyes processed with 1D1, 4C12, or expressing the rh1-GFP transgene are demonstrated in **Fig. 2.8A'-C'** with corresponding p-values of 0.3704, 0.2452, and 0.0474.

GDF11 sequence variants in disease cohorts

Six heterozygous *GDF11* sequence variants were detected in DNA samples from patients with ocular disorders (**Table 2.10**). A three alanine deletion was detected

in 1 of 3 DNA samples from patients exhibiting juvenile RP, also carrying a *GDF6* A249E missense variant. The three alanine deletion is present in 2 of 725 control DNAs. A one alanine insertion is present in 1 of 163 MAC DNA samples and 1 of 252 POAG samples, and is present in 4 of 725 control DNAs. A four alanine insertion was present in 1 of 252 POAG patients and detected in 0 of 725 controls. Representative data for genotyping of controls is displayed in (**Fig. 2.10A**). Chromatograms for DNA samples containing polyalanine sequence variants were verified for number (**Fig. 2.10B**). The 13 polyalanine number is conserved in human and gorilla but is decreased in mice, rats and pigs and absent in zebrafish (**Fig. 2.9**). Missense variant G210V (**Fig. 2.9B)** was present in 2 of 252 POAG samples and in 1 of 245 while controls. G44A (**Fig. 2.9B**) was detected in 1 of 252 POAG samples and in 2 of 618 control DNAs. These amino acids are conserved in gorilla, mouse, rat and pig but not in zebrafish (**Fig. 2.9C**). A single nucleotide insertion, +10_+11insT (**Fig. 2.9B**), was found in a patient with coloboma and inherited from a mother that exhibit cornea plana (data not shown).

Western analysis *GDF11* sequence variants

Western analysis of media and whole cell protein isolates revealed the presence of an approximately 100kDa band in G210V not detected in WT to 10, 14 or 17 polyalanine variants and G44A protein samples (**Fig. 2.11A**). G210V also exhibits reduced levels of a 50kDa pro-*GDF11* band (**Fig. 2.11 A-A'**) as

compared to WT. The mature 15kDa *GDF11* ligand is reduced in G210V, while no gross difference is detected in WT or other *GDF11* sequence variants. No gross differences were detected in whole cell lysates (**Fig. 2.11B**). Secreted alkaline phosphatase and α-tubulin controls suggest no gross difference in loaded protein is accountable for observed *GDF11* band intensities or migration.

Discussion

The expression pattern of zebrafish *gdf11* has many similarities to what is observed in mice. In developing mice eyes, in situ hybridization performed on sectioned eyes show that *Gdf11* is expressed in neuro retinal layers and is detected in the retina and lens of zebrafish in this study [9]. In this study, I show that zebrafish *gdf11* is expressed in the developing eye in early neural retina RPCs and at later stages of development in layers of the eye corresponding to the RGCs, amacrine, and photoreceptor cells **(Fig. 2.1A-B)**. As shown previously [12], *gdf11* is expressed in the hindbrain at 2-3dpf (**Fig. 2.1C-D**). These results document the expression in the eye as well as the presumptive olfactory epithelium corresponding to published *Gdf11* expression in the mouse olfactory epithelium [8].

The effects of reducing *gdf11* activity by morpholino inhibition yielded both similarities and differences to what is observed in *Gdf11* mutant mice. Corresponding with the *gdf11* expression patterns in the eye, MO inhibition resulted in an ocular phenotype of smaller eyes. An explanation as to why the *gdf11*$^{\text{MO-ATG}}$ is more effective generating the phenotypes is that it targets both maternal and zygotically expressed genes. Co-injection of *gdf11* MOs with a p53 MO suggests that the phenotypes are not due to non-specific cell death. However, other experiments could be performed to show that the particular MO is acting through *gdf11* and not through the inhibition of other genes. One assay could be the co-injection of *gdf11* MOs with *gdf11* RNA to evaluate rescue of the

phenotype. One issue that could arise in this experiment is a gross alteration in axis patterning since another member of the BMP family, *gdf6a*, exhibits gross dorsal ventral patterning defects. This may be due to the tissue specific expression pattern of *gdf6a*. To circumvent this non-specific tissue expression pattern, rescue experiment with *gdf6a* and other BMPs are placed in vectors carrying ocular specific promoter elements which then transcribe RNA in a tissue specific manner. Experiments such as rescue experiments and the development of *gdf11* antibodies will add reinforcement to show that the MOs utilized are acting in a gene specific manner.

Another complicating issue with this study is the possibility of developmental delay. Observations of reduced eye size in *gdf11* may be due to the fact that *gdf11* morphants are delayed. To address this issue, larvae were staged according to caudal fin ossification and anal fin condensation [23] and no differences in delay were detected. However, if reduced eye phenotypes are due to changes due to hormonal differences then the presented data would need to be reinterpreted. Perhaps altering *gdf11* activity can affect hormonal levels during development. When *gdf11* is reduced, *otx2* expression is increased in the eye, although this experiment may need to be repeated with another probe. Interestingly human *OTX2* loss of function mutations results in ocular and hormonal deficiency phenotypes [33-34]. This contrast to an apparent increase of *otx2* expression in the eyes of *gdf11* morphants in this study, but other experiments to examine the presence or lack of hormonal deficiencies can be investigated in the future.

Amacrines and rod photoreceptor cells were reduced upon investigation with *runx1* [26] and rod photoreceptor specific antibodies resulting in a similar reduction of rods in *Gdf11* mutant mice. In mice, this has been attributed to a change of cell fate as cells destined to become later born cell types such as amacrines and rod photoreceptors become retinal ganglion cells [9]. No definitive assays to examine relative RGC abundance were performed due to technical issues. Overexpression of *neuroD* in zebrafish causes the differentiation of rod photoreceptor cells [28] but rod and cone IHCs showed a decrease in eyes of *gdf11* morphants despite the increase of *neuroD* expression.

Furthermore, an apparent increase in expression of photoreceptor developmental genes *crx* and *otx2* in 4 and 5dpf may have contributed to aberrant photoreceptor development. Inhibiting *gdf11* seems to increase levels of *crx*, while a complementary in situ for its upstream gene, *otx2* [30], also exhibits increased levels of expression in the eyes of morphants as compared to controls. Loss of *Crx* in mice results in a failure of proper photoreceptor development and functionally silent electroretinograms [32] but c*rx* mutant mice also exhibit increased levels of *NeuroD* protein. In mice, *Crx* is expressed in post-mitotic photoreceptor precursors [35] while zebrafish *crx* functions differently to promote other retinal progenitors as well as photoreceptors [36]. In this study, levels of *crx*, *otx2*, and *neuroD* are increased in *gdf11* morphants while previous investigations in *Gdf11* exhibited decreased levels of *Crx* [9] from which it was inferred that these mice would have decreased rod photoreceptors. Perhaps the increase of expression of *crx*, *otx2*, and *neuroD* is compensating for the loss of

certain retinal cell type populations such as the photoreceptors. Alternatively, mouse *Gdf11* and zebrafish *gdf11* genes may be acting in different pathways to regulate the three photoreceptor development genes.

GDF11 sequence variants were screened in two early onset disorders, juvenile RP and MAC, and a late onset disorder, POAG, which revealed six heterozygous sequence variants. Screening a MAC panel for *GDF11* mutations seemed compatible as *Gdf11* mutant mice exhibit ventral coloboma [9]. A compound heterozygous sequence variant *GDF6* A249E and a deletion of 3 alanines of *GDF11* may mean that the two are interacting to cause faulty photoreceptor development. POAG was screened as null mutations in a TGF-Beta interacting protein *latent-transforming growth factor beta-binding protein 2* (*LTBP2*) are associated with congenital glaucoma [37-38]. No nonsense or frameshift mutations were detected in any of the three disease panels however; mutations may be present in regulatory sequences. Only the *GDF11* exons were sequenced and it may be possible that mutations in regulatory elements were not detected in the screening assay.

Transient transfection of wildtype and variant *GDF11* sequences partially revealed the functional consequence on mature levels of signaling ligand. Only G210V showed a detectable difference in the presence of the mature ligand and exhibited a gross difference in migrating pro-*GDF11*. Gly210 is an evolutionary conserved residue located within the pro-domain of *GDF11*. The gross difference in pro-*GDF11* size and decreased levels of mature ligand may be attributable to a processing defect of *GDF11*. Alternatively, the approximately 100kDa band may

be a dimer of 50kDa of *GDF11* protein that was not fully denatured by the western assay. G210V may be increase inhibitory activity of the prodomain by increasing binding of the prodomain to the mature ligand. *GDF11* G44A and polyalanine variants showed no detectable difference in mature ligand or migration of pro-*GDF11*. *GDF11*'s polyalanine tract is located within the prodomain and any effect on protein processing would be speculative with the results in this thesis. Under normal conditions, the prodomains of BMP and TGF-β proteins are cleaved to produce the mature signaling ligand. However, prodomain molecule can form noncovalent latent complexes with their signaling ligand to limit their bioavailability. In the case of *GDF11*, the prodomain binds to the signaling ligand and has been shown to be sufficient to limit the function of *GDF11* to inhibit aspects of neurogenesis [39]. Whether or not alterations in the polyalanine tract could have an effect on the formation of such latent complexes could be pursued. Other polyalanine tract expansions have been investigated in disease for genes encoding proteins located in the nucleus or the cytoplasm [40]. An expansion of the transcription factor *forkhead box L2* (*FOXL2*) 14 polyalanine tract to 19-24 additional alanine residues cause Blepharophimosis, ptosis and epicanthus inverse type II which presents as eyelid abnormalities as well as premature ovarian failure [41]. The molecular consequence of expansions of the polyalanine tract result in protein aggregates leading to a decrease in *FOXL2* activity [42]. Expansions in cytoplasmic protein *poly(A)-binding protein 2* (PABP2) cause Oculo pharyngeal muscular dystrophy [43]. To my knowledge, no reports of polyalanine expansions or deletions have been documented in

secreted genes such as *GDF11*. Interestingly, certain BMP members exhibit nuclear localization when the nuclear localization domain is altered [44]. Whether this is the case could be documented in future studies

Generally, loss of *Gdf11* results in a change of cell fate as cells destined to be later born cell types become RGCs. Cases of cell fate changes are present in retinal diseases such as *NR2E3* mutations causing Enhanced S Cone Syndrome, a consequence of an increase in the number blue light sensitive cone photoreceptors [45]. Mutations in *Tbx2b* result in a change of retinal cell fates of UV cones to become rods, thereby increasing the number of rod photoreceptors in zebrafish retina [46]. Whether or not loss of *GDF11* causes ocular diseases such as retinal dystrophies and reduced photoreceptor number warrants further investigation.

Studying *gdf11* by MO inhibition in zebrafish and the effects on retinal cell types are summarized in **Fig. 2.12**. Generally, inhibiting *gdf11* results in a loss of photoreceptor number but an upregulation of transcription factors associated with photoreceptor development. This inconsistency should be noted as it may be an interesting question to be answered by future investigators. Perhaps inhibiting *gdf11* activity drastically alters the intrinsic expression pattern of RPCs, an avenue of research that could be pursued in the future.

Figure 2.1 In-situ hybridization reveals *gdf11* expression in the eye, hindbrain, and presumptive olfactory epithelium

A: A dissected 29hpf wildtype zebrafish eye display expression of *gdf11*in the lens and retina proximal to the lens. **B**: At 3dpf, the expression of *gdf11* continues to be detected in the eye as later born cell types arise in the inner retina consisting of the retinal ganglion and amacrine cells. **C-D**: Dorsal views of 2 and 3dpf embryos demonstrate *gdf11* expression throughout the hindbrain. **E-F**: Dorsal flatmounts at 21 and 27hpf embryos illustrate *gdf11* expression in the presumptive olfactory epithelium as indicated by "*". Flatmount eyes and heads were imaged with a 20x lens.

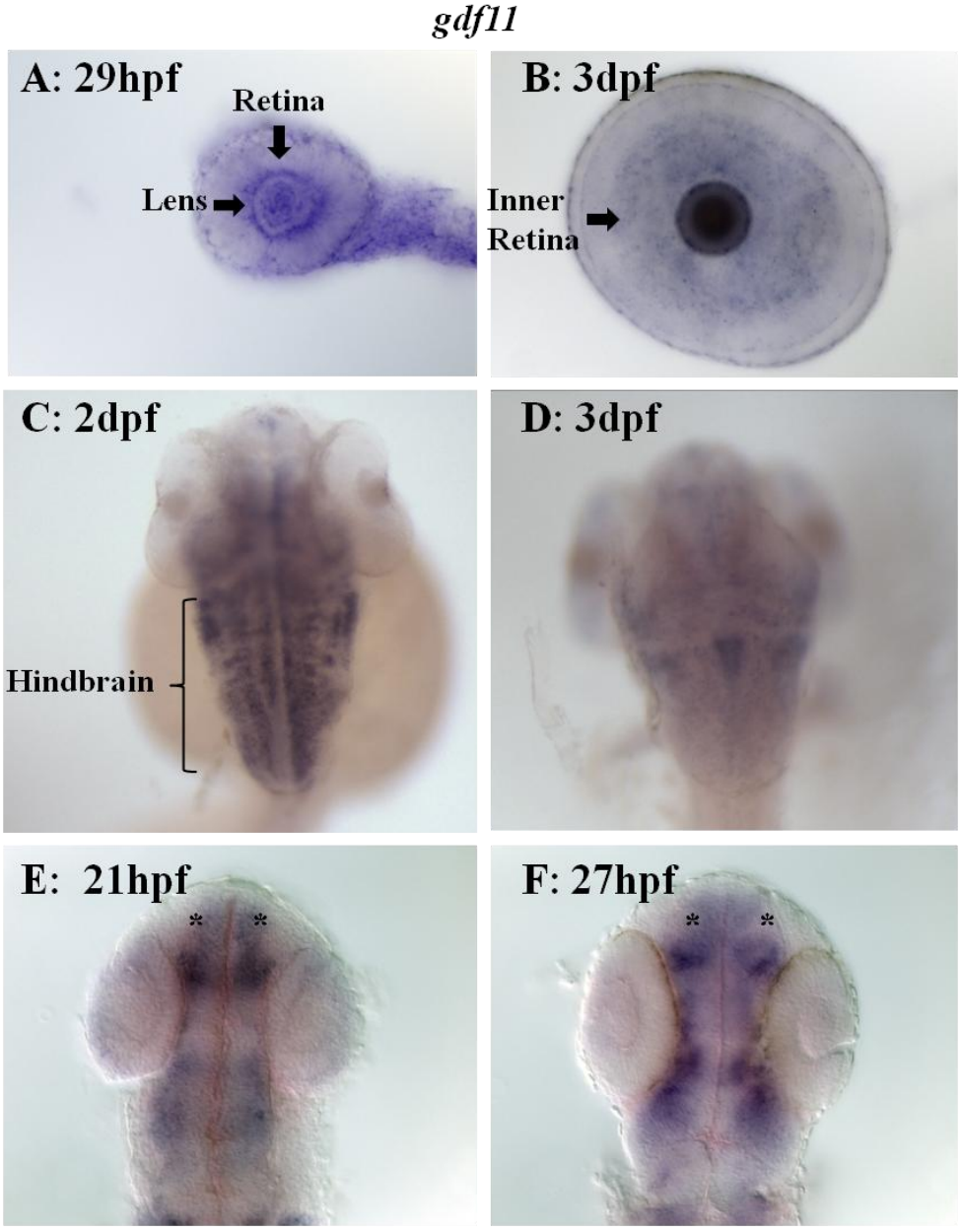

Figure 2.2 Morpholino positions and efficacy studies

A: Schematic illustrating the position of the *gdf11* splice blocking morpholino spanning exon 1 and intron 1. Location of primer F1, R1 and R2 and the expected size of their exon-intron spanning (525bp) or exon junction (392bp) spanning PCR amplicons are indicated. ISH-F/R indicate primer pair used to synthesize the 962bp band for the *gdf11* in situ hybridization probe. **B**: A gel illustrating the efficacy of *gdf11*$^{MO\text{-}splice}$ lack of a properly spliced 392bp band (lane 2) in *gdf11*$^{MO\text{-}splice}$ injected sample (S) in a PCR reaction containing all 3 primers: F1, R1, and R2 while both the 525bp and 392bp are in controls (C). A control amplicon for *ef1*alpha suggests equal loading of PCR products (lanes 4-5). While the amplicon used to generate the *gdf11* WISH probe is detected in a control sample (lane 7) but not in the splice blocking morpholino treated group likely due to the retention of part of the 119kb intron 1 not detectable by this assay (lane 8). Lanes 3, 6 and 9 represent PCR reactions performed without any cDNA template.

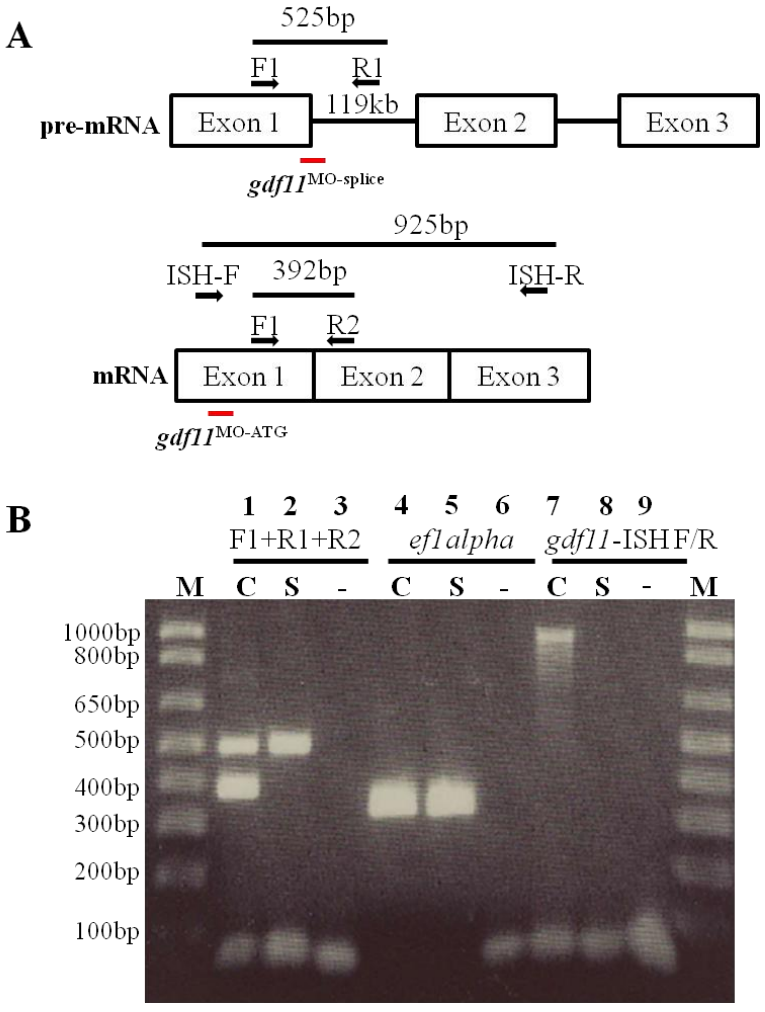

Figure 2.3 Spectrum of *gdf11* morphant phenotypes.

A-B: The yolk extension is present in 3dpf controls but reduced in *gdf11* morphants (*). The black arrow indicates hydrocephaly. **C-D**: Eyes are noticeably smaller in *gdf11* morphants and exhibit cardiac edemas. **E-F**: Controls and morphants exhibit comparatively equal states of caudal fin ossification. **G-H**: The anal fin stage of development suggests evidence for lack of developmental delay. **I**: A representative image of a *gdf11*splice-MO injected morphant that exhibits small eye and cardiac anomalies but not hydrocephaly or reduced yolk extension.

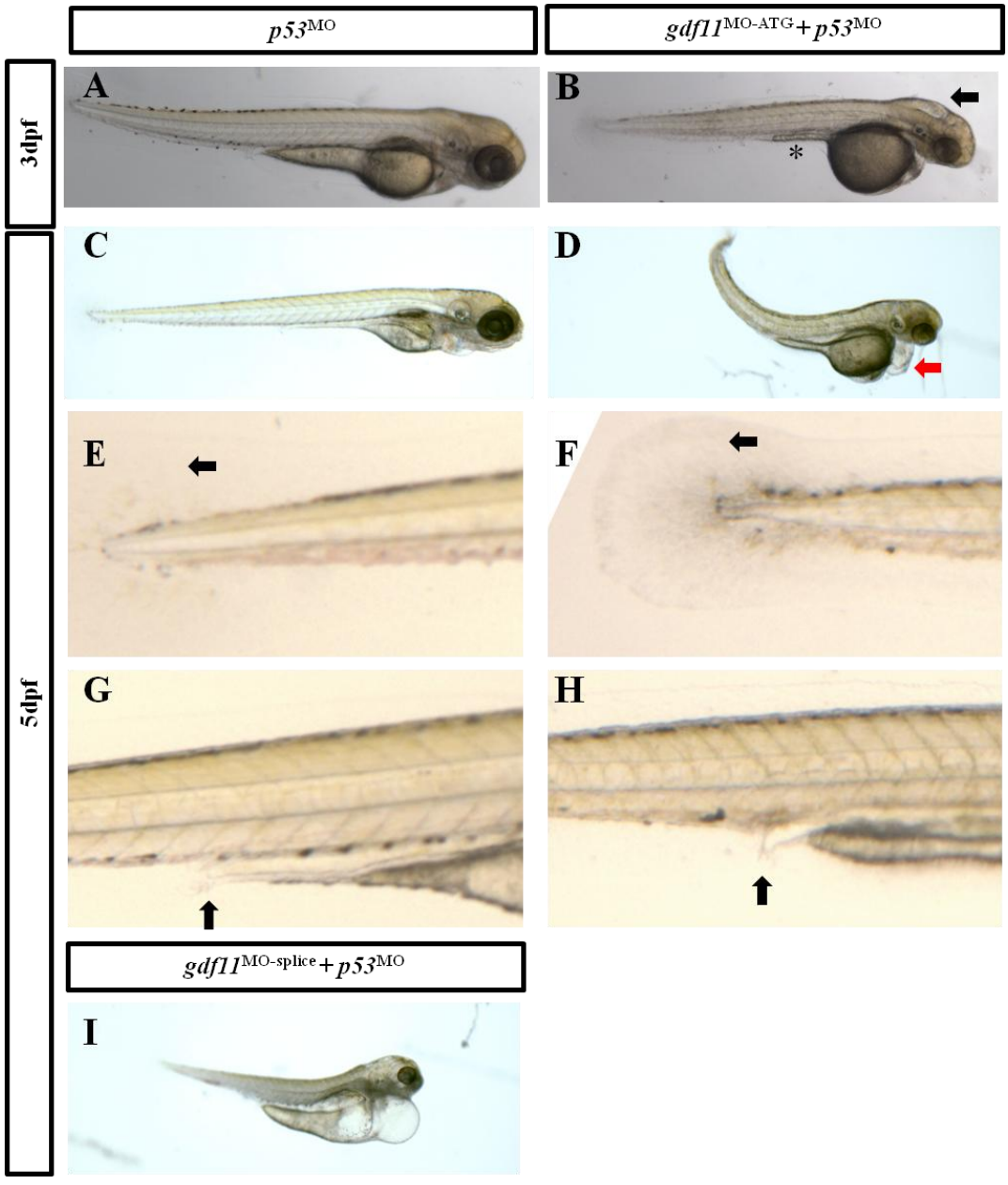

Table 2.9 Phenotype counts of *gdf11* morphants and controls at 3 & 5dpf.

Zebrafish were phenotyped for hindbrain hydrocephaly and decreased yolk extension at 3dpf while tail, cardiac and small eyes were phenotyped at 5dpf. Phenotype data were collected from 3 separate injection trials.

Phenotypes at 3dpf	***p53*^{MO}**	***gdf11*$^{MO\text{-}ATG}$ + *p53*^{MO}**	***gdf11*$^{MO\text{-}splice}$ + *p53*^{MO}**
Hindbrain Hydrocephaly	1% 2/185	50% 100/200	6% 10/169
Decreased Yolk Extension	1% 2/185	48% 96/200	2.5% 5/199
Phenotypes at 5dpf	***p53*^{MO}**	***gdf11*$^{MO\text{-}ATG}$ + *p53*^{MO}**	***gdf11*$^{MO\text{-}splice}$ + *p53*^{MO}**
Tail anomaly	7% 10/139	31% 44/140	9% 15/170
Cardiac edemas	2% 3/139	42% 59/140	12% 20/170
Small Eye	2% 3/139	46% 64/140	24% 40/170

Figure 2.4 Decreased expression of amacrines cell marker *runx1* in *gdf11* morphants at 2 and 3dpf.

A-B: At 2dpf, the expression of *runx1* is detected in the eye in the presumptive amacrine cell layer in controls but is not detected in the smaller *gdf11* morphants eyes. **C-D**: At 3dpf, the expression of *runx1* recovers in *gdf11* morphant eyes but is not in an organized ring like pattern visualized in controls. The proportion of eyes exhibiting the representative phenotype is annotated for each group. All eyes were imaged with a 20x lens.

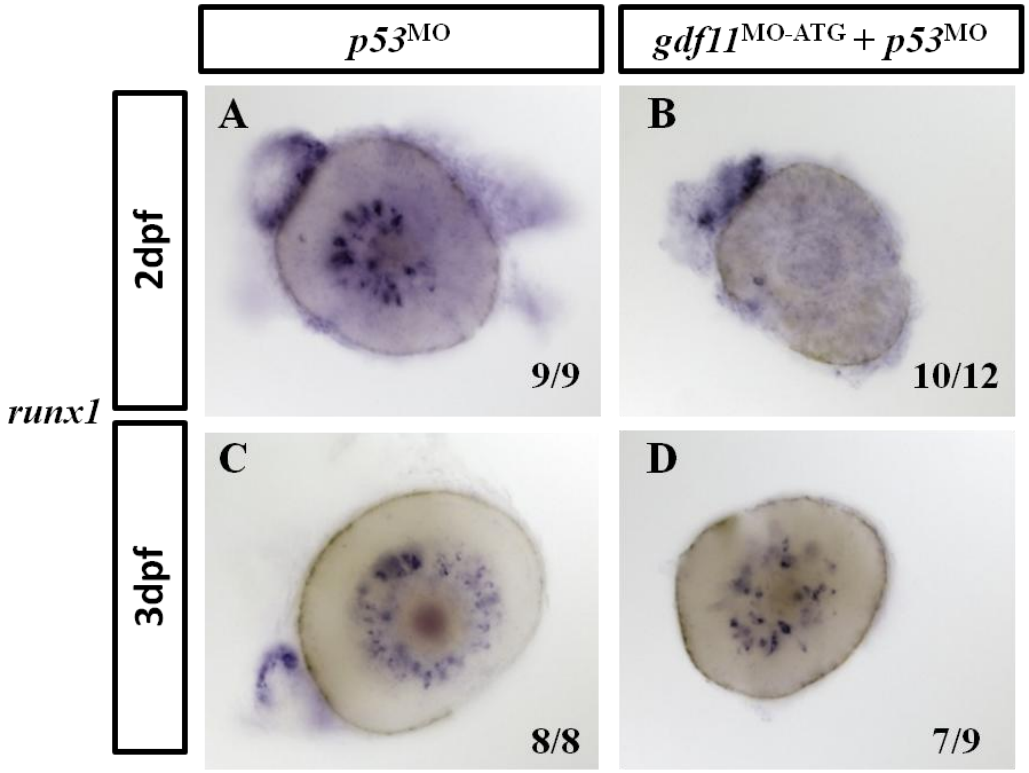

Figure 2.5 Altered expression of the rod photoreceptor cell marker *neuroD* in the eye and the olfactory epithelium at 4 & 5dpf.

A-B: Flatmounts heads display expression of *neuroD* in the eye as well as the presumptive olfactory epithelium marked by two distinct points (*) in *gdf11* morphants not detected in controls. **C-D**: Dissected eyes display gross increase of *neuroD* expression in *gdf11* morphant eyes as *neuroD* is detected throughout the eye but is restricted to the outer nuclear layer in controls. At this time point *gdf11* morphant eyes are slightly smaller than controls. **E-F**: Expression of *neuroD* is no longer detected in controls, but persists in the *gdf11* morphant eyes. The proportion of eyes exhibiting the representative phenotype is annotated for each group. Flatmount heads were imaged with a 10x lens while eyes were imaged with a 20x lens.

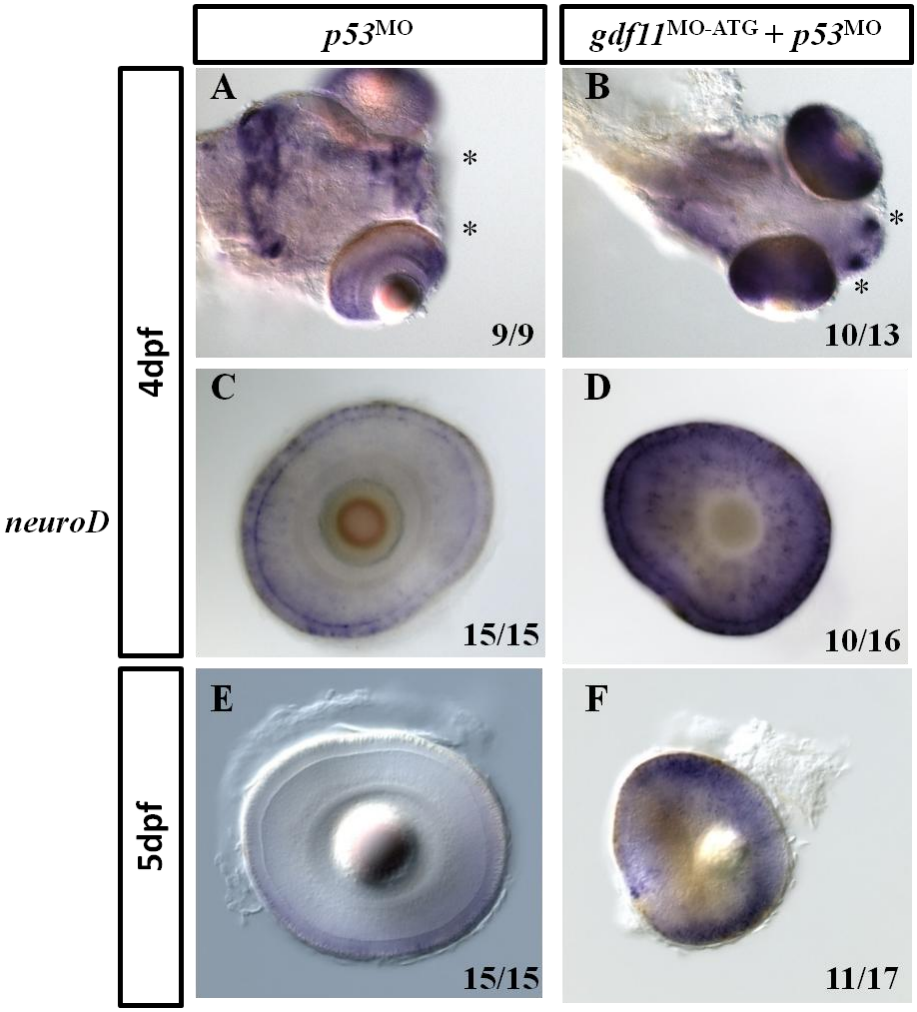

Figure 2.6 Altered expression of photoreceptor cell associated transcription factors *crx* and *otx2*.

A-B: At 4dpf the smaller *gdf11* morphant retinas is increased as compared to controls. **C-D**: At 5dpf broad expression of *crx* is maintained in *gdf11* morphant eyes as compared to controls. **E-F**: *otx2*, known to be upstream of *crx*, is detected throughout the eye at higher levels in *gdf11* morphants as compared to controls where expression is decreased and detected proximal to the lens. The proportion of eyes exhibiting the representative phenotype is annotated for each group. All images were taken at the same magnification with a 20x lens.

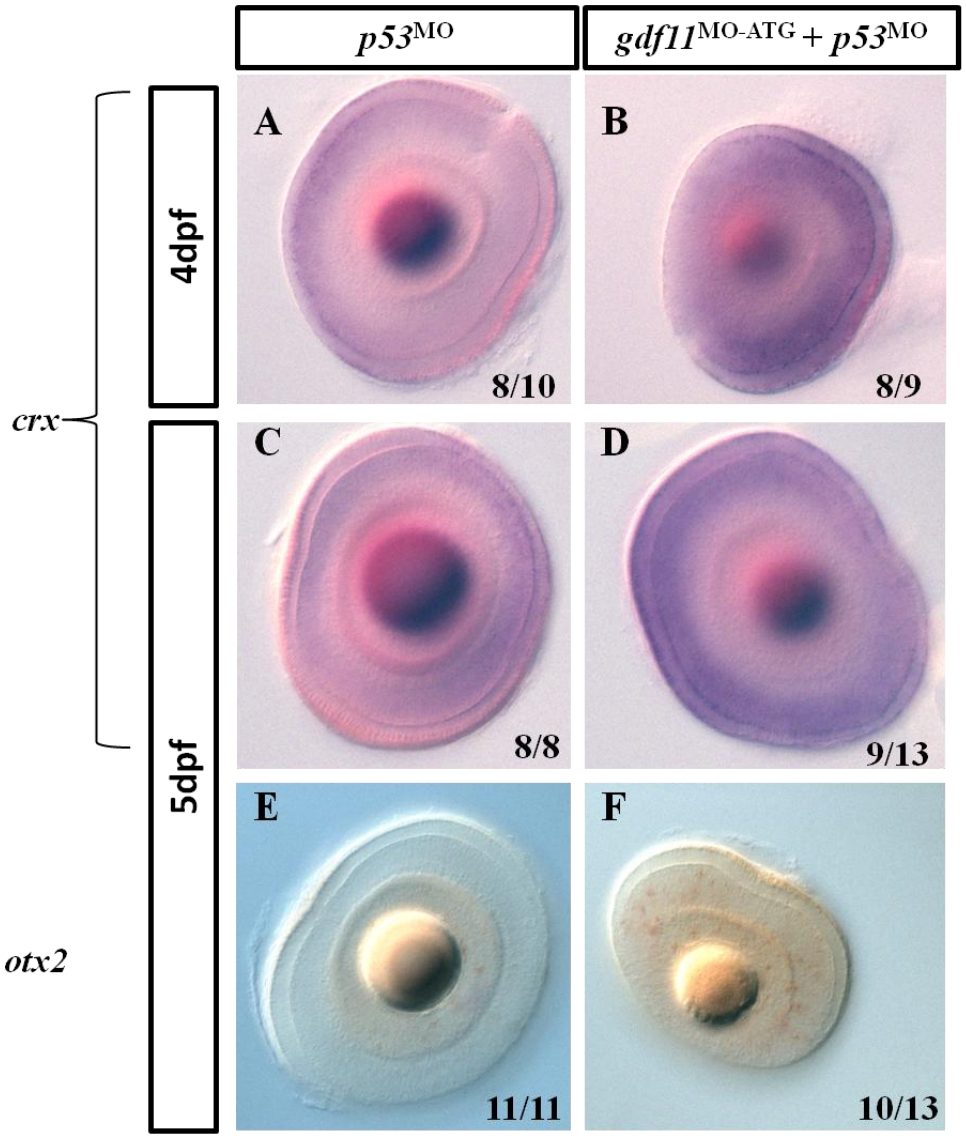

Figure 2.7 Decreased photoreceptor number in gdf11 morphant at 5dpf.

A-B: Compressed z-stacks of IHC processed with the 1D1 (rod) show decreased number of rod photoreceptor in 5dpf smaller eyes of *gdf11* morphants as compared to more abundant rods observed in controls. **C-D**: Another rod antibody, 4C12, displays decreased rod photoreceptor number in morphant eyes while controls have more rod photoreceptors. **E-F**: A decrease in the ventral patch of rods (*rh1*-GFP) is observed in *gdf11* morphants as well as a decrease in the number of rod photoreceptor cells. Signal intensity for a red-green specific antibody, zpr-1, is decreased in morphants as compared to controls. Mean number of cells (x□) and sample sizes are indicated for each group. Eyes were imaged at the same magnification with a 20x lens.

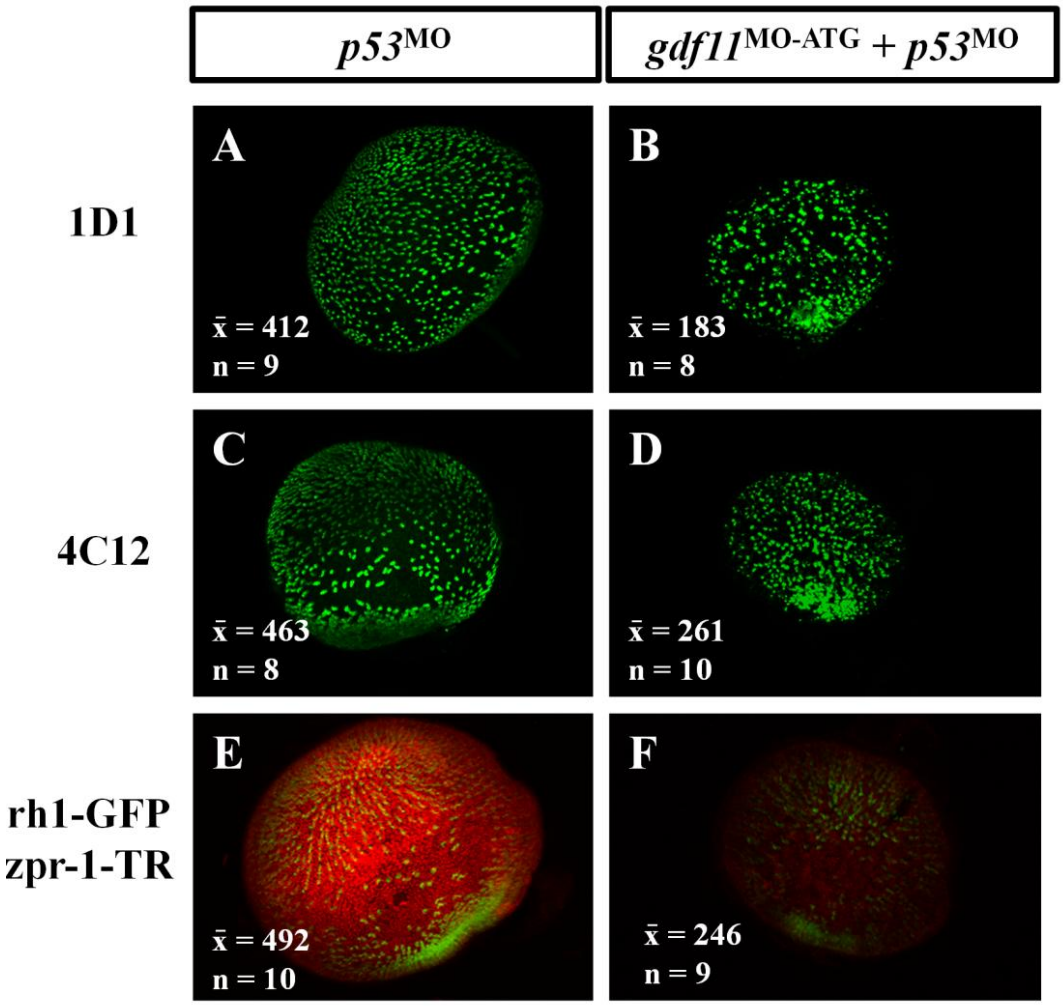

Figure 2.8 Scatter plots for rod photoreceptors 5dpf eyes.

A-C: Raw counts are displayed as scatter plots for eyes processed with 1D1, 4C12, or *rh1*-GFP. **A'-C'**: The y-axes were adjusted to take into account the surface area of the retina (rod #/surface area x 1000).

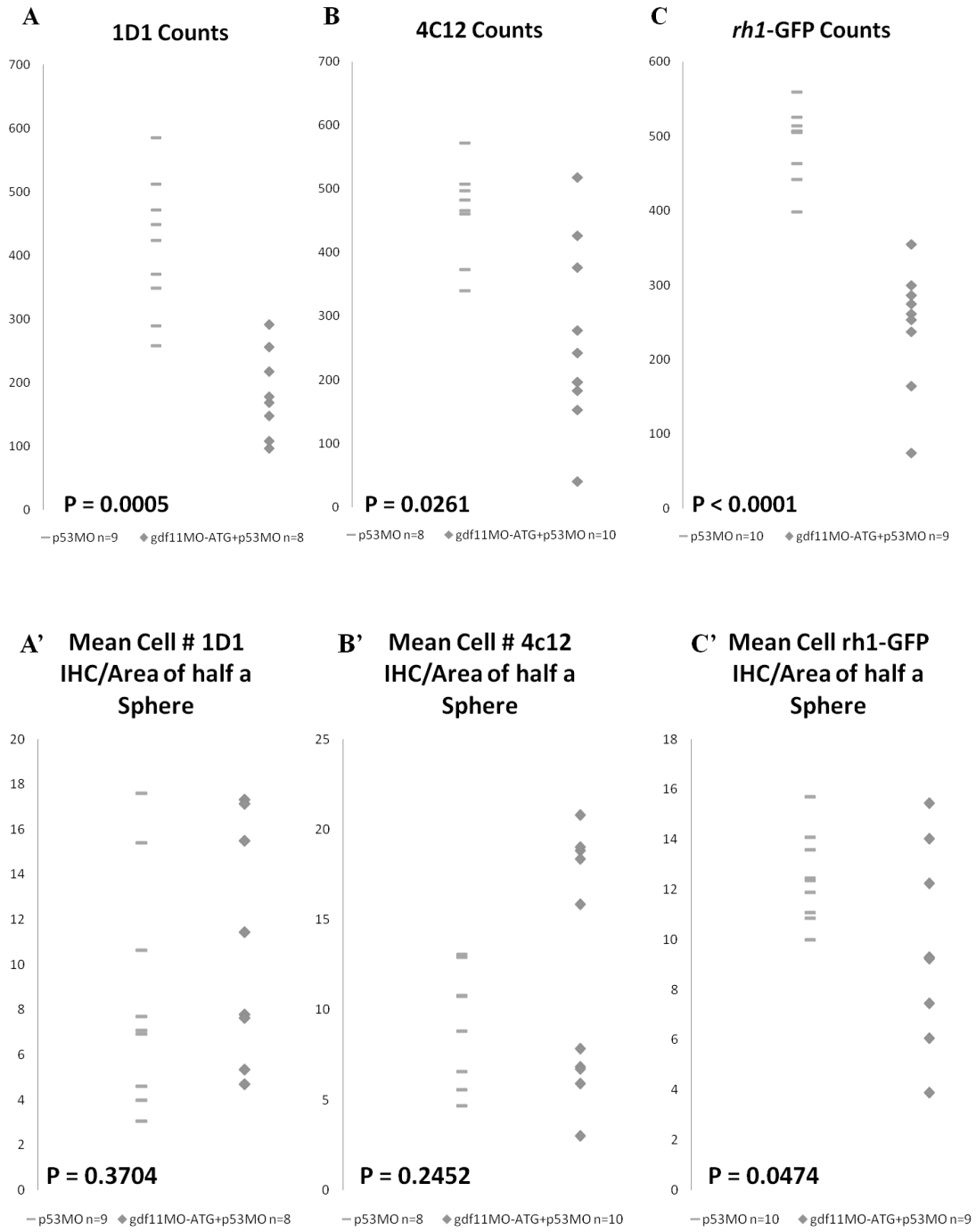

Table 2.10 Frequency of heterozygous *GDF11* Sequence variants in patients and controls.

Six heterozygous *GDF11* sequence variants were detected in patients diagnosed with juvenile RP, MAC, or POAG. The frequency of the *GDF11* sequence variants was detected in controls by either genotyping or restriction enzyme digestion.

***GDF11* Sequence Variant**	**Diagnosis**	**Frequency in Patients**	**Frequency in Controls**	**Screening Method**
3 Ala Del	Juvenile RP	1/3	2/725	Genotyping
1 Ala Ins	MAC	1/163	4/725	Genotyping
3'UTR* +10_+11 insT	Coloboma	2/163	0/862	Genotyping
4 Ala Ins	POAG	1/252	0/725	Genotyping
G210V	POAG	2/252	1/245	RE Digest (TspRI)
1 Ala Ins	POAG	1/252	4/725	Genotyping
G44A	POAG	1/252	2/618	RE Digest (HgaI)

Figure 2.9 Schematic diagram of *GDF11* sequence variants, amino acid conservation and representative restriction enzyme digest of control DNA samples.

A: Schematic depicting human *GDF11* structure as 3 exons and protein domains. *GDF11* protein is composed of 3 domains with enumerated amino acid number (AA#) for the signal peptide, prodomain, and mature ligand positions. The 13 polyalanine wildtype stretch is located at amino acid residues 29-41. **B**: Chromatograms for WT and heterozygous sequence missense variants G44A and G210V. The +10_+11insT (red box) is illustrated with WT and variant nucleotides corresponding to the double peaks observed in the chromatogram. **C**: Protein alignments of affected amino acid residues show that Gly44 is conserved in all species except zebrafish whilst Gly210 is invariant in all species carrying that residue. The 13 polyalanine residues are conserved in gorilla, decreased in mouse, rat, and pig and is absent in zebrafish. **D**: Representative RE digest performed to screen control DNAs for the prevalence of G44A or G210V. Three bands are detected in DNA samples carrying G210V or G44A amino acid substitutions (+) while wildtype (-) samples have two bands.

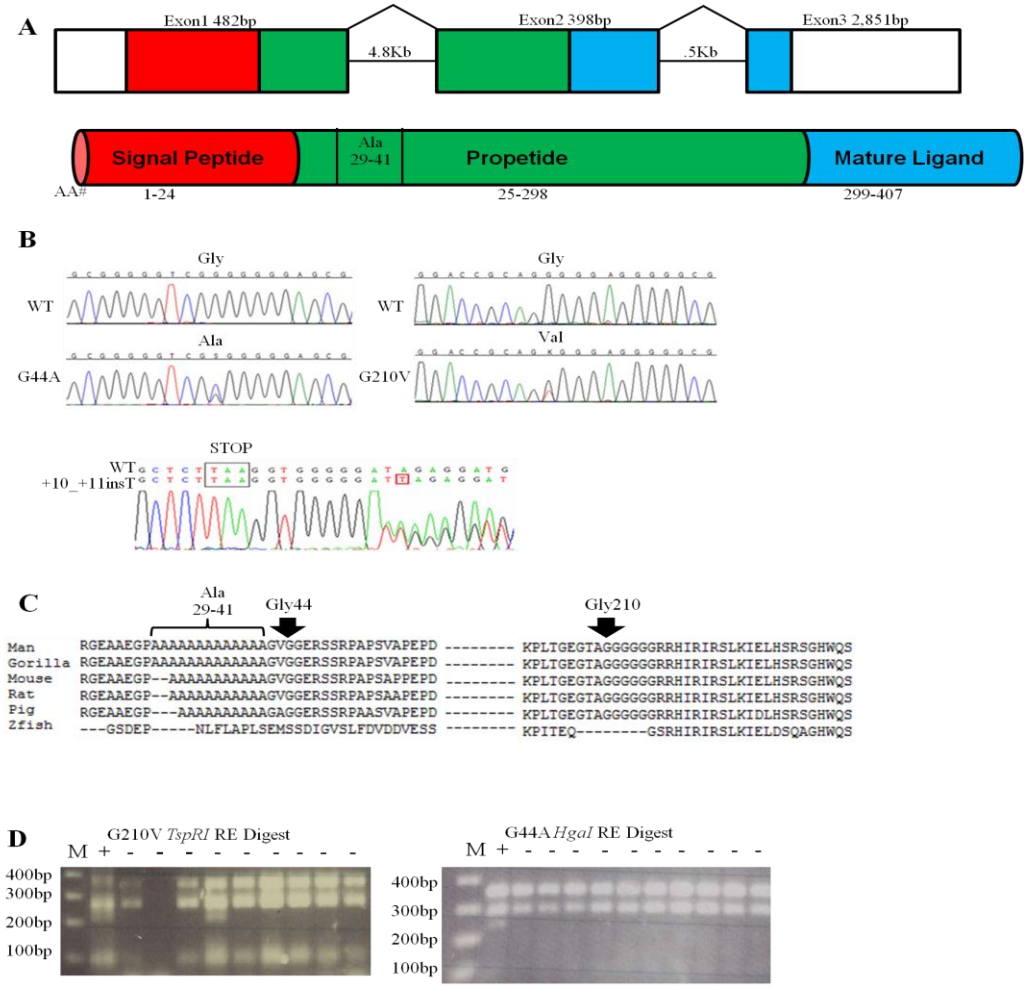

Figure 2.10 Polyalanine genotyping and single allele-sequences.

A: Size fragment genotypes for polyalanine sequence variants are depicted. Relative sizes of PCR fragments containing 10, 14 or 17 alanines are depicted with reference to the wildtype genotype (red rectangle). B: Chromatograms for PCR fragments spanning the polyalanine stretch are displayed with alanine number depicted as boxes over the GCG and GCA alanine triplet codons.

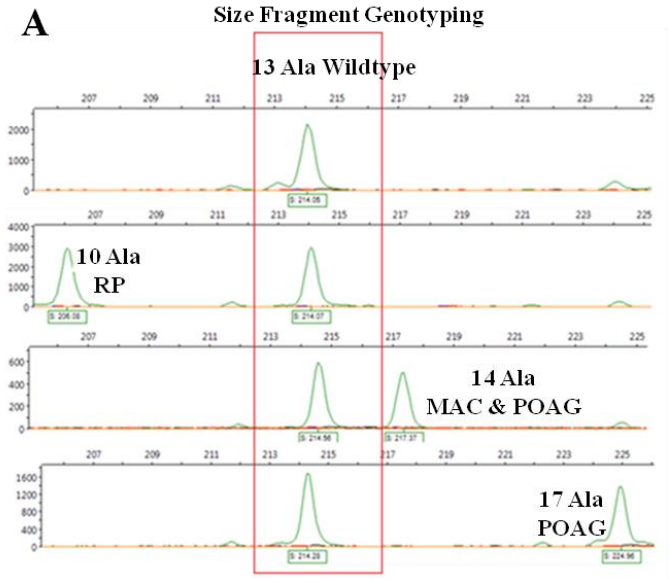

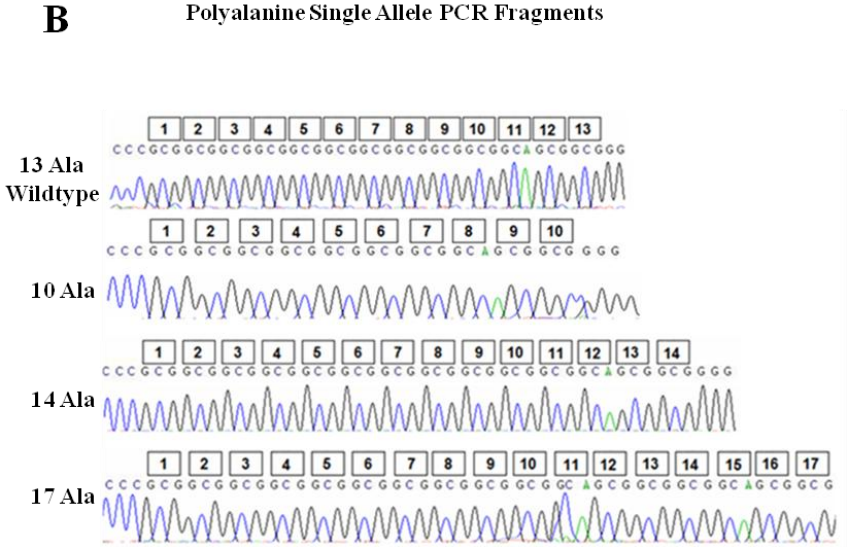

Figure 2.11 Western analysis of *GDF11* sequence variants.

A: Media protein isolates show exhibit an approximately 50kDA band detected in polyalanine sequence variants as well as G44A. G210V displays reduced levels of the 50kDa band and increased levels of an approximately 100kDa band (see red arrows). The 15kDa band thought to represent mature *GDF11* signaling ligand is present but is reduced in G210V as compared to WT. Secreted Alkaline Phosphatase, SEAP, was probed to demonstrate equal loading of protein samples. A': The high abundance of the G210V specific 100kDa band is further illustrated in an over exposed blot that is reduced in the other samples. G210V 50kDa and 15kDa bands are reduced while no gross differences are observed for the other samples with reference to the controls. B: Whole Cell lysates display no gross difference of *GDF11* sequence variant protein samples as compared to WT controls. No appreciable differences were detected in loading of protein samples as demonstrated by equal amounts of a band corresponding to α-tubulin.

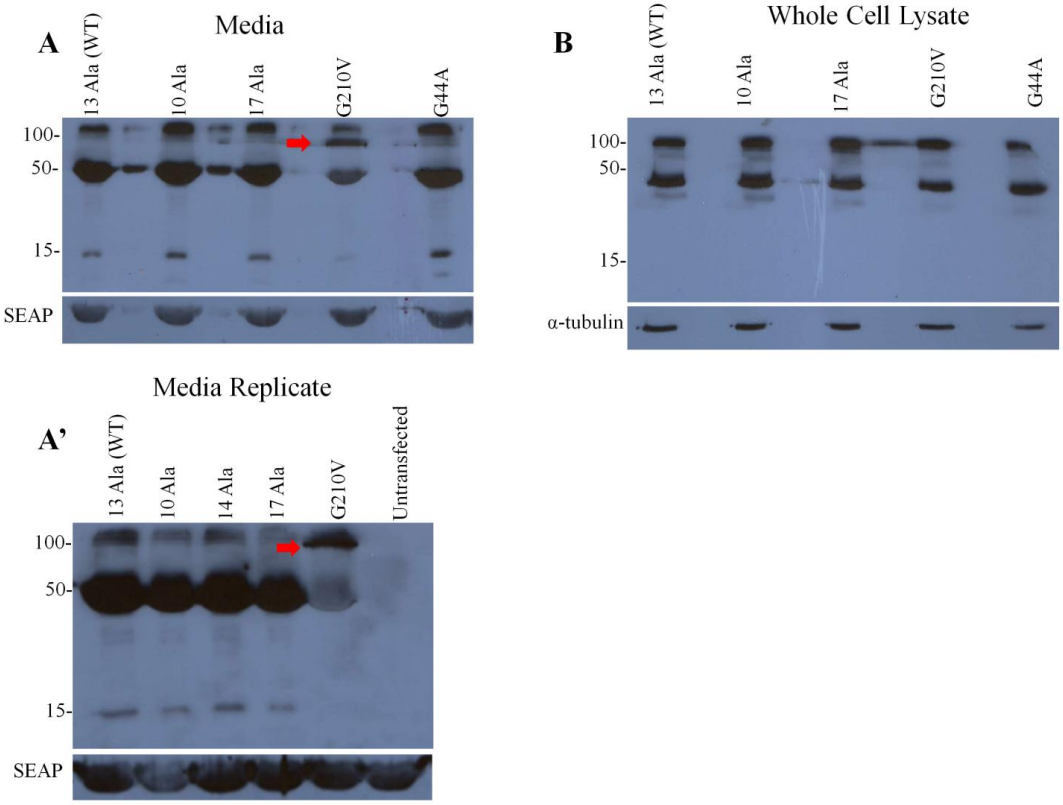

Figure 2.12 Summary of observed changes in retinal populations of *gdf11* morphants.

A general diagram documenting the change of RPC fate upon inhibition of *gdf11* activity. In the normal state, *gdf11* inhibits prolonged RGC proliferation to allow for the birth of later born cell types such as amacrines, rods, and cones which exhibit cell specific markers *runx1*, *otx2*, *crx*, and *neuroD* annotated below the cell type. Interestingly, the transcription factors normally associated with photoreceptor development are increased in this study while the population of photoreceptors are reduced as assayed by IHC. This may indicate a change in the expression profile of RPCs.

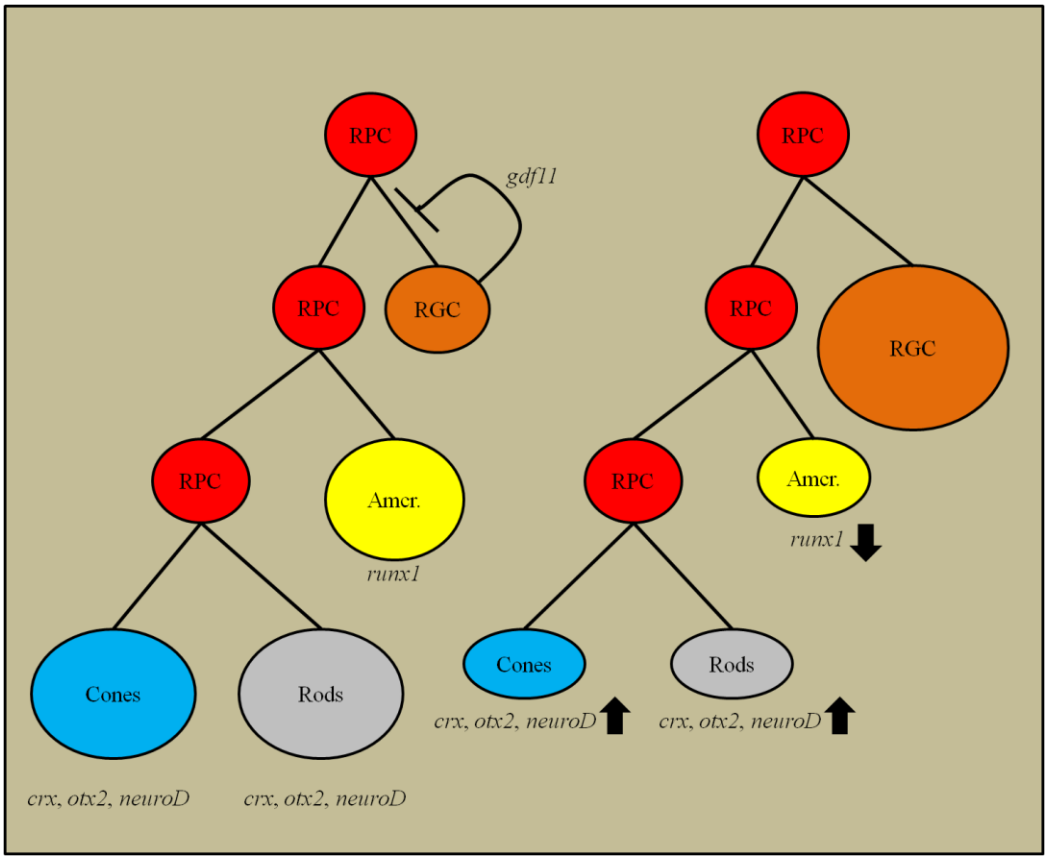

References

1. Gamer LW, Wolfman NM, Celeste AJ, Hattersley G, Hewick R, Rosen V. A novel BMP expressed in developing mouse limb, spinal cord, and tail bud is a potent mesoderm inducer in Xenopus embryos. Dev Biol 1999; 208(1):222-32.

2. Nakashima M, Toyono T, Akamine A, Joyner A. Expression of growth/differentiation factor 11, a new member of the BMP/TGFbeta superfamily during mouse embryogenesis. Mech Dev 1999; 80(2):185-9.

3. McPherron AC, Lawler AM, Lee SJ. Regulation of anterior/posterior patterning of the axial skeleton by growth/differentiation factor 11. Nat Genet 1999; 22(3):260-4.

4. Oh SP, Yeo CY, Lee Y, Schrewe H, Whitman M, Li E. Activin type IIA and IIB receptors mediate Gdf11 signaling in axial vertebral patterning. Genes Dev 2002; 16(21):2749-54.

5. McPherron AC, Lee SJ. Double muscling in cattle due to mutations in the myostatin gene. Proc Natl Acad Sci U S A 1997; 94(23):12457-61.

6. Gamer LW, Cox KA, Small C, Rosen V. Gdf11 is a negative regulator of chondrogenesis and myogenesis in the developing chick limb. Dev Biol 2001; 229(2):407-20.

7. Murali D, Yoshikawa S, Corrigan RR, Plas DJ, Crair MC, Oliver G, Lyons KM, Mishina Y, Furuta Y. Distinct developmental programs require

different levels of Bmp signaling during mouse retinal development. Development 2005; 132(5):913-23.

8. Wu HH, Ivkovic S, Murray RC, Jaramillo S, Lyons KM, Johnson JE, Calof AL. Autoregulation of neurogenesis by GDF11. Neuron 2003; 37(2):197-207.

9. Kim J, Wu HH, Lander AD, Lyons KM, Matzuk MM, Calof AL. GDF11 controls the timing of progenitor cell competence in developing retina. Science 2005; 308(5730):1927-30.

10. Biga PR, Roberts SB, Iliev DB, McCauley LA, Moon JS, Collodi P, Goetz FW. The isolation, characterization, and expression of a novel GDF11 gene and a second myostatin form in zebrafish, Danio rerio. Comp Biochem Physiol B Biochem Mol Biol 2005; 141(2):218-30.

11. Kimmel CB, Ballard WW, Kimmel SR, Ullmann B, Schilling TF. Stages of embryonic development of the zebrafish. Dev Dyn 1995; 203(3):253-310.

12. Farooq M, Sulochana KN, Pan X, To J, Sheng D, Gong Z, Ge R. Histone deacetylase 3 (hdac3) is specifically required for liver development in zebrafish. Dev Biol 2008; 317(1):336-53.

13. Murata Y, Tamura M, Aita Y, Fujimura K, Murakami Y, Okabe M, Okada N, Tanaka M. Allometric growth of the trunk leads to the rostral shift of the pelvic fin in teleost fishes. Dev Biol 2010; 347(1):236-45.

14. Asai-Coakwell M, French CR, Berry KM, Ye M, Koss R, Somerville M, Mueller R, van Heyningen V, Waskiewicz AJ, Lehmann OJ. GDF6, a novel locus

for a spectrum of ocular developmental anomalies. Am J Hum Genet 2007; 80(2):306-15.

15. Ye M, Berry-Wynne KM, Asai-Coakwell M, Sundaresan P, Footz T, French CR, Abitbol M, Fleisch VC, Corbett N, Allison WT, Drummond G, Walter MA, Underhill TM, Waskiewicz AJ, Lehmann OJ. Mutation of the bone morphogenetic protein GDF3 causes ocular and skeletal anomalies. Hum Mol Genet 2010; 19(2):287-98.

16. Wyatt AW, Osborne RJ, Stewart H, Ragge NK. Bone morphogenetic protein 7 (BMP7) mutations are associated with variable ocular, brain, ear, palate, and skeletal anomalies. Hum Mutat 2010; 31(7):781-7.

17. Bakrania P, Efthymiou M, Klein JC, Salt A, Bunyan DJ, Wyatt A, Ponting CP, Martin A, Williams S, Lindley V, Gilmore J, Restori M, Robson AG, Neveu MM, Holder GE, Collin JR, Robinson DO, Farndon P, Johansen-Berg H, Gerrelli D, Ragge NK. Mutations in BMP4 cause eye, brain, and digit developmental anomalies: overlap between the BMP4 and hedgehog signaling pathways. Am J Hum Genet 2008; 82(2):304-19.

18. French CR, Erickson T, French DV, Pilgrim DB, Waskiewicz AJ. Gdf6a is required for the initiation of dorsal-ventral retinal patterning and lens development. Dev Biol 2009; 333(1):37-47.

19. Gosse NJ, Baier H. An essential role for Radar (Gdf6a) in inducing dorsal fate in the zebrafish retina. Proc Natl Acad Sci U S A 2009; 106(7):2236-41.

20. Asai-Coakwell M, French CR, Ye M, Garcha K, Bigot K, Perera AG, Staehling-Hampton K, Mema SC, Chanda B, Mushegian A, Bamforth S, Doschak

MR, Li G, Dobbs MB, Giampietro PF, Brooks BP, Vijayalakshmi P, Sauve Y, Abitbol M, Sundaresan P, van Heyningen V, Pourquie O, Underhill TM, Waskiewicz AJ, Lehmann OJ. Incomplete penetrance and phenotypic variability characterize Gdf6-attributable oculo-skeletal phenotypes. Hum Mol Genet 2009; 18(6):1110-21.

21. Yokoe T, Ohmachi T, Inoue H, Mimori K, Tanaka F, Kusunoki M, Mori M. Clinical significance of growth differentiation factor 11 in colorectal cancer. Int J Oncol 2007; 31(5):1097-101.

22. Fingert JH, Honkanen RA, Shankar SP, Affatigato LM, Ehlinger MA, Moore MD, Jampol LM, Sheffield VC, Stone EM, Alward WL. Familial cavitary optic disk anomalies: identification of a novel genetic locus. Am J Ophthalmol 2007; 143(5):795-800.

23. Parichy DM, Elizondo MR, Mills MG, Gordon TN, Engeszer RE. Normal table of postembryonic zebrafish development: staging by externally visible anatomy of the living fish. Dev Dyn 2009; 238(12):2975-3015.

24. Gerety SS, Wilkinson DG. Morpholino artifacts provide pitfalls and reveal a novel role for pro-apoptotic genes in hindbrain boundary development. Dev Biol 2011; 350(2):279-89.

25. Danilova N, Kumagai A, Lin J. p53 upregulation is a frequent response to deficiency of cell-essential genes. PLoS One 2010; 5(12):e15938.

26. Stewart L, Potok MA, Camper SA, Stifani S. Runx1 expression defines a subpopulation of displaced amacrine cells in the developing mouse retina. J Neurochem 2005; 94(6):1739-45.

27. Hitchcock P, Kakuk-Atkins L. The basic helix-loop-helix transcription factor neuroD is expressed in the rod lineage of the teleost retina. J Comp Neurol 2004; 477(1):108-17.

28. Ochocinska MJ, Hitchcock PF. NeuroD regulates proliferation of photoreceptor progenitors in the retina of the zebrafish. Mech Dev 2009; 126(3-4):128-41.

29. Ochocinska MJ, Hitchcock PF. Dynamic expression of the basic helix-loop-helix transcription factor neuroD in the rod and cone photoreceptor lineages in the retina of the embryonic and larval zebrafish. J Comp Neurol 2007; 501(1):1-12.

30. Nishida A, Furukawa A, Koike C, Tano Y, Aizawa S, Matsuo I, Furukawa T. Otx2 homeobox gene controls retinal photoreceptor cell fate and pineal gland development. Nat Neurosci 2003; 6(12):1255-63.

31. Omori Y, Katoh K, Sato S, Muranishi Y, Chaya T, Onishi A, Minami T, Fujikado T, Furukawa T. Analysis of transcriptional regulatory pathways of photoreceptor genes by expression profiling of the Otx2-deficient retina. PLoS One 2011; 6(5):e19685.

32. Furukawa T, Morrow EM, Li T, Davis FC, Cepko CL. Retinopathy and attenuated circadian entrainment in Crx-deficient mice. Nat Genet 1999; 23(4):466-70.

33. Tajima T, Ohtake A, Hoshino M, Amemiya S, Sasaki N, Ishizu K, Fujieda K. OTX2 loss of function mutation causes anophthalmia and combined pituitary

hormone deficiency with a small anterior and ectopic posterior pituitary. J Clin Endocrinol Metab 2009; 94(1):314-9.

34. Diaczok D, Romero C, Zunich J, Marshall I, Radovick S. A novel dominant negative mutation of OTX2 associated with combined pituitary hormone deficiency. J Clin Endocrinol Metab 2008; 93(11):4351-9.

35. Furukawa T, Morrow EM, Cepko CL. Crx, a novel otx-like homeobox gene, shows photoreceptor-specific expression and regulates photoreceptor differentiation. Cell 1997; 91(4):531-41.

36. Shen YC, Raymond PA. Zebrafish cone-rod (crx) homeobox gene promotes retinogenesis. Dev Biol 2004; 269(1):237-51.

37. Ali M, McKibbin M, Booth A, Parry DA, Jain P, Riazuddin SA, Hejtmancik JF, Khan SN, Firasat S, Shires M, Gilmour DF, Towns K, Murphy AL, Azmanov D, Tournev I, Cherninkova S, Jafri H, Raashid Y, Toomes C, Craig J, Mackey DA, Kalaydjieva L, Riazuddin S, Inglehearn CF. Null mutations in LTBP2 cause primary congenital glaucoma. Am J Hum Genet 2009; 84(5):664-71.

38. Narooie-Nejad M, Paylakhi SH, Shojaee S, Fazlali Z, Rezaei Kanavi M, Nilforushan N, Yazdani S, Babrzadeh F, Suri F, Ronaghi M, Elahi E, Paisan-Ruiz C. Loss of function mutations in the gene encoding latent transforming growth factor beta binding protein 2, LTBP2, cause primary congenital glaucoma. Hum Mol Genet 2009; 18(20):3969-77.

39. Ge G, Hopkins DR, Ho WB, Greenspan DS. GDF11 forms a bone morphogenetic protein 1-activated latent complex that can modulate nerve growth factor-induced differentiation of PC12 cells. Mol Cell Biol 2005; 25(14):5846-58.

40. Messaed C, Rouleau GA. Molecular mechanisms underlying polyalanine diseases. Neurobiol Dis 2009; 34(3):397-405.

41. De Baere E, Beysen D, Oley C, Lorenz B, Cocquet J, De Sutter P, Devriendt K, Dixon M, Fellous M, Fryns JP, Garza A, Jonsrud C, Koivisto PA, Krause A, Leroy BP, Meire F, Plomp A, Van Maldergem L, De Paepe A, Veitia R, Messiaen L. FOXL2 and BPES: mutational hotspots, phenotypic variability, and revision of the genotype-phenotype correlation. Am J Hum Genet 2003; 72(2):478-87.

42. Caburet S, Demarez A, Moumne L, Fellous M, De Baere E, Veitia RA. A recurrent polyalanine expansion in the transcription factor FOXL2 induces extensive nuclear and cytoplasmic protein aggregation. J Med Genet 2004; 41(12):932-6.

43. Brais B, Bouchard JP, Xie YG, Rochefort DL, Chretien N, Tome FM, Lafreniere RG, Rommens JM, Uyama E, Nohira O, Blumen S, Korczyn AD, Heutink P, Mathieu J, Duranceau A, Codere F, Fardeau M, Rouleau GA. Short GCG expansions in the PABP2 gene cause oculopharyngeal muscular dystrophy. Nat Genet 1998; 18(2):164-7.

44. Felin JE, Mayo JL, Loos TJ, Jensen JD, Sperry DK, Gaufin SL, Meinhart CA, Moss JB, Bridgewater LC. Nuclear variants of bone morphogenetic proteins. BMC Cell Biol 2010; 11:20.

45. Haider NB, Jacobson SG, Cideciyan AV, Swiderski R, Streb LM, Searby C, Beck G, Hockey R, Hanna DB, Gorman S, Duhl D, Carmi R, Bennett J, Weleber RG, Fishman GA, Wright AF, Stone EM, Sheffield VC. Mutation of a nuclear receptor gene, NR2E3, causes enhanced S cone syndrome, a disorder of retinal cell fate. Nat Genet 2000; 24(2):127-31.

46. Alvarez-Delfin K, Morris AC, Snelson CD, Gamse JT, Gupta T, Marlow FL, Mullins MC, Burgess HA, Granato M, Fadool JM. Tbx2b is required for ultraviolet photoreceptor cell specification during zebrafish retinal development. Proc Natl Acad Sci U S A 2009; 106(6):2023-8.

Chapter 3 Evidence for additional *FREM1* heterogeneity in Manitoba Oculotrichoanal syndrome

A version of this chapter has been submitted to

Molecular Vision

Robertino Karlo Mateo, Royce Johnson, and Ordan J. Lehmann

Introduction

Manitoba Oculotrichoanal (MOTA) syndrome is a rare autosomal recessive disorder, first documented in the Island Lake region of Northern Manitoba [1]. Individuals of native Aboriginal descent (Canada's First Nations peoples) exhibited ocular anomalies, most notably a fusion of the upper eyelid to the globe, known as subtotal cryptophthalmos or hidden eye. Associated phenotypes included facial anomalies with aberrant hair distribution extending below the brow, nasal dimpling, as well as ano-genital anomalies [2-3]. The existence of a similar disorder in the Inuit [4], who are ancestrally related to the First Nations, suggested a common genetic etiology. MOTA syndrome is phenotypically similar to Fraser Syndrome (FS), with common features including cryptophthalmos, nasal and genital anomalies [5-6]; however MOTA probands are less severely affected and to our knowledge do not exhibit cognitive impairment, syndactyly, renal, auricular or limb defects.

Both disorders are autosomal recessively inherited [2]. Fraser syndrome cases are attributable to mutations in either *FRAS1* (Fraser syndrome 1) or *FREM2* (FRAS1-related extracellular matrix protein 2) [7-9], with these genes accounting for approximately 40% of cases. Other FRAS/FREM gene family members (*FREM1* and *FREM3*) form multi-protein complexes in the extracellular matrix that interact with *GRIP1*,(glutamate receptor-interacting protein 1) which serves to anchor *FRAS/FREM* proteins [10-11], and in which mutations were recently

detected in FS probands [12]. Linkage analysis of Fraser Syndrome to the vicinity of *FREM1* (chromosome 9p22.3) was reported 5 years ago, however no disease causing mutations were identified [13]. More recently, homozygous *FREM1* mutations were shown in a Middle Eastern sibship [14] to be associated with a bifid nose, anorectal and renal anomaly phenotype, but which lacked cryptophthalmos, suggesting that *FRAS/FREM* variants may contribute to a diverse spectrum of related disorders [15].

The *Fras/Frem* and*Grip1 genes* have been extensively studied in murine models, strains, collectively referred to as "bleb" mutants, due to epidermal blistering during embryonic development [16-19]. These exhibit cryptophthalmos, syndactyly and renal defects that correspond with those phenotypes observed in FS patients. *Fras/Frem* genes, which are expressed in a tissue specific manner and encode proteins that are secreted into the extracellular matrix, regulate the bioavailability of growth factors during development [20] and so have key roles in tissue morphogenesis [21-22]. *FRAS/FREM* proteins contain chondroitin sulfate proteoglycan (CSPG) domains, and their tissue specific expression is thought to maintain epithelial-mesenchymal integrity during development via a mechanism similar to *CSPG4* (or *NG2*), directly binding collagens V and VI as well as fibroblast growth factor (*FGF*) and epidermal growth factor (*EGF*) [23-24].

At the commencement of this study MOTA syndrome was molecularly undefined, with no *FRAS/FREM* family members known to underlie MOTA. We utilized homozygosity mapping, an approach that permits mapping of genes responsible

for autosomal recessive disorders [25-28]. Single nucleotide polymorphisms (SNPs) were used to identify regions that are Identical By Descent (IBD) in multiple affected individuals and so determine the genomic interval responsible for disease [29-30]. This methodology takes advantage of the geographically isolated nature of the First Nations community studied and MOTA's reported inheritance pattern, enabling the molecular basis to be elucidated using a very small number of patient samples.

Methods

Patients and genomic DNA collection

Affected individuals were derived from three pedigrees of Cree ancestry living in a geographically isolated region in Northern Alberta (**Fig. 3.1**). Since the area is only accessible during the winter by ice roads, this was anticipated to result in high levels of consanguinity in the approximately 1000 inhabitants. Blood samples were collected from four probands (1.III-1, 2.V-2, 3.III-1, and 3.III-7) and the unaffected parent (mother) that accompanied each child for oculoplastic surgery at the regional ophthalmic center, followed by genomic DNA extraction. *Ethical approval was provided by the University of Alberta Hospital Health Research Ethics Board, and informed consent was obtained from all participants.*

Genotyping and Homozygosity Mapping

Genotyping was performed using a 61*0-Quad* SNP array (*Illumina Inc. San Diego USA) comprising* approximately *28,000 Copy Number Variant (CNV) probes and 592,000 SNPs, spaced at a mean distance of 1 SNP per 2.7kb across the genome, and processed by deCODE genetics in Reykjavík, Iceland.* Raw data were analyzed using GenomeStudio software (Illumina), non-Mendelian genotypes removed using the software's Heritability Report algorithm, and then exported to PLINKv1.07 for homozygosity analysis [31]. Homozygous regions were then

analyzed to define IBD intervals common amongst the probands. Initial homozygosity analysis performed using default PLINK parameters [homozygous region >1Mb] did not identify an IBD interval common to all four probands. Subsequently, criteria were altered to permit detection of smaller homozygous segments [> 300kb] comprising at least 100 consecutive homozygous SNPs. In addition the percentage homozygosity of each genome was calculated utilizing the total length of homozygous regions >300kb divided by that of the autosomes [NCBI Build 36] [32] .

SNP Visualization of Genotype and CNV status

Two values were calculated from the array data to determine if any copy number variants were present. The first [B-Allele Frequency (BAF)] is derived from the relative ratio of fluorescent intensities of the two alleles at each SNP [Cy5 (green) A allele; Cy3 (red) B allele] with a heterozygous SNP having a BAF of 0.5, whilst homozygous SNPs are either 1 or 0. The second criterion used, is the logarithm of the ratio of the observed to the expected intensities at each SNP [Log_2R ratio (LRR)], with deviations from zero (log_21) providing evidence of a CNV [deletion = -1, duplication = 0.5, normal = 0]. Additional software [CnvPartition 3.1.6, Illumina *San Diego USA*] was used in parallel with LRR data to assign a CNV value for each SNP, and so detect any potential deletions or duplications.

Candidate Gene Sequencing

The coding and splice junctions of three genes lying in or adjacent to the genomic region of interest [*FREM1*, *CER1* [33] and *ZDHHC21* [34]] were sequenced using published primers [14] or those designed with Primer3 (**Table 3.3 and 3.4**). Genomic DNA from a single affected individual (1.III-1) was used as template and sequence data generated [ABI Prism 3100, Applied Biosystems, Foster City, USA] was analyzed relative to the ENSEMBL reference sequence [Sequencher 4.6, GeneCodes, Madison USA].

Evolutionary Conserved Regions (ECRs) within the IBD Region

In an effort to identify potential regulatory elements within the IBD interval, non-coding genomic sequences conserved in vertebrates were defined using ECR Browser [35], with appropriate correction for the different genomic builds [SNP array, Build 36, ECR Brower, Build 37] using the UCSC LiftOver Tool [32]. Criteria consisted of ECRs with a minimum length of 90bp and greater than 70% conservation of the human sequence against chimpanzee, rhesus monkey, cow, dog, opossum, rat, mouse, chicken, frog, pufferfish, or zebrafish genomes. ECRs conserved between human and xenopus (**Table 3.2**) were selected for further analysis and sequenced with primers designed by Primer 3 (**Table 3.5**).

Results

Phenotypic analysis

The four MOTA cases displayed a spectrum of ocular anomalies with considerable variation in phenotypic severity. There were both bilateral and unilateral involvement (**Fig. 3.2**), and cases with partial upper eyelid involvement most frequently affected the medial segment. Additional features included fusion of the eyelid to the cornea, which ranged in severity from total fusion (**Fig. 3.2D**) to focal synechiae (**Fig. 3.2E & F**), as well as frequent corneal opacification and corneal vascularisation (**Fig. 3.2G & H**). Aberrant facial development was evident from extension of hair distribution from the scalp to reach the eyebrow (**Fig. 3.2B & C**) as well as nasal dimpling (**Fig. 3.2B & D**).

Molecular analyses

Only a small number of SNPs [67 – 95 (~0.01%), (**Table 3.6**)] were excluded due to non-Mendelian errors, indicating that the genotyping data were of high quality. High homozygosity levels were observed in the four affected individuals [range: 9.3% – 15.8%] (**Table 3.7**), indicating very substantial degrees of consanguinity that contrast with the ~6% theoretically calculated for the offspring of a first cousin marriage [36-37]. Homozygosity mapping analysis identified only a single segment that is identical by descent in the four affected individuals. This 330kb

interval on 9p22.3 [Chr.9: 14,377,817 - 14,711,766, flanking SNPs rs2382470 and rs1494359] lies approximately 16kb 3' to the last exon of *FREM1* and the SNPs in this IBD interval display BAF values of 1 or 0 in the probands (demonstrating homozygosity) whilst the unaffected parents are heterozygous (BAF = ~0.5) (**Fig. 3.3A** upper panels). Equally, the LRR values cluster around zero for the 152 SNPs in the IBD region, demonstrating the absence of any CNVs (**Fig. 3.3A** lower panels). In particular, the SNPs encompassing *FREM1* [9: 14,727,151 - 14,900,234] have normal LRR values and additional automated CNV analysis (CnvPartition) demonstrated that no CNVs were detectable in either the IBD (data not shown) or *FREM1* intervals (**Fig. 3.3B**). Similarly, no CNVs or additional IBD regions were detected in the intervals encompassing *FRAS1*, *FREM2*, *FREM3*, or *GRIP1* (data not shown).

The IBD region contains two genes *CER1* (a TGF-β signalling antagonist) [33] and *ZDHCC21* (a regulator of hair follicle development) [34] and as illustrated (Fig. 4) its border is distinct from that of *FREM1*. Sequencing was performed initially for *CER1* and *ZDHCC21*, with no coding or splice site mutations identified. Notwithstanding the homozygosity mapping data, the 38 exons of *FREM1* were next sequenced and did not identify any causative variants. Ten homozygous variants were present: seven that result in synonymous amino acid substitutions, one non synonymous SNP (A1212S) present in 28% of controls (dbSNP rs35870000), and a 5'UTR variant [Table 1]. Notably a variant (c.5556A>G) that was recently described as contributing to MOTA [38], did not

segregate in an autosomal recessive pattern [homozygous 1.III-1; heterozygous 3.III-1 and 3.III-7; homozygous wildtype 2.V-2]. Seven non-coding regions within the IBD interval were found to be evolutionarily conserved with > 70% identity between humans and xenopus. Sequencing these seven regions identified a homozygous T>C base pair substitution that segregated with the disease phenotype [all probands: C/C, unaffected parents T/C (**Fig. 3.5**)].

Discussion

This study's key finding is the identification of a 330kb region on 9p22.3 that is associated with MOTA syndrome. This illustrates the value of studying consanguineous populations such as the First Nations with homozygosity analysis. These findings localize the causative variant to an interval adjacent to *FREM1*, which represents an excellent candidate on the basis of the recapitulation of the human phenotypes in *Frem1* mutant mice [39-40], and related phenotypes induced by mutation of other *FRAS/FREM* gene family members. This study was predicated on the assumption that the level of homozygosity in a geographically isolated population, living on a remote reserve, would be increased. The range of autosomal homozygosity observed (9.3% - 15.8%), which in some cases exceeds that observed in other consanguineous populations or in the offspring of first cousin marriages [36], validates the approach used and contrasts with the far lower rates observed in a general population (1.9% - 4.6%) [37]. These data, derived from a very small number of affected individuals, illustrate the applicability of homozygosity mapping in the First Nations and suggest that it may permit other causes of this population's disproportionately large disease burden to be identified.

Whilst this manuscript was in preparation, two papers were published that substantially advanced understanding of *FREM1*'s role in these disorders [15, 38]. The first, reported several *FREM1* mutations in MOTA cases of either First

Nations or European ancestry [38] including: an inframe deletion of exons 8-23, one nonsense, two missense, and a synonymous alteration (c.5556A>G). Notably, neither of the two variants identified in First Nations patients [deletion of exons 8 – 23 or c.5556A>G (G1853G)] is the cause in our cases, in view of the absence of CNVs in the 330kb region (**Fig. 3.3**) and the fact that c.5556A>G's does not segregate with disease (data not shown). Since a second causative allele was not identified in some individuals of Oji-Cree ancestry reported in Slavotinek et al.'s 2011 paper, the possibility therefore exists that a still to be identified allele is common to both the Oji-Cree and First Nations populations. The second publication describes heterozygous *FREM1* deletions and 3 missense variants that associate with metopic craniosynostosis as well as documenting the contribution of *FREM1* in patterning the murine cranial skeleton [15]. Accordingly our study demonstrates additional genetic heterogeneity amongst the First Nations, who would have been anticipated to have a single cause for the phenotype.

The most parsimonious explanation for our findings is that a sequence variant within the 330kb IBD interval, which is located 16kb 3' of *FREM1*'s last known exon, causes MOTA. This is most likely to represent a regulatory element; however the possibility that an additional exon remains to be defined, cannot be excluded. Support for the concept of a regulatory variant is provided by the *Frem1*^{bfd} murine strain, which lacks a coding *Frem1* mutation and is believed to have a variant in a control region that causes cryptophthalmos-like phenotypes [40]. *Frem1*'s role during development suggests that its temporal-spatial

expression is tightly controlled, in keeping with the regulatory elements and tissue specific enhancers defined for a range of other developmental regulatory genes [41]. There are several examples of such mutated sequences in both ocular and systemic diseases, with regulatory mutations 3' to *PAX6* causing aniridia and demonstrated to be functionally relevant by murine transgenesis rescue experiments [42-43]. In an attempt to define such elements, seven regions conserved across vertebrates were sequenced, identifying a homozygous T>C base pair substitution (ECR-7) that segregated with the phenotype. Bioinformatics analysis for regulatory elements using the VISTA Enhancer Browser online data base [44] yielded no tissue specific enhancers for this region (data not shown). The most likely explanation is that this variant is in linkage disequilibrium with the true mutation, and it should be noted that sequence conservation is not necessarily a criteria of all regulatory elements [45]. Future research directions to support the relevancy of the identified 330kb IBD region could include assaying *FREM1* expression from mRNA isolated from skin fibroblasts of MOTA probands, relative to a housekeeping gene and control samples. In parallel, next generation sequencing of the 330kb IBD interval is increasingly feasible. It is interesting to note that the transcription factor delta-Np63 has been shown to control expression of members of the Fras/Frem gene family and displays enhancer activity in the murine nose, eyelids, genitals, and digits [46-47], the tissue domains affected in FS, BNAR, and MOTA.

In summary, this study extends *FREM1* heterogeneity in MOTA syndrome of First Nations ancestry. Homozygosity mapping defined one 330kb IBD region on 9p22.3 comprising 152 SNPs in 4 probands. Sequencing the genes in or adjacent to this interval (*FREM1*, *CER1*, and *ZDHHC21*) revealed no disease-causing mutations. Accordingly, we infer that a variant within this region is responsible for MOTA syndrome, and suggest that future studies are indicated to define the causative mutation and by facilitating genetic counselling, reduce the high prevalence of MOTA syndrome in these isolated populations.

Table 3.1 Sequence variants identified in 1.III-1

Sequence variants are homozygous base pair substitutions that result in synonymous amino acid changes with the exception of A1212S, present in 28% of controls (Coriell Collection). Variant annotations are based on *ZDHHC21* (ENST00000380916), and *FREM1* (ENST00000422223) transcripts where the A of the start codon = 1. No sequence variants were identified in *CER1*.

Gene	Exon	Variant	Amino Acid Residue	dbSNP Reference Number
ZDHHC21	exon 6	c.318 T>C	C106C	rs17215796
FREM1	exon 3	c.-135C>G	N/A	
	exon 5	c.456 A>G	Q152Q	rs10961757
	exon 21	c.3634 G>T	A1212S	rs35870000
	exon 26	c.4785 C>T	A1595A	rs10733289
	exon 26	c.4791 T>C	D1597D	rs1032474
	exon 27	c.5004 C>A	I1668I	rs17219005
	exon 31	c.5556 A>G	G1853G	Not described
	exon 34	c.5859 T>C	V1953V	rs4741426

Table 3.2 Conserved Regions identified within the 330kb IBD Region

Non-coding genomic regions within the IBD interval are of approximately 100bp or larger, >70% sequence conservation in vertebrate species are listed in the table as well as their genomic positions on chromosome 9 (Build 37). % identity refers to sequence conservation for vertebrate genomes within the confines of ECR Browser, human, chimpanzee, rhesus macaque, cow, dog, opossum, rat, mouse, chicken, and frog. No ECRs of the stated criteria were found to be conserved in puffer fish or zebrafish.

ECR	Genomic position chr9	Length (bp)	% identity
1	14423929-14424022	94	89%
2	14443290-14443585	296	80%
3	14520772-14520883	112	71%
4	14521314-14521641	328	74%
5	14521719-14522534	816	78%
6	14522575-14522705	131	72%
7	14549013-14549211	199	71%

Figure 3.1 MOTA pedigrees investigated

The three MOTA pedigrees exhibit an inheritance pattern compatible with autosomal recessive disease. [Asterisks denote individuals that provided blood samples]

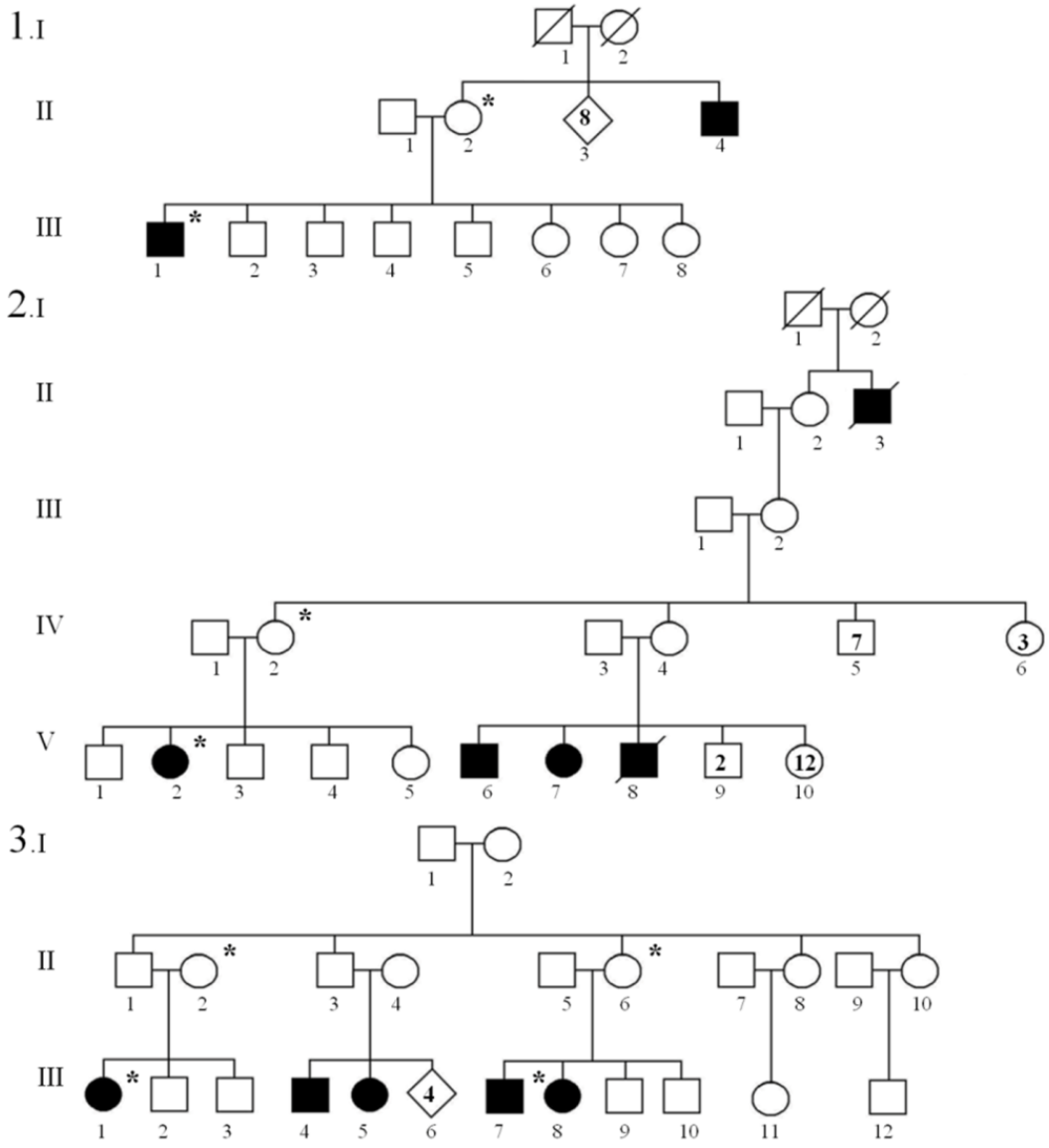

Figure 3.2 MOTA phenotypic spectrum in Albertan First Nations pedigrees

The oculo-facial phenotypes observed are diverse, ranging from isolated ocular anomalies to broader characteristics including dimpled noses (white arrows) and aberrant hair wedges where hair extends across the forehead to reach the eyebrow (black arrows). As evident from the montage, the ocular malformations can be bilateral (A, B) or unilateral (C, D), and vary in terms of the degree of lid involvement from isolated fusion (D) to abortive cryptophthalmos (E). Associated features include corneopalpebral synechiae (E, F), corneal opacification (G) and vascularisation (H).

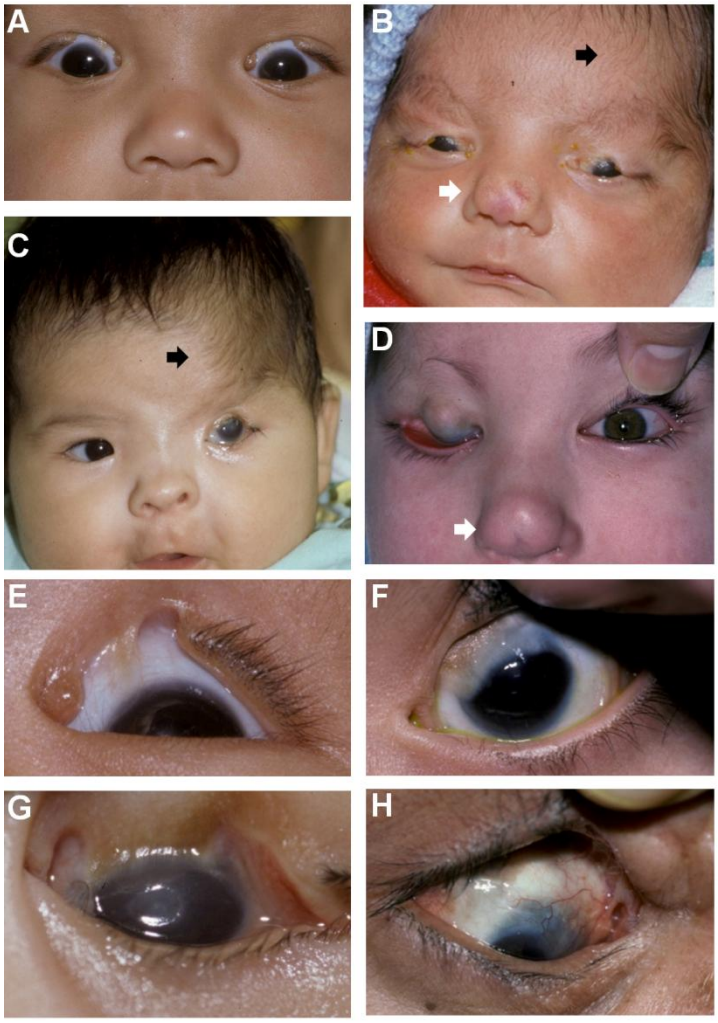

Figure 3.3 Montage illustrating representative genotype and copy number data across the IBD interval and *FREM1*

A: Genotype status (upper panels) and copy number data (lower panels) are provided for the first 55 SNPs in the IBD region (Chr9: 14,377,817-14,484,388). The BAF plots demonstrate homozygosity in the probands (BAF = 1 or 0) and heterozygosity in the unaffected parents (BAF = 0.5). The LRR plots also suggest no CNVs are present (LRR ~ 0). **B:** The lack of CNVs in *FREM1* (14,727,151-14,900,234) is evident from LRR plots. CnvPartition did not detect any CNVs in this region as all 96 SNPs in this region were assigned a normal CNV value of 2.

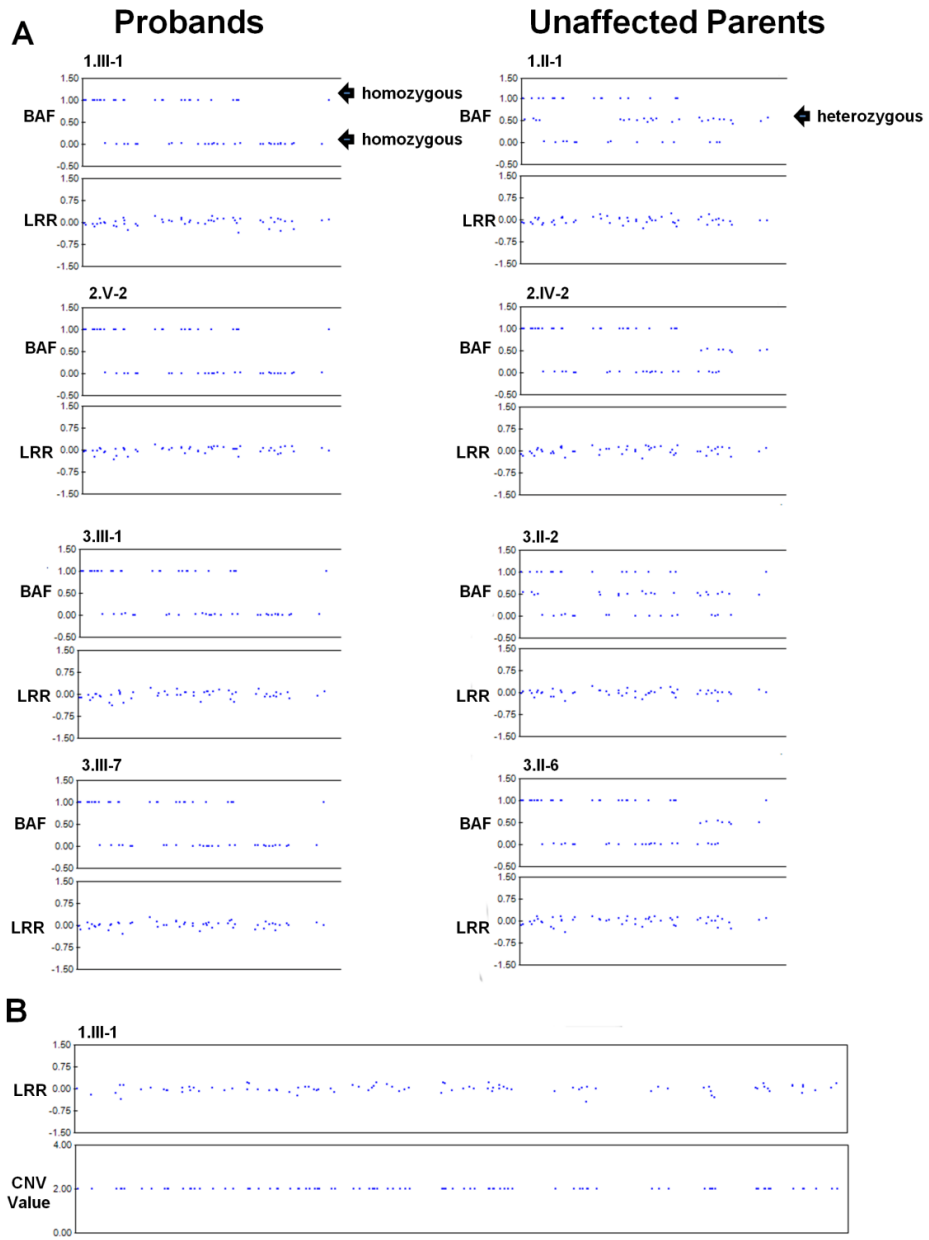

Figure 3.4 Illustration of the homozygous regions and IBD interval in the four probands

The regions of homozygosity, which range from 330kb to 10.4Mb, include a 330kb IBD interval common to all probands (red line). This interval contains *ZDHHC21* and *CER1*, and is 16kb 3 prime of *FREM1*'s last exon. Homozygosity mapping defined one IBD interval suggesting that mutation responsible for MOTA lies within the narrow 330kb region.

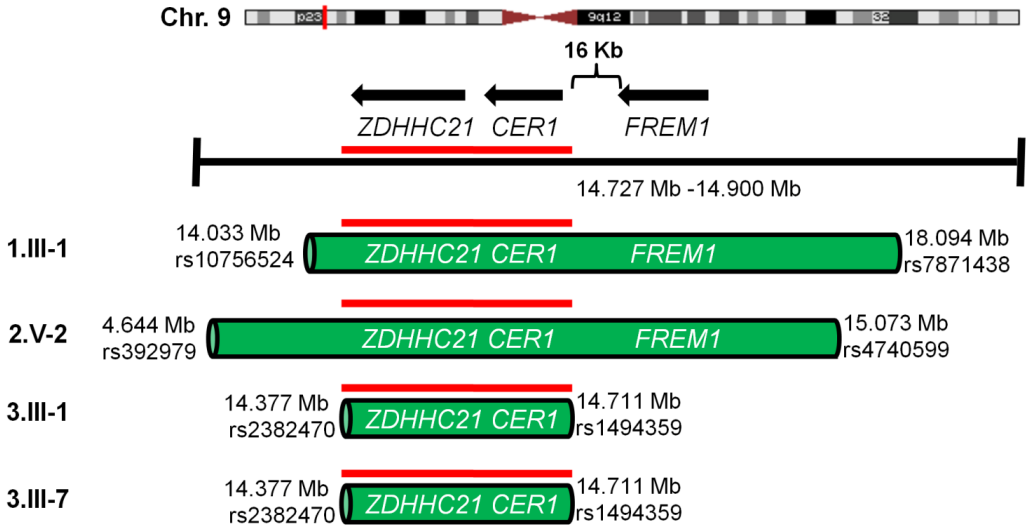

Table 3.3 Primers used to amplify *CER1* and *ZDHHC21*

Amplicon	Forward Primer (5' to 3')	Reverse Primer (5' to 3')
CER1		
1	CCGCCAGGCAGGTATCTAT	CTACTCTCCATCCATCCCAG
2-1	TCCATAGCTTCTGCATTATGTG	TTTCAAGTCACCTTTCCCTG
2-2	CAGGATTCCTTTATCCCAGG	TTGCTGGTGATTTGACACAC
ZDHHC21		
1	CCAGGTGCAAGCGCTCTGGA	GCACCGAGAAACCCCCGGGT
2	TCTACAAAAGGGCAGGTTGG	CCTTCACACCAGGCTTTACC
3	TGGGTGGGATATGAAAGCAC	TTGCTAACTGACAATTAAGTGCATC
4	CTACAGAAAGAAAATGTCAAATATGC	GGTCTTCATGCACTTTGCAG
5	ATGGTGGCCAAATCTGTTTTCCCTT	TGGTGAAACTGCCGGGGTGC
6	GCAGCATTTATGGCAAACAC	GGGAGTTGACAGAACCATATAATC
7	TGTGGACTTCCTTTGTGAAGTG	CTGGGGTTCACGCCATTC
8	GCTCAATTCTTGATTATTATTGCG	GCATGGGTAATTTTCTCCTTTG
9	TTTTCCAAGGGGATTCCAG	GCACAGGCCTCAGACAATG
10-1	GCTGCATGCCATAATGAAAG	TTGTTCACTCCTATGCTGCTG
10-2	TCAAATTAGCTTTCCACAGGG	ATGCCCACTGGTCAGGAG
10-3	TTCACCAAAACCAACATGAAAG	GCTACTAGTAAAAGGTCTCTCAATGC
10-4	GAGAACTCCTGACCAGTGGGCA	TCCAAACCCTTGTGCCTGACATGA
10-5	TGAAAGTAAGGAACAATACCTGGG	TGCCCAGTACCCACTGCTAC

Table 3.4 Primers used to amplify *FREM1*

	Forward (5' to 3')	Reverse (5' to 3')
1	TCTGCATTATTGGGATCACG	ATTCTCACGCATGCTCCAC
2	CCAACCAGCAGAAGGCAC	TCACACAAACAATCTCTGGG
3-1	AGGCTGGTTGAAAGATCCCT	GGTTGATGCTGATGAAGGTG
3-2	CACAGAAGCCCTCCTTTGTT	TCGTCTTTGATGGCTTGAGG
4	GAGGTGGTGGTGGTGAAGAC	CTCAGGCCTCCAGTTTCTGT
5	CAAATTTGGTGAAGGCCAAT	TCATCATGGTGGAAGGTGAG
6	CATGGGACGGAGTACTGGTT	AGCACAGGAACTCTCCCTGG
7	CAGGCTTCAGGTCACTGCTA	AGGAACCTGAGGGTTTAGGG
8	CTGAATCCACTGTGTGTGGG	AAACTACCTTTCTTTCCTGACCC
9	GCACGTTGGCATGTCATAGA	GGTTTAAACAATGAGCCACG
10	CAGCCTCTACTGTATTGATGCTT	CTCGGACACAATTTCAGCAA
11	TGCAGATTCCTTGGGTACAT	GGGTCCCATAGTTAAATGACCTT
12	CTGTGACTAGGTGATTGTGGG	CCTGACCAATGGAGCAAGTAA
13	TGGACTTAATGCTAGAATCTCCC	GACCAACATTCTCAGGCACA
14	CAAAGTGATGATGGTGGCAT	GACTCCCTTCTCCCTGCTTT
15	TGCATGTGAAGATAATACTGGAA	TGTGTTAAGTGGCATGTTGG
16	GCCTTGGAAGAGCTCATGTATC	CTCCAGAGTCATGAGCCAAA
17	TGCCTGTCATTCTGACTATGAG	GACTGTTTGATTATGGGAGCC
18	TTTCCTTGCTGTTTCAATGC	AAGGACAATTCCATATGGTGG
19	TTTGCACGTGGGAGGCTT	GCCCGGTGCTTTAAACATT
20	GCAGCCCTTGATAGCAAGATA	TGTGTTAATGCACTTGGAGCA
21	TCCTTTGTCCTTCATGGAAAT	AATCCTCCCACCCTCAGC
22	TTCACCCTACTGCACTGATAAA	CGAAGACTTGCTTCTTTGGG
23	GAGCCTGTTTCATTCCTCTCA	AGCATGAATTCACCCTGAAC
24	TGAAACCCTTTGGTTGAAGC	AAAGCAGGTGAGAAGCCAAA
25	GCCTTTGTCTTCTGCCTTTG	AGCTGCACCAGAGCTGAAA
26	TCATTTGAGTCACAACACGACA	TGAAGTGAGCCAAGATCACG
27	TTGCTGAGGCTGTTGTGAAC	CAAATGGGCCTGCACTTAAT
28	AGCTCGCTGCATTTGAGTTT	TCCATGAGCTTGTGAAATGG
29	TTTCCATCACTGGTGTAGGTTG	AGGGCCAAGGAGGTTTTGTGCT
30	TCCAGTATGAGGGAGAATAGCTG	TCCCTGAGGAGTTTCTAGTTGG
31	TCGGGCTACTGCAGTCTAGC	TTATCAAGCACGTTGGCTGT
32	TAATGACAAGCTGCTCCAGG	AAACAGCTTCTTCAGTGTTTCAG
33-34	GCAAGATCTTACTTGGTGGTTT	CCCAACCTTGGAGGCTATTT

35	GAAGACCCAAAGGAGGTGAA	GCAGGAAGATGTAGCATGGG
36	TGAAGTTAGGGAACTCGTAGGAC	ATGAATGAAGCAGCTCTCCG
37	CCCACCCTGCAGATACTTT	TGGCTAGATCTATTGGTTGCC
38	AACCTGGGCCCACACTTGCA	GCTCCAAAGGGACAACTTTGCGG

Table 3.5 Primers used to amplify ECRs

Amplicon	Forward Primer (5' to 3')	Reverse Primer (5' to 3')
1	CCCCACACACAACACACTTGCA	TCCTGGACAGCAAACCCAGTGAA
2	ACTCCCAGTGAGGTGGGTTCCC	TGCTGTTTGCAAAAGAAGTGGGCA
3	ACGTTGAGCTTTCACGAGACGCC	TGGGGAGGGGTATGGCCAGC
4	ACTACCTCTCATCCCAGCACTCTGA	CTGCTATTGTGGCCGGGGGC
5-1	TTTCACAGCAGCCGGCCTGG	AGCAGTTAGCCGCCCACTTGC
5-2	AGCTGTCCGACGTTTTCCCAGC	GCACCAGGCCCATTGCCTCC
6	GCAAGTGGGCGGCTAACTGCT	GCACCAGGCCCATTGCCTCC
7	GCCACCCTGGGACCCATCCT	CCCCCTCCACCTGAGCTTGC

Table 3.6 Erroneous SNPs identified

GenomeStudio's heritability report algorithm was used to identify potentially discrepant parent-child relationships and reveal non-Mendelian genotyping errors. Erroneous SNPs were removed prior to homozygosity analysis with PLINK. More than 99.9% of SNPs were inherited in a Mendelian manner (from unaffected mothers to probands) verifying correct parent child relationship.

Proband	Unaffected Parent	Correct SNPs	Erroneous SNPs	Total SNPs	P-C Heritability Freq
1.III-1	1.II-2	591009	69	591078	0.9998832
2.V-2	2.IV-2	590820	83	590903	0.9998595
3.III-1	3.II-2	590903	95	590998	0.9998392
3.III-7	3.II-6	590934	67	591001	0.9998866

Table 3.7 Percentage genome homozygosity of individuals studied

Percentage homozygosity was derived from the ratio of the total length of all autosomal homozygous regions, divided by the length of all autosomes (2867Mb).

Individual	Homozygous Regions (Mb)	% Genome Homozygosity
1.II-2	362.77	12.6
1.III-1	396.50	13.8
2.IV-2	367.93	12.8
2.V-2	344.77	12.0
3.II-2	187.58	6.5
3.III-1	267.57	9.3
3.II-6	388.21	13.5
3.III-7	451.87	15.8

Figure 3.5 A homozygous point mutation within ECR7 segregates with MOTA

Electropherograms of a point mutation found to segregate with the disease are shown for the four probands and the unaffected parents in a ECR-7, a region identified by ECR Browser to be conserved from human, chimpanzee, rhesus macaque, cow, opossum, rat, mouse, chicken and frog, but not in puffer fish or zebrafish. Probands are homozygous C/C while unaffected parents are C/T. The genomic reference used to compare sequence is T/T in this position.

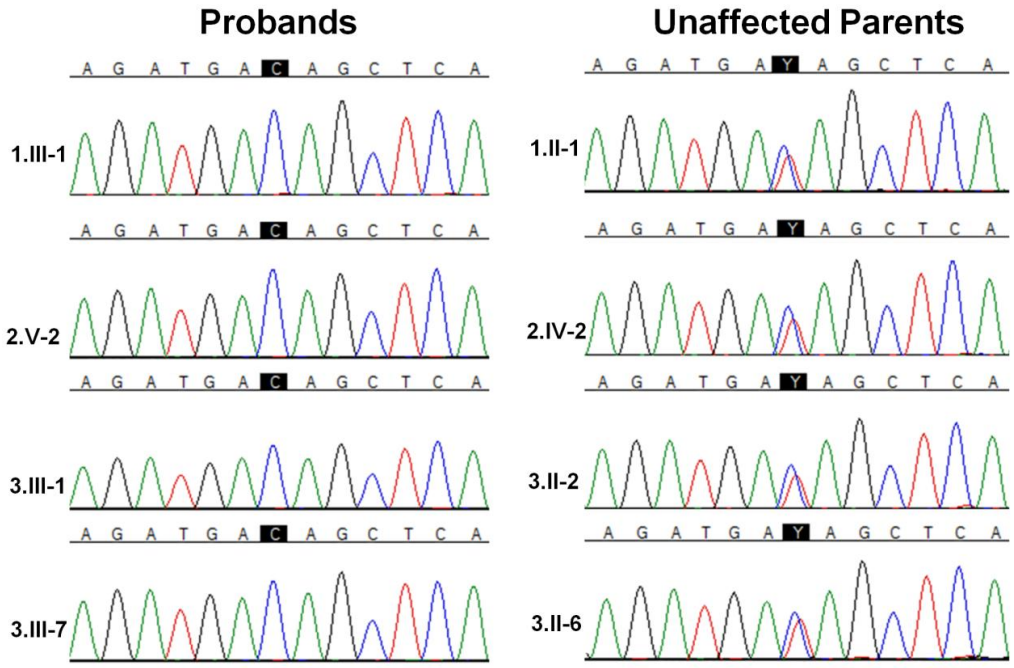

Table 3.8 SNP genotypes for probands and unaffected parents in the Identity By Descent region and *FREM1*

SNPs are shown for the Identity By Descent region (14,377,817 - 14,711,766), the coding region of *FREM1* (14,727,506-14,909,539), and the region between the two for the probands and unaffected mothers. Missed genotype calls are indicated by a "-". SNPs in the IBD region are in italics while SNPs within *FREM1* are in bold. Homozygous genotypes in the probands are highlighted in blue, orange, red, or green. Heterozygous genotypes found in either probands or parents are highlighted in brown. Chromosomal positions are based on NCBI Build 36.

Chr9 Position	SNP Name	1.III-1	1.II-2	2.V-2	2.IV-2	3.III-1	3.II-2	3.III-7
14369104	rs1108676	CC	AC	AA	AA	AC	AC	AC
14370070	rs12341650	AA	AG	GG	GG	AG	AG	AG
14370528	rs568008	GG	AG	AA	AA	AG	AG	AG
14370945	rs630973	AA	AA	AA	AA	AA	AA	AA
14373316	rs17708974	AA	AC	CC	CC	AC	AC	AC
14374950	rs679613	GG	GG	GG	GG	GG	AG	GG
14374976	rs10810134	GG	AG	AA	AA	AG	AG	AG
14377817	*rs2382470*	GG	GG	GG	GG	GG	GG	GG
14379011	*rs717932*	GG	AG	GG	GG	GG	AG	GG
14381869	*rs2382474*	CC	CC	CC	CC	CC	CC	CC
14382785	*rs2208919*	GG	AG	GG	GG	GG	AG	GG
14383854	*rs10810136*	GG	AG	GG	GG	GG	AG	GG
14385035	*rs2076872*	GG	GG	GG	GG	GG	GG	GG
14385595	*rs1807429*	CC	AC	CC	CC	CC	AC	CC
14386833	*rs10481545*	GG	GG	GG	GG	GG	GG	GG
14387276	*rs16931705*	AA	AA	AA	AA	AA	AA	AA
14391281	*rs17709614*	GG	GG	GG	GG	GG	GG	GG
14391932	*rs1323349*	CC	CC	CC	CC	CC	CC	CC
14392446	*rs7873382*	AA	AA	AA	AA	AA	AA	AA
14395158	*rs7042750*	GG	GG	GG	GG	GG	GG	GG
14395555	*rs11788403*	CC	CC	CC	CC	CC	CC	CC
14395801	*rs1570499*	AA	AA	AA	AA	AA	AA	AA
14397184	*rs1407837*	AA	AA	AA	AA	AA	AA	AA
14400591	*rs10961505*	AA	AA	AA	AA	AA	AA	AA
14401546	*rs4740570*	AA	AA	AA	AA	AA	AA	AA
14409053	*rs10756549*	GG	GG	GG	GG	GG	GG	GG
14412035	*rs7875762*	GG	GG	GG	GG	GG	AG	GG
14412288	*rs7018762*	GG	GG	GG	GG	GG	AG	GG
14414929	*rs2031195*	AA	AA	AA	AA	AA	AA	AA
14416289	*rs1028704*	AA	AA	AA	AA	AA	AA	AA
14420286	*rs373034*	GG	GG	GG	GG	GG	AG	GG
14420328	*rs303737*	AA	AG	AA	AA	AA	AG	AA

14422097	*rs991115*	GG	AG	GG	GG	GG	GG	GG
14423910	*rs501360*	GG	GG	GG	GG	GG	GG	GG
14424284	*rs958957*	GG	AG	GG	GG	GG	AG	GG
14427476	*rs508259*	AA	AA	AA	AA	AA	AA	AA
14427593	*rs1556031*	CC	AC	CC	CC	CC	CC	CC
14430552	*rs303727*	AA	AG	AA	AA	AA	AG	AA
14432045	*rs10810147*	AA	AG	AA	AA	AA	AG	AA
14433468	*rs551112*	CC	CC	CC	CC	CC	CC	CC
14433784	*rs10491775*	AA	AC	AA	AA	AA	AA	AA
14434316	*rs1323339*	AA	AC	AA	AA	AA	AC	AA
14436001	*rs1556032*	AA	AG	AA	AA	AA	AG	AA
14438497	*rs535076*	AA	AA	AA	AA	AA	AA	AA
14442729	*rs10810150*	GG	AG	GG	GG	GG	GG	GG
14443468	*rs17711118*	AA	AA	AA	AA	AA	AA	AA
14444393	*rs1323342*	CC	CC	CC	CC	CC	AC	CC
14445325	*rs184230*	GG	GG	GG	GG	GG	GG	GG
14446012	*rs7021022*	AA	AG	AA	AA	AA	AA	AA
14454744	*rs913416*	AA	AG	AA	AA	AA	AG	AA
14455961	*rs877451*	AA	AC	AA	AC	AA	AC	AA
14458321	*rs1998495*	AA	AG	AA	AG	AA	AG	AA
14459146	*rs303723*	AA	AA	AA	AA	AA	AG	AA
14460833	*rs10961534*	AA	AG	AA	AA	AA	AA	AA
14462090	*rs10491773*	AA	AA	AA	AA	AA	AA	AA
14463378	*rs1323344*	AA	AA	AA	AC	AA	AC	AA
14463556	*rs303721*	AA	AG	AA	AA	AA	AA	AA
14465352	*rs501463*	AA	AG	AA	AG	AA	AG	AA
14468209	*rs549157*	AA	AG	AA	AG	AA	AG	AA
14469228	*rs487674*	AA	AC	AA	AC	AA	AA	AA
14481347	*rs439269*	AA	AG	AA	AG	AA	AG	AA
14484388	*rs1323348*	GG	AG	GG	AG	GG	GG	GG
14501645	*rs7023433*	AA	AA	AA	AA	AA	AC	AA
14505364	*rs1318729*	GG	AG	GG	AG	GG	AG	GG
14507555	*rs4741389*	GG	AG	GG	AG	GG	AG	GG
14508829	*rs873553*	AA	AA	AA	AA	AA	AA	AA
14509170	*rs2382475*	GG	AG	GG	AG	GG	--	GG
14509301	*rs1106726*	AA	AG	AA	AG	AA	AA	AA
14514438	*rs927969*	AA	AA	AA	AA	AA	AC	AA
14514741	*rs16931893*	GG	GG	GG	GG	GG	AG	GG
14514784	*rs4741390*	AA	AA	AA	AG	AA	AA	AA
14515980	*rs913418*	GG	AG	GG	GG	GG	AG	GG
14518901	*rs4142081*	AA	AA	AA	AG	AA	AG	AA
14520882	*rs10810173*	AA	AG	AA	AG	AA	AA	AA
14522236	*rs13284733*	GG	AG	GG	GG	GG	GG	GG

14524103	*rs7046317*	AA	AA	AA	AG	AA	AA	AA
14525343	*rs7020007*	AA	AA	AA	AA	AA	AA	AA
14525957	*rs10810175*	GG	GG	GG	GG	GG	AG	GG
14528257	*rs2182856*	AA	AA	AA	AG	AA	AA	AA
14528577	*rs10961558*	GG	GG	GG	AG	GG	GG	GG
14529758	*rs10961560*	AA	AG	AA	AA	AA	AA	AA
14530539	*rs7847421*	AA	AG	AA	AA	AA	AA	AA
14531236	*rs7850989*	AA	AA	AA	AG	AA	AA	AA
14533181	*rs16931920*	CC	AC	CC	AC	CC	AC	CC
14533548	*rs927971*	GG	GG	GG	GG	GG	AG	GG
14534555	*rs2149104*	AA	AG	AA	AG	AA	AA	AA
14536071	*rs9987778*	AA	AA	AA	AC	AA	AA	AA
14537633	*rs12002454*	GG	AG	GG	AG	GG	AG	GG
14538852	*rs3736996*	GG	AG	GG	GG	GG	GG	GG
14540138	*rs10491772*	AA	AA	AA	AA	AA	AG	AA
14542236	*rs1327999*	AA	AA	AA	AG	AA	AA	AA
14542292	*rs1536647*	AA	AC	AA	AC	AA	AC	AA
14542979	*rs7875776*	GG	GG	GG	GG	GG	GG	GG
14546625	*rs4741404*	GG	GG	GG	GG	GG	AG	GG
14546659	*rs10756576*	AA	AG	AA	AG	AA	AA	AA
14547806	*rs10961571*	GG	GG	GG	AG	GG	GG	GG
14549910	*rs10961573*	AA	AA	AA	AA	AA	AA	AA
14551712	*rs10961576*	CC	CC	CC	AC	CC	CC	CC
14552630	*rs1556029*	AA	AG	AA	AG	AA	AG	AA
14552698	*rs1004800*	AA	AA	AA	AC	AA	AA	AA
14554090	*rs10491771*	AA	AG	AA	AA	AA	AG	AA
14554285	*rs10961580*	AA	AG	AA	AG	AA	AG	AA
14556116	*rs7867360*	AA	AA	AA	AA	AA	AA	AA
14556156	*rs7867377*	AA	AG	AA	AA	AA	AA	AA
14556406	*rs7040652*	AA	AA	AA	AA	AA	AC	AA
14557981	*rs16932018*	CC	CC	CC	CC	CC	CC	CC
14563137	*rs12352208*	GG	GG	GG	GG	GG	GG	GG
14563613	*rs10116154*	GG	GG	GG	GG	GG	AG	GG
14575052	*rs7029906*	CC	CC	CC	CC	CC	AC	CC
14578049	*rs12238310*	AA	AA	AA	AA	AA	AG	AA
14578910	*rs1047720*	AA	AG	AA	AA	AA	AA	AA
14579173	*rs1047717*	AA	AG	AA	AA	AA	AA	AA
14580805	*rs7857143*	AA	AA	AA	AA	AA	AG	AA
14582180	*rs2225163*	CC	AC	CC	CC	CC	CC	CC
14584501	*rs11794863*	AA	AA	AA	AA	AA	AA	AA
14593494	*rs7859506*	GG	GG	GG	GG	GG	AG	GG
14594822	*rs7850166*	AA	AA	AA	AA	AA	AA	AA
14600591	*rs1343706*	AA	AA	AA	AA	AA	AG	AA

14600866	*rs1343705*	AA	AG	AA	AA	AA	AA	AA
14606166	*rs10756585*	AA	AA	AA	AA	AA	AA	AA
14606371	*rs4741411*	GG	AG	GG	GG	GG	AG	GG
14606590	*rs12236525*	AA	AG	AA	AA	AA	AG	AA
14612952	*rs7874535*	AA	AG	AA	AA	AA	AA	AA
14617829	*rs1343567*	GG	AG	GG	GG	GG	GG	GG
14623299	*rs4620377*	GG	AG	GG	GG	GG	GG	GG
14625546	*rs4490946*	AA	AG	AA	AA	AA	AG	AA
14629380	*rs13302629*	GG	GG	GG	GG	GG	AG	GG
14629666	*rs13284172*	AA	AA	AA	AA	AA	AG	AA
14635813	*rs10120588*	GG	GG	GG	GG	GG	AG	GG
14636278	*rs7870354*	AA	AA	AA	AA	AA	AA	AA
14638118	*rs7849273*	GG	GG	GG	GG	GG	GG	GG
14639728	*rs10961636*	GG	GG	GG	GG	GG	GG	GG
14641283	*rs11790280*	AA	AA	AA	AA	AA	AG	AA
14644900	*rs7853156*	GG	GG	GG	GG	GG	GG	GG
14646681	*rs10119411*	GG	AG	GG	GG	GG	GG	GG
14647139	*rs10756597*	CC	CC	CC	CC	CC	CC	CC
14650700	*rs10481503*	GG	AG	GG	GG	GG	GG	GG
14652171	*rs10961640*	AA	AA	AA	AA	AA	AA	AA
14652260	*rs17215796*	GG	GG	GG	GG	GG	AG	GG
14652459	*rs6474850*	AA	AG	AA	AA	AA	AG	AA
14653394	*rs7867569*	AA	AG	AA	AA	AA	AG	AA
14660890	*rs7875420*	AA	AA	AA	AA	AA	AG	AA
14660949	*rs10961649*	GG	GG	GG	GG	GG	AG	GG
14661208	*rs11793517*	GG	GG	GG	GG	GG	GG	GG
14662267	*rs2890992*	GG	AG	GG	GG	GG	AG	GG
14666174	*rs10961655*	GG	GG	GG	GG	GG	AG	GG
14666870	*rs10810211*	AA	AA	AA	AA	AA	AA	AA
14668017	*rs17216147*	AA	AC	AA	AA	AA	AC	AA
14679088	*rs10810220*	GG	GG	GG	GG	GG	GG	GG
14679594	*rs2890988*	AA	AC	AA	AA	AA	AA	AA
14681897	*rs4740585*	GG	AG	GG	GG	GG	AG	GG
14684302	*rs2382479*	GG	GG	GG	GG	GG	GG	GG
14684372	*rs1574768*	AA	AG	AA	AA	AA	AA	AA
14684536	*rs4326470*	AA	AC	AA	AA	AA	AA	AA
14687022	*rs1317294*	GG	AG	--	--	--	--	GG
14691616	*rs12685826*	GG	GG	GG	GG	GG	GG	GG
14699151	*rs10961677*	GG	AG	GG	GG	GG	AG	GG
14702257	*rs7024505*	AA	AA	AA	AA	AA	AA	AA
14711766	*rs1494359*	AA	AA	AA	AA	AA	AA	AA
14712616	rs10115703	GG	GG	AA	AA	AG	GG	AG
14713637	rs7035643	AA	AA	CC	CC	AC	AA	AC

14716304	rs11794846	AA	AA	AA	AA	AA	AG	AA
14717180	rs1494351	AA	AA	AA	AA	AA	AG	AA
14718730	rs12345917	AA	AG	GG	AG	AG	AA	AG
14720124	rs1494338	GG	AG	GG	GG	GG	GG	GG
14720234	rs10511595	AA	AG	GG	AG	AG	AG	AG
14723896	rs1494340	AA	AG	AA	AA	AA	AA	AA
14723912	rs1494341	GG	GG	AA	AG	AG	AG	AG
14725053	rs1048070	AA	AG	AA	AA	AA	AA	AA
14725187	rs7047712	GG	GG	GG	GG	GG	AG	GG
14727506	**rs10961689**	AA	AC	AA	AA	AA	AC	AA
14730682	**rs8181217**	GG	GG	GG	GG	GG	GG	GG
14736261	**rs4124592**	AA	AA	AA	AA	AA	AA	AA
14737133	**rs2270529**	GG	AG	GG	GG	GG	AG	GG
14737412	**rs4741426**	GG	AG	AA	AG	AG	AG	AG
14738039	**rs1112042**	GG	AG	GG	GG	GG	AG	GG
14741872	**rs2890993**	CC	CC	AA	AC	AC	AC	AC
14744010	**rs2035987**	GG	AG	GG	GG	GG	AG	GG
14746969	**rs12348146**	GG	AG	GG	AG	GG	AG	GG
14747744	**rs10738377**	CC	CC	CC	CC	CC	AC	CC
14747877	**rs7864052**	AA	AC	CC	AC	AC	AC	AC
14751226	**rs1724**	GG	GG	GG	AG	GG	GG	GG
14751260	**rs10124839**	AA	AC	CC	AC	AC	AA	AC
14752700	**rs12685742**	AA	AA	AA	AG	AA	AA	AA
14753056	**rs16932272**	GG	GG	GG	GG	GG	GG	GG
14753855	**rs7039708**	AA	AG	GG	GG	AG	AG	AG
14755030	**rs923926**	AA	AA	AA	AA	AA	AA	AA
14757916	**rs6474855**	AA	AG	GG	GG	AG	AA	AG
14760658	**rs17219005**	AA	AA	CC	CC	AC	AC	AC
14762384	**rs7852390**	CC	CC	CC	--	CC	AC	CC
14765779	**rs1874108**	AA	AA	GG	AG	AG	AA	AG
14765853	**rs1032474**	GG	GG	GG	GG	GG	GG	GG
14766140	**rs10961700**	GG	AG	GG	GG	GG	GG	GG
14768244	**rs4415414**	CC	CC	CC	CC	CC	CC	CC
14770698	**rs923921**	CC	CC	AA	AA	AC	AC	AC
14772367	**rs10810237**	AA	AA	AA	AA	AA	AG	AA
14772497	**rs1494354**	AA	AA	CC	AC	AC	AC	AC
14772585	**rs1494355**	GG	GG	GG	GG	GG	GG	GG
14775224	**rs7027322**	AA	AA	GG	AG	AG	AG	AG
14776962	**rs12685522**	AA	AA	AA	AA	AA	AA	AA
14777156	**rs1546135**	GG	GG	AA	AA	AG	AG	AG
14778886	**rs16932282**	GG	AG	AA	AA	AG	AG	AG
14779521	**rs10810243**	GG	GG	GG	GG	GG	AG	GG
14780841	**rs2291681**	CC	CC	AA	AA	AC	AC	AC

14781348	**rs13296345**	AA	AA	AA	AG	AA	AA	AA
14781715	**rs1389733**	CC	CC	AA	AC	AC	CC	AC
14784476	**rs10756613**	GG	AG	GG	GG	GG	AG	GG
14785265	**rs12338615**	AA	AA	GG	GG	AG	AA	AG
14789407	**rs10810246**	AA	AG	AA	AA	AA	AG	AA
14790779	**rs10738379**	AA	AC	AA	AA	AA	AC	AA
14792948	**rs12350382**	GG	GG	GG	GG	GG	GG	GG
14793857	**rs13294097**	CC	CC	CC	CC	CC	AC	CC
14794141	**rs17220118**	CC	AC	AA	AC	AC	AC	AC
14794733	**rs10810248**	AA	AA	AA	AA	AA	AA	AA
14797218	**rs10756614**	AA	AC	AA	AC	AA	AC	AA
14798325	**rs10810251**	GG	GG	GG	GG	GG	GG	GG
14799826	**rs1389738**	AA	AA	AA	AA	AA	AA	AA
14801009	**rs10217611**	GG	GG	AA	AG	AG	GG	AG
14801971	**rs12000514**	AA	AA	AA	AA	AA	AA	AA
14809370	**rs7023244**	CC	AC	CC	AC	CC	AC	CC
14809813	**rs10961730**	AA	AA	CC	AC	AC	AA	AC
14810223	**rs2779502**	GG	GG	AA	AG	AG	GG	AG
14811819	**rs2779503**	GG	GG	GG	GG	GG	GG	GG
14814286	**rs1332805**	GG	AG	GG	AG	GG	AG	GG
14815709	**rs2493630**	GG	AG	AA	AA	AG	AG	AG
14816616	**rs2818939**	GG	AG	AA	AA	AG	AG	AG
14819767	**rs10756618**	GG	GG	GG	GG	GG	GG	GG
14820010	**rs2779507**	AA	AG	GG	GG	AG	AG	AG
14820821	**rs7868862**	AA	AA	AA	AA	AA	AA	AA
14820989	**rs10810258**	AA	AG	GG	GG	AG	AG	AG
14822349	**rs9792613**	AA	AG	GG	GG	AG	AG	AG
14822366	**rs10081714**	GG	GG	GG	GG	GG	GG	GG
14823401	**rs11506374**	GG	GG	GG	GG	GG	GG	GG
14824172	**rs12555189**	AA	AC	CC	CC	AC	AC	AC
14825081	**rs10961746**	AA	AG	GG	GG	AG	AG	AG
14834777	**rs10810269**	AA	AG	AA	AA	AA	AA	AA
14838892	**rs1021493**	GG	GG	GG	GG	GG	GG	GG
14840256	**rs16932354**	GG	GG	GG	AG	GG	AG	GG
14840816	**rs2779499**	GG	GG	GG	GG	GG	GG	GG
14841841	**rs729491**	AA	AA	AA	AG	AA	AG	AA
14842141	**rs1874105**	AA	AA	AA	AA	AA	AG	AA
14844072	**rs2151206**	GG	GG	AA	AA	AG	GG	--
14856389	**rs7020282**	AA	AA	AA	AA	AA	AA	AA
14857958	**rs16932386**	AA	AA	AA	AA	AA	AG	AA
14860153	**rs11788565**	AA	AA	AA	AA	AA	AA	AA
14868376	**rs10810280**	GG	GG	GG	GG	GG	AG	GG
14869464	**rs10511601**	CC	CC	CC	CC	CC	AC	CC

14869870	**rs2065482**	CC	CC	CC	CC	CC	CC	CC
14870104	**rs7862066**	AA	AA	AA	AA	AA	AA	AA
14870667	**rs7862716**	AA	AA	AA	AA	AA	AA	AA
14879834	**rs16892**	AA	AA	AA	AA	AA	AA	AA
14880268	**rs1996893**	GG	GG	GG	GG	GG	GG	GG
14881670	**rs10810285**	GG	AG	AA	AA	AG	GG	AG
14881810	**rs11790595**	GG	GG	GG	GG	GG	GG	GG
14882721	**rs9776129**	GG	AG	AA	AA	AG	GG	AG
14882993	**rs10961773**	CC	CC	CC	CC	CC	CC	CC
14888142	**rs7044651**	AA	AG	AA	AA	AA	AG	AA
14888161	**rs10961780**	AA	AA	AA	AA	AA	AA	AA
14890356	**rs4740593**	AA	AA	GG	GG	AG	AG	AG
14890516	**rs4740594**	AA	AA	GG	GG	AG	AG	AG
14890565	**rs4741443**	GG	GG	AA	AA	AG	AG	AG
14893275	**rs12337423**	AA	AA	AA	AA	AA	AG	AA
14896868	**rs940120**	AA	AA	GG	GG	AG	AA	AG
14898056	**rs7034380**	CC	CC	AA	AA	AC	AC	AC
14909539	**rs3850442**	AA	AA	GG	GG	AG	AA	AG
14912124	rs11553867	AA	AA	AA	AA	AA	AA	AA
14912224	rs11553861	AA	AA	AA	AA	AA	AA	AA
14912877	rs10756626	GG	GG	AA	AA	AG	AG	AG
14918013	rs10511602	AA	AA	AA	AA	AA	AG	AA
14918594	rs10756627	GG	GG	AA	AA	AG	AG	AG
14924638	rs4295763	AA	AA	CC	CC	AC	AA	AC
14927012	rs1523211	GG	GG	AA	AA	AG	AG	AG
14932035	rs10810293	AA	AA	GG	GG	AG	AA	AG
14937083	rs7043477	AA	AA	GG	GG	AG	AA	AG
14939190	rs9969815	GG	GG	AA	AA	AG	GG	AG
14950217	rs1357474	GG	GG	AA	AA	AG	GG	AG
14952799	rs1412723	GG	GG	GG	GG	GG	AG	GG

Acknowledgements

This work was supported by the Women and Children's Health Research Institute and the Canadian Institutes of Health Research. We thank Azam Khorshidi and Dr. Sameer Pant for assistance with bioinformatic analysis. Data presented at Women and Children Health Research Institute Research Day (November 24th 2010), and the Department of Medical Genetics Research Day (March 9th 2011).

Conflict of Interest Statement

The authors state no conflicts of interest.

References

1. Marles SL, Greenberg CR, Persaud TV, Shuckett EP, Chudley AE. New familial syndrome of unilateral upper eyelid coloboma, aberrant anterior hairline pattern, and anal anomalies in Manitoba Indians. Am J Med Genet 1992; 42(6):793-9.

2. Li C, Marles SL, Greenberg CR, Chodirker BN, van de Kamp J, Slavotinek A, Chudley AE. Manitoba Oculotrichoanal (MOTA) syndrome: report of eight new cases. Am J Med Genet A 2007; 143A(8):853-7.

3. Li C. Manitoba Oculotrichoanal Syndrome. Gene Reviews 2008.

4. Ehlers N. Cryptophthalmos with orbito-palpebral cyst and microphthalmos (report of a bilateral case). Acta Ophthalmol (Copenh) 1966; 44(1):84-94.

5. Slavotinek AM, Tifft CJ. Fraser syndrome and cryptophthalmos: review of the diagnostic criteria and evidence for phenotypic modules in complex malformation syndromes. J Med Genet 2002; 39(9):623-33.

6. Fraser GR. Our genetical 'load'. A review of some aspects of genetical variation. Annals of Human Genetics 1962; 25(4):387-415.

7. Shafeghati Y, Kniepert A, Vakili G, Zenker M. Fraser syndrome due to homozygosity for a splice site mutation of FREM2. Am J Med Genet A 2008; 146A(4):529-31.

8. Jadeja S, Smyth I, Pitera JE, Taylor MS, van Haelst M, Bentley E, McGregor L, Hopkins J, Chalepakis G, Philip N, Perez Aytes A, Watt FM, Darling SM, Jackson I, Woolf AS, Scambler PJ. Identification of a new gene

mutated in Fraser syndrome and mouse myelencephalic blebs. Nat Genet 2005; 37(5):520-5.

9. van Haelst MM, Maiburg M, Baujat G, Jadeja S, Monti E, Bland E, Pearce K, Hennekam RC, Scambler PJ. Molecular study of 33 families with Fraser syndrome new data and mutation review. Am J Med Genet A 2008; 146A(17):2252-7.

10. Long J, Wei Z, Feng W, Yu C, Zhao YX, Zhang M. Supramodular nature of GRIP1 revealed by the structure of its PDZ12 tandem in complex with the carboxyl tail of Fras1. J Mol Biol 2008; 375(5):1457-68.

11. Cavalcanti DP, Matejas V, Luquetti D, Mello MF, Zenker M. Fraser and Ablepharon macrostomia phenotypes: concurrence in one family and association with mutated FRAS1. Am J Med Genet A 2007; 143(3):241-7.

12. Vogel MJ, van Zon P, Brueton L, Gijzen M, van Tuil MC, Cox P, Schanze D, Kariminejad A, Ghaderi-Sohi S, Blair E, Zenker M, Scambler PJ, Ploos van Amstel HK, van Haelst MM. Mutations in GRIP1 cause Fraser syndrome. J Med Genet 2012.

13. Short K, Wiradjaja F, Smyth I. Let's stick together: the role of the Fras1 and Frem proteins in epidermal adhesion. IUBMB Life 2007; 59(7):427-35.

14. Alazami AM, Shaheen R, Alzahrani F, Snape K, Saggar A, Brinkmann B, Bavi P, Al-Gazali LI, Alkuraya FS. FREM1 mutations cause bifid nose, renal agenesis, and anorectal malformations syndrome. Am J Hum Genet 2009; 85(3):414-8.

15. Vissers LE, Cox TC, Maga AM, Short KM, Wiradjaja F, Janssen IM, Jehee F, Bertola D, Liu J, Yagnik G, Sekiguchi K, Kiyozumi D, van Bokhoven H, Marcelis C, Cunningham ML, Anderson PJ, Boyadjiev SA, Passos-Bueno MR, Veltman JA, Smyth I, Buckley MF, Roscioli T. Heterozygous mutations of FREM1 are associated with an increased risk of isolated metopic craniosynostosis in humans and mice. PLoS Genet 2011; 7(9):e1002278.

16. Varnum DS, Fox SC. Head blebs: a new mutation on chromosome 4 of the mouse. J Hered 1981; 72(4):293.

17. Timmer JR, Mak TW, Manova K, Anderson KV, Niswander L. Tissue morphogenesis and vascular stability require the Frem2 protein, product of the mouse myelencephalic blebs gene. Proc Natl Acad Sci U S A 2005; 102(33):11746-50.

18. Chiotaki R, Petrou P, Giakoumaki E, Pavlakis E, Sitaru C, Chalepakis G. Spatiotemporal distribution of Fras1/Frem proteins during mouse embryonic development. Gene Expr Patterns 2007; 7(4):381-8.

19. Takamiya K, Kostourou V, Adams S, Jadeja S, Chalepakis G, Scambler PJ, Huganir RL, Adams RH. A direct functional link between the multi-PDZ domain protein GRIP1 and the Fraser syndrome protein Fras1. Nat Genet 2004; 36(2):172-7.

20. Pavlakis E, Chiotaki R, Chalepakis G. The role of Fras1/Frem proteins in the structure and function of basement membrane. Int J Biochem Cell Biol 2011; 43(4):487-95.

21. McGregor L, Makela V, Darling SM, Vrontou S, Chalepakis G, Roberts C, Smart N, Rutland P, Prescott N, Hopkins J, Bentley E, Shaw A, Roberts E, Mueller R, Jadeja S, Philip N, Nelson J, Francannet C, Perez-Aytes A, Megarbane A, Kerr B, Wainwright B, Woolf AS, Winter RM, Scambler PJ. Fraser syndrome and mouse blebbed phenotype caused by mutations in FRAS1/Fras1 encoding a putative extracellular matrix protein. Nat Genet 2003; 34(2):203-8.

22. Smyth I, Scambler P. The genetics of Fraser syndrome and the blebs mouse mutants. Hum Mol Genet 2005; 14 Spec No. 2:R269-74.

23. Burg MA, Tillet E, Timpl R, Stallcup WB. Binding of the NG2 proteoglycan to type VI collagen and other extracellular matrix molecules. J Biol Chem 1996; 271(42):26110-6.

24. Goretzki L, Burg MA, Grako KA, Stallcup WB. High-affinity binding of basic fibroblast growth factor and platelet-derived growth factor-AA to the core protein of the NG2 proteoglycan. J Biol Chem 1999; 274(24):16831-7.

25. Lander ES, Botstein D. Homozygosity mapping: a way to map human recessive traits with the DNA of inbred children. Science 1987; 236(4808):1567-70.

26. Thiadens AA, den Hollander AI, Roosing S, Nabuurs SB, Zekveld-Vroon RC, Collin RW, De Baere E, Koenekoop RK, van Schooneveld MJ, Strom TM, van Lith-Verhoeven JJ, Lotery AJ, van Moll-Ramirez N, Leroy BP, van den Born LI, Hoyng CB, Cremers FP, Klaver CC. Homozygosity mapping reveals PDE6C mutations in patients with early-onset cone photoreceptor disorders. Am J Hum Genet 2009; 85(2):240-7.

27. Littink KW, Koenekoop RK, van den Born LI, Collin RW, Moruz L, Veltman JA, Roosing S, Zonneveld MN, Omar A, Darvish M, Lopez I, Kroes HY, van Genderen MM, Hoyng CB, Rohrschneider K, van Schooneveld MJ, Cremers FP, den Hollander AI. Homozygosity mapping in patients with cone-rod dystrophy: novel mutations and clinical characterizations. Invest Ophthalmol Vis Sci 2010; 51(11):5943-51.

28. den Hollander AI, Lopez I, Yzer S, Zonneveld MN, Janssen IM, Strom TM, Hehir-Kwa JY, Veltman JA, Arends ML, Meitinger T, Musarella MA, van den Born LI, Fishman GA, Maumenee IH, Rohrschneider K, Cremers FP, Koenekoop RK. Identification of novel mutations in patients with Leber congenital amaurosis and juvenile RP by genome-wide homozygosity mapping with SNP microarrays. Invest Ophthalmol Vis Sci 2007; 48(12):5690-8.

29. Wissinger B, Jagle H, Kohl S, Broghammer M, Baumann B, Hanna DB, Hedels C, Apfelstedt-Sylla E, Randazzo G, Jacobson SG, Zrenner E, Sharpe LT. Human rod monochromacy: linkage analysis and mapping of a cone photoreceptor expressed candidate gene on chromosome 2q11. Genomics 1998; 51(3):325-31.

30. Connell F, Kalidas K, Ostergaard P, Brice G, Homfray T, Roberts L, Bunyan DJ, Mitton S, Mansour S, Mortimer P, Jeffery S. Linkage and sequence analysis indicate that CCBE1 is mutated in recessively inherited generalised lymphatic dysplasia. Hum Genet 2010; 127(2):231-41.

31. Purcell S, Neale B, Todd-Brown K, Thomas L, Ferreira MA, Bender D, Maller J, Sklar P, de Bakker PI, Daly MJ, Sham PC. PLINK: a tool set for whole-

genome association and population-based linkage analyses. Am J Hum Genet 2007; 81(3):559-75.

32. Kent WJ, Sugnet CW, Furey TS, Roskin KM, Pringle TH, Zahler AM, Haussler D. The human genome browser at UCSC. Genome Res 2002; 12(6):996-1006.

33. Belo JA, Bachiller D, Agius E, Kemp C, Borges AC, Marques S, Piccolo S, De Robertis EM. Cerberus-like is a secreted BMP and nodal antagonist not essential for mouse development. Genesis 2000; 26(4):265-70.

34. Mill P, Lee AW, Fukata Y, Tsutsumi R, Fukata M, Keighren M, Porter RM, McKie L, Smyth I, Jackson IJ. Palmitoylation regulates epidermal homeostasis and hair follicle differentiation. PLoS Genet 2009; 5(11):e1000748.

35. Ovcharenko I, Nobrega MA, Loots GG, Stubbs L. ECR Browser: a tool for visualizing and accessing data from comparisons of multiple vertebrate genomes. Nucleic Acids Res 2004; 32(Web Server issue):W280-6.

36. Woods CG, Cox J, Springell K, Hampshire DJ, Mohamed MD, McKibbin M, Stern R, Raymond FL, Sandford R, Malik Sharif S, Karbani G, Ahmed M, Bond J, Clayton D, Inglehearn CF. Quantification of homozygosity in consanguineous individuals with autosomal recessive disease. Am J Hum Genet 2006; 78(5):889-96.

37. Broman KW, Weber JL. Long homozygous chromosomal segments in reference families from the centre d'Etude du polymorphisme humain. Am J Hum Genet 1999; 65(6):1493-500.

38. Slavotinek AM, Baranzini SE, Schanze D, Labelle-Dumais C, Short KM, Chao R, Yahyavi M, Bijlsma EK, Chu C, Musone S, Wheatley A, Kwok PY, Marles S, Fryns JP, Maga AM, Hassan MG, Gould DB, Madireddy L, Li C, Cox TC, Smyth I, Chudley AE, Zenker M. Manitoba-oculo-tricho-anal (MOTA) syndrome is caused by mutations in FREM1. J Med Genet 2011; 48(6):375-82.

39. Kiyozumi D, Sugimoto N, Sekiguchi K. Breakdown of the reciprocal stabilization of QBRICK/Frem1, Fras1, and Frem2 at the basement membrane provokes Fraser syndrome-like defects. Proc Natl Acad Sci U S A 2006; 103(32):11981-6.

40. Smyth I, Du X, Taylor MS, Justice MJ, Beutler B, Jackson IJ. The extracellular matrix gene Frem1 is essential for the normal adhesion of the embryonic epidermis. Proc Natl Acad Sci U S A 2004; 101(37):13560-5.

41. Noonan JP, McCallion AS. Genomics of long-range regulatory elements. Annu Rev Genomics Hum Genet 2010; 11:1-23.

42. Fantes J, Redeker B, Breen M, Boyle S, Brown J, Fletcher J, Jones S, Bickmore W, Fukushima Y, Mannens M, et al. Aniridia-associated cytogenetic rearrangements suggest that a position effect may cause the mutant phenotype. Hum Mol Genet 1995; 4(3):415-22.

43. Kleinjan DA, Seawright A, Schedl A, Quinlan RA, Danes S, van Heyningen V. Aniridia-associated translocations, DNase hypersensitivity, sequence comparison and transgenic analysis redefine the functional domain of PAX6. Hum Mol Genet 2001; 10(19):2049-59.

44. Visel A, Minovitsky S, Dubchak I, Pennacchio LA. VISTA Enhancer Browser--a database of tissue-specific human enhancers. Nucleic Acids Res 2007; 35(Database issue):D88-92.

45. Cooper GM, Brown CD. Qualifying the relationship between sequence conservation and molecular function. Genome Res 2008; 18(2):201-5.

46. Koster MI, Dai D, Marinari B, Sano Y, Costanzo A, Karin M, Roop DR. p63 induces key target genes required for epidermal morphogenesis. Proc Natl Acad Sci U S A 2007; 104(9):3255-60.

47. Antonini D, Rossi B, Han R, Minichiello A, Di Palma T, Corrado M, Banfi S, Zannini M, Brissette JL, Missero C. An autoregulatory loop directs the tissue-specific expression of p63 through a long-range evolutionarily conserved enhancer. Mol Cell Biol 2006; 26(8):3308-18.

Chapter 4 General discussion and future directions

The World Health Organization estimates that 138 million individuals are visually impaired and about 37 million of these are blind globally [1]. Vision acuity can drastically impact the quality and duration of life and estimates that the rate of mortality by increases 1.1 – 4.1 times [2]. Visually impairments leads to a lack of mobility and depending on the severity of vision loss may require aids such as walking sticks or guide dogs. These physical challenges compound into psychological conditions causing social withdrawal and depression [3], factors which decrease ability of individuals to pursue careers and personal pursuits of which they otherwise might be capable. The two projects described in this thesis add to the growing body information that genetic factors are responsible for inherited ocular disease. *GDF11* and *FREM1* encode proteins which control different aspects of eye development.

Future directions of *gdf11* in development

The first project involved selecting a *GDF11* as a candidate gene, pursuing its role in determining retinal cell development in a zebrafish model organism, and screening disease cohorts for sequence variants. Although sequence variants detected were rare, no mutations were found to be directly responsible for disease. Sequence variants resulting in amino acid substitutions of G210V, G44A, or 1 alanine insertion detected in POAG DNAs and relating causation by comparison of frequency in controls exhibits the caveat that POAG may have been undiagnosed or has yet to develop in the controls. Alterations in protein processing were detected in one missense variant, G210V, and not in *GDF11* sequence variants with altered alanine number. The functional consequence of

the *GDF11* sequence variants on activity could be pursued by luciferase assays with responsive elements sensitive for *GDF11* signal transduction. Cell localization assays could prove fruitful as alterations in polyalanine number in other genes resulted in aggregation or mis-localization of protein. Modeling the effects of *gdf11* inhibition in zebrafish resulted in alterations of genes required for development of retinal cell types and whole eyes exhibiting a decrease in photoreceptor number. While it may be tempting to translate these results with human patient phenotypes like MAC or juvenile RP, it should be noted that no model exist explaining retinal differentiation in vertebrates as genes in one model organism plays different roles in other organisms [4]. The differing retinal composition may be due to the different visual needs of an organism such as temporal activity (day or night) or the state of their environment (land or water).

The differences and similarities of this study investigating *gdf11* in retinal development should be contrasted with the two other zebrafish *gdf11* publications which employed MOs to inhibit gene activity [5-6] and the *Gdf11* knockout mouse [7-8]. The *Gdf11* knockout nice exhibits changes in retinal cell type composition (less rods), a ventral coloboma at E14.5 (see supplemental Fig 2). The *gdf11* investigations in this thesis mirror the loss of rod photoreceptor phenotype in that there is a decrease in rods and amacrines. No experiments were performed to examine the retinal ganglion cell population. Expression of *Crx* is decreased in *Gdf11* mutant mice while *NeuroD* is decreased at one time point, but recovers to normal levels. It may be that *Crx* and *NeuroD* cause the

differentiation of cell types differently in zebrafish and mice. In zebrafish *Farooq et al.* 2008 inhibited *gdf11* function with a translation blocking MO resulting in alteration in aspects of liver development and in Fig. 12 *gdf11* morphants display smaller eyes at 2-3dpf, but a small eye phenotype is not detected at 5dpf [5]. Another group inhibited *gdf11* function with a splice blocking MO and no gross changes in eye size were noted or are observed in larvae [6]. Interestingly, neither group mentioned the presence of cardiac edema as their focus may have been solely on liver or skeletal patterning. To further decipher the role of *gdf11* in zebrafish, other experiments should examine other retinal populations such as the RGCs which are increased in *Gdf11* mice and horizontal cells which are unaltered [7].

The role of *GDF11* in retinal cell development of axons or dendrite connections is another point of interest which could be investigated. This has been observed in the increase of dendrite production of RGCs exposed to *Gdf11* protein in xenopus [9]. It would be interesting to detect what processes occur in zebrafish when *gdf11* activity is reduced. This could lead to faulty development of the retinal circuit as RGCs may not properly connect to inner neurons like amacrines.

Other than ocular phenotypes, several other lines of study could be further investigated such as a possible role of *gdf11*'s in brain development. In the developing spinal cord, *Gdf11* controls the segmentation by the homeobox (*Hox*) genes [10]. The *Hox* genes are transcription factors that control segmentation of the spinal cord as well as the hindbrain [11]. Neuronal development as it pertains to *hox* genes and hindbrain compartmentalization in zebrafish brain could be

pursued as *gdf11* is expressed in the hindbrain. Interestingly *gdf11* morphants exhibit a hindbrain phenotype, while *neuroD* in situs show expression between the putative midbrain and hindbrain which is lost in *gdf11* morphants. Whether or not this is due to altered brain segmentation or altered expression of genes required for brain segmentation would be interesting avenues to study.

While morpholinos are an important and fruitful tool to study development, subsequent studies will be far more powerful if *gdf11* mutants are made available. The advantageous of having *gdf11* mutants is that gene activity will be very little or null as compared to the temporary and variable knockdown yielded in MO usage. This would make it possible to study phenotypes manifesting in adult zebrafish. It is interesting to note that another group was able to document alterations in pelvic positioning of *gdf11* morphants at 44-60dpf using a *gdf11* splice blocking MO [6]. The work in this thesis employs a translation blocking MO resulting in ocular, skeletal, and cardiac anomalies in morphants incapable of swimming properly by 5dpf. Also no *gdf11* antibody exists to test for knockdown specificity to further support MO efficacy. The use of homozygous or heterozygous *gdf11* mutant zebrafish would increase the power of the studies as off targeting effects such as non-specific cell death caused by some MOs would not be present. One potential approach to create *gdf11* mutants is employing zinc finger nucleases [12-13]. While zinc finger nucleases and other emerging mutagenesis technologies could be employed to generate a *gdf11* null model, it should be noted that the Sanger Center created a founder line which did generate a mutant strain. The high throughput mutagenesis system employed by the Sanger

Center raises the possibility that the zebrafish carrying the *gdf11* null mutation were lost during the creation of a founder line. Background genetics of founder strains as well as careful maintenance of detected alleles should be taken into consideration should any future researchers wish to invest time and effort to create a null *gdf11* mutant. Another option would be to create a hypomorph with reduced *gdf11* activity which reminds viable for life. Doing so would require further characterization of *gdf11* protein residues that could be altered but still retain partial functionality.

Towards the characterization of genetic factors responsible for MOTA

My second project mapped a causative locus responsible for Manitoba Oculotrichoanal syndrome, an inherited ocular condition present in First Nations communities. While the results of this thesis are encouraging, subsequently outlined future directions could potentially progress and improve the health outcomes of the First Nations. No biochemically characterized disease causing definitive variants were discovered or assayed. Instead, what is shown is a relatively small 330kb region shown to segregate with MOTA syndrome probands. Traditionally, homozygous regions are regions that are greater than 1Mb however this not a standardized criteria. Historically, homozygosity mapping papers focus on regions greater than 1 Mb because it is thought that smaller regions would be due to homozygosity by chance instead of by descent. This may have been an arbitrary cut off point set at a time when arrays had an average density of 10 SNPs over 1Mb. The MOTA syndrome in this thesis

utilizes an array that has 30 times more coverage for the same 1Mb region and contains 152 SNPs in the critical 330kb region. Other studies have used smaller cut offs as a study investigating human height examined homozygous regions that are approximately 500kb [14]. The genotyping data were deemed to be high quality as < 0.01% were due to non-Mendelian error, this value is likely an underestimate since the paternal genotypes are not known.

The causal region identified in this MOTA study is small but further defining the critical interval with microsatellite markers could complement the SNP data. Other mapping strategies could be performed but this may be redundant and not necessary in this case, as homozygosity mapping analysis has defined just one autosomal region shared by probands and not unaffected individuals. Furthermore, the numerous *Frem1* mouse mutant strains describe its role in maintaining epithelial integrity [15-16]. A relatively recent report in another set of MOTA syndrome afflicted samples do not document any mutations [17] found in this study supports the conclusion that additional mutations cause MOTA syndrome. It is interesting that even in an isolated and genetically homogenous population such as the First Nations, there are tentatively two alleles (a mutation in linkage with c.5556A>G and an exonic in frame deletion). This is not unique in that other diseases exhibited by apparently consanguineous populations have occurred [18-20].

Another possibility is that *ZDHHC21* and *CER1* could be contributing to the phenotypes attributable to MOTA syndrome. The functional role of *ZDHHC21* in hair development may have roles in patterning the aberrant hair wedge exhibited

by MOTA phenotypes if *ZDHCC21* expression is altered [21]. Altered antagonism of growth factors by *CER1* could change the bioavailability of growth factors [22]. FS patients exhibit renal phenotypes while *Cer1* patterns kidney development [23]. There may be a sub-clinical kidney deficit not detected in MOTA probands in this study. Loss of function mutations in the *FRAS/FREM* family of genes results in phenotypes compatible with MOTA and FS syndrome but the contributing role that *ZDHHC21* and *CER1* should not be discounted. While no exon or exon-intron boundary mutations were detected, sequence variants may be present in areas previously unknown to regulate gene expression. The ultimate goal of mapping genetic disorders is to identify causal alleles, but the region identified may not be due to mutations within coding regions of genes. A possible explanation proposed is the existence of an altered regulatory element. One strategy that could be employed is targeted next generation sequencing and comparisons of the critical interval for both parents and probands.

The subsequent process of identifying and characterizing may be extremely difficult. Approximately 50% of the genome is mis-termed "junk DNA" in that it does not contain the 45% repetitive elements or 1.5% of protein coding DNA. This junk DNA may actually contain elaborate programming and expression information in the form of gene regulatory elements such as enhancer, silencers, or promoters. Enhancers recruit additional transcription factors to increase gene and loss of enhancer activity subsequently decreases gene activity [24]. Enhancers can be located tens to hundreds of kilobases upstream or downstream of the transcriptional start site of their target genes. Circularized Chromosome

Conformation Capture (4C) is one method that could document the DNA looping of putative *FREM1* enhancers [25]. Enhancers have been documented in the online VISTA Enhancer database for activity in forebrain, midbrain and limb tissues [26]. This is not an exhaustive a definitive description of enhancers as the particular reporter assay test at only one embryonic time point and the number of tested sequences continues to grow so the VISTA database should be checked periodically for updated assayed sequences. Silencers turn off gene transcription, but may not cause MOTA as heterozygous *FREM1* mutations act in a dominant gain of function mechanism to cause craniosynostosis [27]. Promoters are located 5' upstream of the transcribed gene and this does not fit with the downstream positional location of the IBD region with respect to *FREM1*. No doubt there are multiple strategies to identify and characterize plausible disease implicated regulatory elements responsible for MOTA which would be an interesting project to pursue in the future. Should a pathogenic variant be discovered and biochemically validated, populations at risk could be screened for mutation carriers in order to provide information including the relative risk and complicating factors that arise from giving birth to a child afflicted with MOTA syndrome.

A point of potential further interest is the apparently high rate of homozygosity in this study which could theoretically be applied to explain the roles of genetic factors in complex traits. For example, homozygous interval map genes associated with schizophrenia in apparently unrelated Caucasian individuals [28]. A study on a Croatian cohort demonstrate that consanguinity accounts for 36%

increase blood pressure in a particular population [29]. Higher measurements of heterozygosity in approximately 2700 individuals correlate with lower levels of low-density lipoproteins [30]. These studies show that complex traits may have recessively acting genetic factors. Only eight samples were genotyped in the work presented in this thesis since the goal of finding genetic loci implicated in what appeared to be an autosomal recessive disease. To expand on the role that consanguinity plays in the First Nations would require genotyping many more samples as well as documenting quantitative traits of the phenotype of interest for a particular disease.

Treatment and patient management

The ultimate goal of research is to improve the health outcome of patients. One notable, success of ocular genetics are gene replacement strategies in patients with mutations in retinal pigment epithelium-specific 65kDa (*RPE65*) which cause LCA. This was originally performed on treating dogs employing the use of viral vectors [31]. Subsequently, treatment in three human patients displayed improved visual acuity was maintained 1.5 years [32]. One reason that this treatment has proved successful is that the ocular structure requiring the *RPE65* protein, the RPE and photoreceptors, remains intact in patients with LCA. Gene replacement for other LCA or juvenile RP mutation causing genes may prove more difficult if their eyes lack retinal cell types such as photoreceptors. Treatment of congenital ocular conditions such as MAC may prove more elusive. Currently, patient management consists of first assessing eyes for light sensitivity [33]. Socket expanders may be inserted in patients with no visual perception (anopthalmia) to

minimize facial deformities which could lead to difficulties regarding social interaction. Patients with residual light perception (microphthalmia or coloboma) are fitted with prosthesis that goes over the eye to promote orbital growth. Impaired vision in MOTA syndrome patients can be caused by the constant exposure of the cornea leading to inflammation and irritation which are improved in certain cryptophthalmos cases by surgery to release eyelid fusion from cornea or iris [34].

Much of the current work with regards to inherited ocular diseases focuses on characterizing the diseases at a fundamental molecular level. This work will eventually lead to the treatment and better patient management of such disorders. Preventing blindness has many intrinsic benefits to the individual increasing self reliance as well as well being and extrinsic benefits to the general populace such as increased economic productivity and decreased demand on public health resources. Ongoing research will no doubt be exciting on a fundament scientific level and fruitful to patients by improving their quality of life.

References

1. Resnikoff S, Pascolini D, Etya'ale D, Kocur I, Pararajasegaram R, Pokharel GP, Mariotti SP. Global data on visual impairment in the year 2002. Bull World Health Organ 2004; 82(11):844-51.

2. Cook J, Frick KD, Baltussen R, Resnikoff S, Smith A, Mecaskey J, Kilima P. Loss of Vision and Hearing. 2006.

3. Varma R, Lee PP, Goldberg I, Kotak S. An assessment of the health and economic burdens of glaucoma. Am J Ophthalmol 2011; 152(4):515-22.

4. Adler R, Raymond PA. Have we achieved a unified model of photoreceptor cell fate specification in vertebrates? Brain Res 2008; 1192:134-50.

5. Farooq M, Sulochana KN, Pan X, To J, Sheng D, Gong Z, Ge R. Histone deacetylase 3 (hdac3) is specifically required for liver development in zebrafish. Dev Biol 2008; 317(1):336-53.

6. Murata Y, Tamura M, Aita Y, Fujimura K, Murakami Y, Okabe M, Okada N, Tanaka M. Allometric growth of the trunk leads to the rostral shift of the pelvic fin in teleost fishes. Dev Biol 2010; 347(1):236-45.

7. Kim J, Wu HH, Lander AD, Lyons KM, Matzuk MM, Calof AL. GDF11 controls the timing of progenitor cell competence in developing retina. Science 2005; 308(5730):1927-30.

8. Lee YJ, McPherron A, Choe S, Sakai Y, Chandraratna RA, Lee SJ, Oh SP. Growth differentiation factor 11 signaling controls retinoic acid activity for axial vertebral development. Dev Biol 2010; 347(1):195-203.

9. Hocking JC, Hehr CL, Chang RY, Johnston J, McFarlane S. TGFbeta ligands promote the initiation of retinal ganglion cell dendrites in vitro and in vivo. Mol Cell Neurosci 2008; 37(2):247-60.

10. Liu JP. The function of growth/differentiation factor 11 (Gdf11) in rostrocaudal patterning of the developing spinal cord. Development 2006; 133(15):2865-74.

11. Alexander T, Nolte C, Krumlauf R. Hox genes and segmentation of the hindbrain and axial skeleton. Annu Rev Cell Dev Biol 2009; 25:431-56.

12. Ekker SC. Zinc finger-based knockout punches for zebrafish genes. Zebrafish 2008; 5(2):121-3.

13. Foley JE, Yeh JR, Maeder ML, Reyon D, Sander JD, Peterson RT, Joung JK. Rapid mutation of endogenous zebrafish genes using zinc finger nucleases made by Oligomerized Pool ENgineering (OPEN). PLoS One 2009; 4(2):e4348.

14. Yang TL, Guo Y, Zhang LS, Tian Q, Yan H, Papasian CJ, Recker RR, Deng HW. Runs of homozygosity identify a recessive locus 12q21.31 for human adult height. J Clin Endocrinol Metab 2010; 95(8):3777-82.

15. Smyth I, Du X, Taylor MS, Justice MJ, Beutler B, Jackson IJ. The extracellular matrix gene Frem1 is essential for the normal adhesion of the embryonic epidermis. Proc Natl Acad Sci U S A 2004; 101(37):13560-5.

16. Theiler K, Varnum DS, Nadeau JH, Stevens LC, Cagianut B. A new allele of ocular retardation: early development and morphogenetic cell death. Anat Embryol (Berl) 1976; 150(1):85-97.

17. Slavotinek AM, Baranzini SE, Schanze D, Labelle-Dumais C, Short KM, Chao R, Yahyavi M, Bijlsma EK, Chu C, Musone S, Wheatley A, Kwok PY, Marles S, Fryns JP, Maga AM, Hassan MG, Gould DB, Madireddy L, Li C, Cox TC, Smyth I, Chudley AE, Zenker M. Manitoba-oculo-tricho-anal (MOTA) syndrome is caused by mutations in FREM1. J Med Genet 2011; 48(6):375-82.

18. Benayoun L, Spiegel R, Auslender N, Abbasi AH, Rizel L, Hujeirat Y, Salama I, Garzozi HJ, Allon-Shalev S, Ben-Yosef T. Genetic heterogeneity in two consanguineous families segregating early onset retinal degeneration: the pitfalls of homozygosity mapping. Am J Med Genet A 2009; 149A(4):650-6.

19. Laurier V, Stoetzel C, Muller J, Thibault C, Corbani S, Jalkh N, Salem N, Chouery E, Poch O, Licaire S, Danse JM, Amati-Bonneau P, Bonneau D, Megarbane A, Mandel JL, Dollfus H. Pitfalls of homozygosity mapping: an extended consanguineous Bardet-Biedl syndrome family with two mutant genes (BBS2, BBS10), three mutations, but no triallelism. Eur J Hum Genet 2006; 14(11):1195-203.

20. Miano MG, Jacobson SG, Carothers A, Hanson I, Teague P, Lovell J, Cideciyan AV, Haider N, Stone EM, Sheffield VC, Wright AF. Pitfalls in homozygosity mapping. Am J Hum Genet 2000; 67(5):1348-51.

21. Mill P, Lee AW, Fukata Y, Tsutsumi R, Fukata M, Keighren M, Porter RM, McKie L, Smyth I, Jackson IJ. Palmitoylation regulates epidermal homeostasis and hair follicle differentiation. PLoS Genet 2009; 5(11):e1000748.

22. Belo JA, Bachiller D, Agius E, Kemp C, Borges AC, Marques S, Piccolo S, De Robertis EM. Cerberus-like is a secreted BMP and nodal antagonist not essential for mouse development. Genesis 2000; 26(4):265-70.

23. Chi L, Saarela U, Railo A, Prunskaite-Hyyrylainen R, Skovorodkin I, Anthony S, Katsu K, Liu Y, Shan J, Salgueiro AM, Belo JA, Davies J, Yokouchi Y, Vainio SJ. A secreted BMP antagonist, Cer1, fine tunes the spatial organization of the ureteric bud tree during mouse kidney development. PLoS One 2011; 6(11):e27676.

24. Noonan JP, McCallion AS. Genomics of long-range regulatory elements. Annu Rev Genomics Hum Genet 2010; 11:1-23.

25. Zhao Z, Tavoosidana G, Sjolinder M, Gondor A, Mariano P, Wang S, Kanduri C, Lezcano M, Sandhu KS, Singh U, Pant V, Tiwari V, Kurukuti S, Ohlsson R. Circular chromosome conformation capture (4C) uncovers extensive networks of epigenetically regulated intra- and interchromosomal interactions. Nat Genet 2006; 38(11):1341-7.

26. Visel A, Minovitsky S, Dubchak I, Pennacchio LA. VISTA Enhancer Browser--a database of tissue-specific human enhancers. Nucleic Acids Res 2007; 35(Database issue):D88-92.

27. Vissers LE, Cox TC, Maga AM, Short KM, Wiradjaja F, Janssen IM, Jehee F, Bertola D, Liu J, Yagnik G, Sekiguchi K, Kiyozumi D, van Bokhoven H, Marcelis C, Cunningham ML, Anderson PJ, Boyadjiev SA, Passos-Bueno MR, Veltman JA, Smyth I, Buckley MF, Roscioli T. Heterozygous mutations of

FREM1 are associated with an increased risk of isolated metopic craniosynostosis in humans and mice. PLoS Genet 2011; 7(9):e1002278.

28. Lencz T, Lambert C, DeRosse P, Burdick KE, Morgan TV, Kane JM, Kucherlapati R, Malhotra AK. Runs of homozygosity reveal highly penetrant recessive loci in schizophrenia. Proc Natl Acad Sci U S A 2007; 104(50):19942-7.

29. Rudan I, Smolej-Narancic N, Campbell H, Carothers A, Wright A, Janicijevic B, Rudan P. Inbreeding and the genetic complexity of human hypertension. Genetics 2003; 163(3):1011-21.

30. Campbell H, Carothers AD, Rudan I, Hayward C, Biloglav Z, Barac L, Pericic M, Janicijevic B, Smolej-Narancic N, Polasek O, Kolcic I, Weber JL, Hastie ND, Rudan P, Wright AF. Effects of genome-wide heterozygosity on a range of biomedically relevant human quantitative traits. Hum Mol Genet 2007; 16(2):233-41.

31. Acland GM, Aguirre GD, Ray J, Zhang Q, Aleman TS, Cideciyan AV, Pearce-Kelling SE, Anand V, Zeng Y, Maguire AM, Jacobson SG, Hauswirth WW, Bennett J. Gene therapy restores vision in a canine model of childhood blindness. Nat Genet 2001; 28(1):92-5.

32. Simonelli F, Maguire AM, Testa F, Pierce EA, Mingozzi F, Bennicelli JL, Rossi S, Marshall K, Banfi S, Surace EM, Sun J, Redmond TM, Zhu X, Shindler KS, Ying GS, Ziviello C, Acerra C, Wright JF, McDonnell JW, High KA, Bennett J, Auricchio A. Gene therapy for Leber's congenital amaurosis is safe and effective through 1.5 years after vector administration. Mol Ther 2010; 18(3):643-50.

33. Ragge NK, Subak-Sharpe ID, Collin JR. A practical guide to the management of anophthalmia and microphthalmia. Eye (Lond) 2007; 21(10):1290-300.

34. Li C. Manitoba Oculotrichoanal Syndrome. Gene Reviews 2008.